Biomaterial Scaffolds and Genetically Modified Stem Cells - *An Investigation of their Potential in Bone Repair*

A thesis submitted to the National University of Ireland as fulfillment of the requirement for the degree of

Doctor of Philosophy

By

Saraswathi Sadasivan

Regenerative Medicine Institute (REMEDI),

College of Medicine, Nursing & Health Sciences,

National University of Ireland, Galway

Thesis Supervisor:

Prof. Frank Barry

Table of Contents

LIST OF TABLES

CHAPTER 1:

LIST OF FIGURES

CHAPTER 1:

LIST OF ABBREVIATIONS

µg	Microgram
µg/ml	microgram per millilitre
µl	Microliter
µm	Microns
^{0}C	Degrees Celsius
2D	Two-dimensional
3D	Three-dimensional
ml/min	millilitre per minute
ALP	Alkaline phosphatase
ANOVA	Analysis of variance
ARCO	Association Research Circulation Osseous
AVN	Avascular necrosis
BCP	Biphasic calcium phosphate
OCN	Osteocalcin
BMP	Bone morphogenetic protein
BMSC	bone marrow stromal cells
BSP	Bone sialoprotein
CA	Calcium apatite
CaP	Calcium phosphate
CD	cluster of differentiation
cDNA	complementary DNA
CFU-F	colony-forming unit-fibroblasts
CHA	Calcium hydroxyapatite
CO_2	Carbon dioxide
Col1A1	Collagen, type I, alpha 1
CTB	Cell titre blue
CXCL12	C-X-C motif chemokine 12
dH_2O	Distilled water
DMEM	Dulbecco's Modified Eagle Medium

DNA	Deoxyribonucleic acid
dNTP	Deoxynucleotide
dsRED	Discosoma sp. red fluorescent protein
E. coli	Escherichia coli
ECM	Extracellular matrix
ECs	Endothelial cells
EDX	Energy-dispersive X-ray spectroscopy
ELISA	enzyme-linked immunosorbent assay
EPCs	Endothelial progenitor cells
Eph	Erythropoietin-producing human hepatocellular
ESC	Embryonic stem cells
FDA	Food and Drug Administration
FGF	Fibroblast growth factors
FTIR	Fourier Transform Infra-red
GAG	Group-specific antigen
GAPDH	Granulocyte-colony stimulating factor
GDF	granulocyte-derived factor
GM	Growth media
GPa	Giga Pascal
HA	Hydroxyapatite
HCl	Hydrochloric acid
HEK 293T	Human Embryonic Kidney 293 cells
HLA	human leukocyte antigen
hMSC	human mesenchymal stem cells
hr.	hour
HSCs	Haematopoietic stem cell
HUVEC	Human Umbilical Vein Endothelial Cells
IBSP	integrin binding sialoprotein
IGF-1	Insulin-like growth factor 1
IL	Interleukin

IR	Infrared
ISO	International Organization for Standardization
LB	Lysogeny broth
LIF	Leukaemia inhibitory factor
M	Molar
mA	Milliamps
$MBCP^+$	Micro Macroporous Resorbable Biphasic Calcium Phosphate
MCP-1	Monocyte chemoattractant protein-1
M-CSF	macrophage colony-stimulating factor
mM	mill molar
MMP	Matrix metalloproteinase
MP	Mesenchymal progenitor
MPa	Megapascal
MRI	Magnetic resonance imaging
N	Newton
nm	Nanometre
Ob	Osteoblast
OC	Osteocalcin
Oct4	octamer-binding transcription factor 4
OD	Optical density
OEC	Outgrowth endothelial cells
OM	Osteo media
ON	Osteonecrosis
ONFH	Osteonecrosis of the femoral head
ONN	Osteonectin
OP	Osteopontin
OPG	Osteoprotegerin
OSX	Osterix
PBS	Phosphate buffered saline
PDGF	Platelet derived growth factor

PDZ	acronym combining the first letters of three proteins — post synaptic density protein
PGA	poly(glycolic acid)
PLA	Poly(lactic acid)
PLGA	poly(lactic-co-glycolic acid)
pNPP	para-Nitrophenylphosphate
PTHrP	Parathyroid hormone-related protein
qPCR	quantitative polymerase chain reaction
RANKL	Receptor activator of nuclear factor kappa-B ligand
RGD	Arginylglycylaspartic acid
RNA	ribonucleic acid
RPM	Revolutions per minute
RT	Room temperature
RT-PCR	Reverse transcription polymerase chain reaction
RUNX2	Runt-related transcription factor 2
SaoS 2	Sarcoma osteogenic
SBF	Simulated body fluid
SC	Stem cell
SCF	Stem cell factor
SD	Standard deviation
SDF-1	stromal cell-derived factor 1
SEM	Scanning electron microscope
sFLT-1	Soluble fms-like tyrosine kinase-1
SOX	SRY (sex determining region Y)-box
SSEA	stage-specific embryonic antigen
SVF	Stromal vascular fraction
TCP	Tricalcium phosphate
TE	Tissue Engineered
TGA	Thermo gravimetric analysis
TNF-α	Tumour necrosis factor alpha

TRAP	Tartrate-resistant acid phosphatase
U/ml	Units per millilitre
USA	United States of America
UT	Untransduced
VEGF	Vascular endothelial growth factor
VEGFR-2	vascular endothelial growth factor receptor 2
XPS	X-ray photoelectron spectroscopy
ΔCT	Delta threshold cycle

ACKNOWLEDGEMENT

I wish to convey my sincere gratitude to my supervisor Prof. Frank Barry for his guidance, encouragement and insightful ideas throughout the course of my Ph.D. Thank you so much for providing me an opportunity to start my international career at a leading lab. Special thanks to Ms. Georgina Shaw for being generous with her time in helping and tutoring me in good lab practices. Dr. Linda Howard- your advice and help on the Ephrin Chapter were invaluable and I cannot thank you enough for it. Special thanks also to the project collaborators at DePuy Synthes and in particular James Anderson for the useful discussions and advice during our update meetings at Galway and Leeds.

I would like to particularly mention Dr. Siobhan Gaughan for helping me get oriented to working at REMEDI. Thanks to everyone in the Ortho group and REMEDI who have helped me in one way or the other during my four fruitful years in Galway. Many Thanks to Andrea Keogh for your empathy and encouragement during the last few months of our respective Ph.D. when we used to dominate virus cell culture!! Thank you to Stephanie Boomkamp for your positivity and moral support when I was completing the experiments. I would also like to thank my GRC members- Dr. Mary Murphy and Prof. Matt Griffin for your helpful advice and support.

Last but not any means least, my gratitude to my super amazing parents who continuously supported my endeavor and efforts in my academic pursuits. Appa, I can't thank you enough for permitting me to go alone to a country where I knew no one when everyone else was opposed to the idea. The experience is something I will always cherish. Million thanks to my sister , my true best friend , for believing in me and supporting me and also my brother-in-law who provided constant encouragement.

To my super team of Aces –

Amma, Appa, Akka & Athimber

Abstract

The task of repairing large sections of bone tissue lost due to major trauma or pathology poses a significant challenge in orthopedic healthcare. The medical intervention often resorted to consists of a combination of grafting procedures, internal and external prostheses and fixation devices. However, the quantity of available harvested autologous bone is often not sufficient to create an effective graft. Very often the outcome is limited restoration of functional tissue. One example of such a condition is avascular necrosis (AVN) of the hip, which occurs when blood flow to a section of bone is interrupted. AVN typically affects people between the ages of 25 and 50, and between 30% and 70% of patients who are diagnosed with AVN in one hip will subsequently be diagnosed with the same disease in their other hip. Despite the high performance of current joint replacements, these patients may reasonably expect to require two or more revision surgeries in their lifetimes. These factors combine to make early intervention therapies that delay or remove the need for total hip replacement vital for the long-term management of this disease. Although many such treatments exist, the success rate is relatively low. A promising strategy is to devise methods that will lead to the restoration of functional bone tissue.

The objective of this research project is to develop a tissue engineered construct to enable bone regeneration and to restore the vascular supply. Two scaffolds were tested to evaluate osteoinductivity. Biosel, manufactured by DePuy Synthes (was the candidate material initially selected for the study).This material is fabricated as 3mm cubes consisting of 75% hydroxyapatite (HA) and 25% β-tricalcium phosphate (TCP). The Biosel scaffold provided a non-toxic environment capable of supporting cellular proliferation but did not enhance osteogenesis significantly.

The second material to be tested was microporous biphasic calcium phosphate ($MBCP^+$, Biomatlante, France) which consisted of HA and TCP particles. The ratio of HA: TCP for this material is 20:80 .The $MBCP^+$ scaffold provided an environment for cells to remain viable and proliferate like Biosel. Further, the $MBCP^+$ scaffold, being particulate in nature, presented an environment with a greater degree of freedom, allowing populating cells to

proliferate and self-synthesise a three-dimensional environment. Interestingly, although these scaffolds degraded faster than the Biosel, they supported osteogenesis even in the absence of osteogenic differentiation medium. Since the differentiation step can potentially be bypassed, the $MBCP^+$ has several advantages- reduced time, cost and reduced risk of contamination.

In order to enhance angiogenesis, hMSCs were modified with a lentiviral vector to overexpress Ephrin B2, a molecule known for its pro-osteogenic and pro-angiogenic capabilities. Results indicated a significant enhancement of both osteogenesis and angiogenesis as indicated by increased calcium deposition and tubule formation in Ephrin B2 transduced hMSCs in comparison to controls. It was noted that hMSCs (both transduced and untransduced) displayed a reduction in their angiogenic potential following osteogenic induction.

Therefore, it is proposed to combine the spontaneous osteogenic differentiation capabilities of the $MBCP^+$ and seed it with non-differentiated Ephrin B2 overexpressing hMSC (in order to take advantage of their potent angiogenic capabilities) which would result in a construct that would potentially prove highly therapeutic to the Avascular Necrotic environment.

DECLARATION

I declare that all of the work in this thesis was performed personally. No part of this work has been submitted for consideration as part of any other degree or award

CHAPTER 1: INTRODUCTION

SECTION A: BONE BIOLOGY AND REPAIR

1.1 Bone biology

1.1.1 Function

Bone tissue serves as a structural support to the body. It acts as a lever for muscles enabling locomotion functions of the body. It also protects the underlying soft tissues and vital organs[1]. Additionally bone tissue serves as a mineral reservoir containing calcium and phosphate which are important for regulating ion concentration in the extracellular fluid. Bone marrow contains Mesenchymal stem cells (MSCs), - multipotent cells with the capacity to differentiate into bone, cartilage, tendon, muscle, dermis and fat tissue. The bone marrow contains hematopoietic cells that produce red and white blood vessels required for both nutrient transport and immune resistance[2].

1.1.2 Structure and Mechanics

The adult skeleton typically contains 80% cortical (compact) bone and 20% trabecular (cancellous) bone (Figure 1.1.1)[3]. Cortical bone is hard and dense and surrounds the marrow cavities[4]. Cortical bone being only 10% porous, allows room for only a small number of cells and blood vessels. Cortical bone is comprised of a structure of Haversian systems or osteons. At the center of each osteon is a Haversian canal which is lined by endosteum that contains blood vessels, nerves, and loose connective tissue. Each canal is surrounded by 4-20 concentric lamellae of collagen fibers[4]. The Haversian canals are round or oval in cross-section and generally run in a longitudinal direction. In the longitudinal direction, strength values reported are between 79-151 MPa in tension and 131-224 MPa in compression. The moduli range from 17-20 GPa for tension as well as compression[2]. The cortical surface of the bone is covered with a fibrous connective tissue called periosteum, which constitutes blood vessels, nerve fibers, osteoblasts, and osteoclasts. However, this tissue is absent in certain joints which are covered by articular cartilage[5].

Trabecular bone is spongy with a porosity reaching 50-90% and is found in the ribs, spine, and the ends of long bones[6]. It consists of an interconnected

network of small bone trusses aligned in the direction of loading stress[4]. The porous volume consists of vasculature and bone marrow, which provides little mechanical support compared to cortical bone. The strength and moduli of trabecular bone differ with density but are reported to be between 5-10 MPa and 50-100 MPa respectively (for tension as well as compression)[2].

The unique mechanical properties of bone are due to the interaction of its chemical components at the nanoscale level. Bone is comprised roughly of 60% inorganic material, 30% organic material and 10% water. Calcium phosphate crystals, primarily hydroxyapatite (HA) form the inorganic phase, while the organic phase consists mostly of collagen. Rigid HA crystals contribute to the compressive strength of the bone, while collagen fibers, capable of energy dissipation, provide tensile strength to bone.

1.1.3 Classification

Bones are commonly classified by their shape: long, short, flat, or irregular. Long bones are the primary target of injury. Long bones consist of three regions: the diaphysis, epiphysis, and epiphyseal plates. The diaphysis portion of the bone is comprised principally of cortical or compact bone. The epiphysis consists mainly of cancellous (or spongy) bone and is covered in articular cartilage which assists in low friction contact with other bones. The epiphyseal plate, or growth plate, is only active for growing bones and plays a role in bone lengthening through endochondral ossification. The epiphyseal plate ossifies when the bone reaches a mature size (typically between the ages of 20 and 30 years)[7].

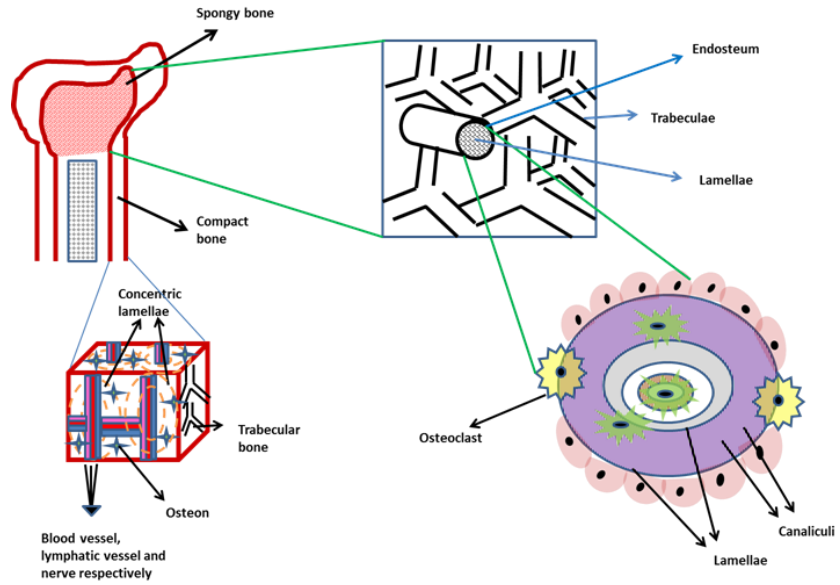

Figure 1.1.1: Trabecular and cortical bone

Table 1.1.1: Types of bone

Bone shape	Types
Long bones	Clavicles,humeri,radii,ulnae,metacarpals,femur,tibiae,fibulae,metatarsels,and phalanges
Short bones	Carpal and tarsal bones, patellae and sesamoid bones.
Flat bones	Skull,mandible,scapulae,sternum and ribs
Irregular bones	Vertebrae,sacrum,coccyx, and hyoid bones

1.1.4 Cellular components

The inorganic-organic composite structure of bone is made up of three types of cells. *Osteoblasts* :derived from MSCs and secrete collagenous proteins that help in the formation of the organic matrix of bone called osteoid[8]. Mature osteoblasts surrounded by osteoid stop secreting this matrix and become osteocytes, which play a crucial role in transduction of mechanical signals[1,6]. *Osteocytes*: are terminally differentiated osteoblasts and comprise 90-95% of all bones and persist for decades in the mineralized human bone. Osteocyte apoptosis, as observed by empty lacunae in aged bone is detrimental to bone structure. Figure 1.1.2 shows the mechanisms thought to lead to osteocyte formation from osteoblasts. The third cell type, called *Osteoclasts* are derived

from hematopoietic cells of the marrow and secrete acids and proteolytic enzymes which aid in dissolving mineral salts and digesting the organic bone matrix. Osteoblasts and osteoclasts turn over frequently but operate in a balanced way to remodel the bone tissue in response to various chemical, biological and mechanical factors[7,9].

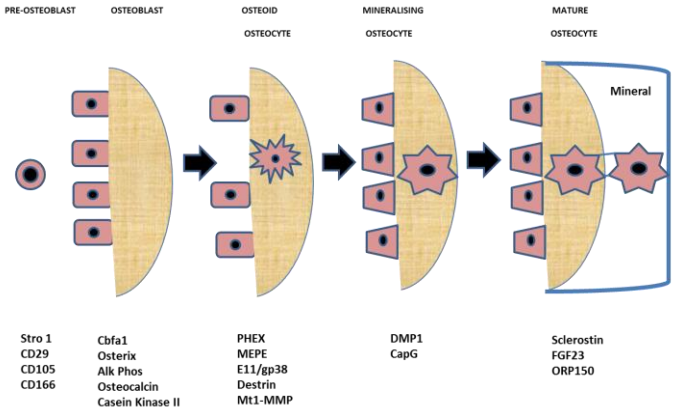

Figure 1.1.2: Stages in osteocyte differentiation along with markers at each stage of the differentiation process

1.2 The hematopoietic stem cell niche in the bone marrow

The bone marrow consists of both hematopoietic and nonhematopoietic stem cells and is encased within a region of vascularization. Cells of the metaphysis are in close proximity to the bone surface due to the protruding trabecular bone. The bone-bone marrow boundary is referred to as the endosteum and is lined by osteoblasts and osteoclasts. The invading arteries supply oxygen and nutrients and further extend into the sinusoids where they function as venous circulation. Sinusoids are dedicated venules that enable to and fro passage of cells during circulation. Therefore, the endosteum, due to the presence of arteries and sinusoids, is an especially vascular rich region.

Within the bone marrow, hematopoietic stem cells (HSCs) are mainly found beside sinusoids. HSCs maintenance is brought about by MSCs and endothelial cells which produce stem cell factor (SCF), C-X-C motif chemokine 12 (CXCL12) and potentially other bioactive factors. The HSC niche is further maintained by sympathetic nerves, non-myelinating Schwann

cells, macrophages, osteoclasts, Extracellular matrix (ECM), calcium, and osteoblasts.

1.2.1 Haematopoietic stem cells (HSCs)

Haematopoietic stem cells (HSCs) represent the best characterised of adult stem cells. Since the time they were first identified, technological advances have accomplished near homogenous purification of adult mouse HSCs. Functionally, HSCs are characterised by their potential to repopulate (for long term) all blood cell lineages and form CFUs in the spleen following transplantation to lethally irradiated recipients. This is known as long term repopulating (LTR) activity.

Functional HSCs are present in the subset of bone marrow cells that do not express the cell-surface markers that are usually present in lineage (Lin)-committed haematopoietic cells. However, they express high levels of stem-cell antigen 1 (SCA 1) and KIT. Therefore, this population of bone marrow cells that contain HSCs are referred to as LSK ($Lin^-SCA1^+KIT^+$). Further, only certain phenotypical HSCs possess LTR activity and are CD 34^-, fms-related tyrosine kinase 3 $(FLT)^-$ and CD 150^+ and these are classified as long-term(LT) HSCs. Short-term (ST) HSCs are CD 34^+FLT3^- and possess only limited self-renewal capacity. A study[10] has shown that 100 LSK HSCs are capable of providing protection from lethal irradiation. Many studies[11,12] however have shown reconstitution of all haematopoietic lineages from a single, purified HSC- proving that HSCs are true adult stem cells that are capable of multi lineage reconstitution and long-term self-renewal[13].

1.2.2 Role of osteoblasts in hematopoiesis

Osteoblasts play a fundamental role in hematopoiesis. A common mesenchymal stem cell is responsible for giving rise to all components of the Bone marrow stromal cell (BMSC) system that constitute the stem cell (SC) niche. Studies[14-16] have established that osteoblasts of the endosteum, along with their precursors are important in generating the SC niche and may contribute to the maintenance, proliferation, and differentiation of SCs.

Further, osteoblasts have been shown to express regulatory factors which most likely contribute to this process. Additionally, cell-cell interactions between osteoblasts and stem cells and other cell types could also influence the maintenance of the stem cell niche.

.

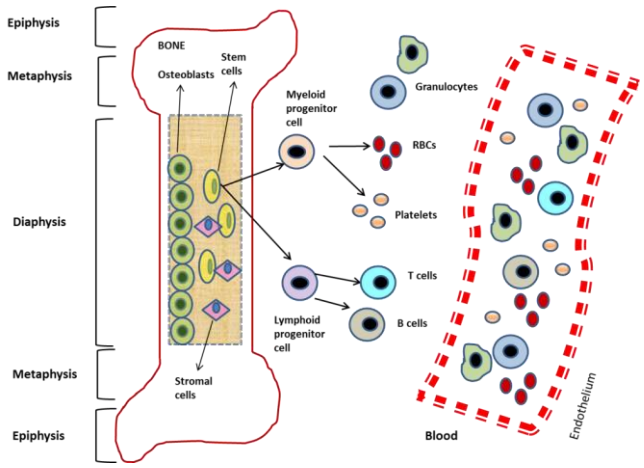

Figure 1.2.1: The hematopoietic stem cell niche in the Bone marrow

Studies[17-20] have shown that primary murine osteoblast cells, along with their transformed cell lines secrete a range of cytokines that control hematopoiesis. Hematopoietic stem cells receive instructive information from the bone and therefore, hematopoiesis is restricted to the bone. These include, among others, granulocyte-colony stimulating factor (G-CSF), macrophage colony-stimulating factor (M-CSF),IL(interleukin)-1, and IL-6. Primary human osteoblasts have been shown to express factors that are known to influence hematopoiesis:

G-CSF, CM-SCF,M-CSF,IL-1β,IL-6,IL-7, Leukaemia inhibitory factor (LIF), Osteoprotegerin (OPG), Receptor activator of nuclear factor kappa-B ligand (RANKL), stromal cell-derived factor-1 (SDF-1), Tumour necrosis factor alpha (TNF-α) and Vascular endothelial growth factor(VEGF) (Figure 1.2.2) .

Also, HSC-Ob adhesion has been shown to influence the creation of the niche. A variety of growth factors and adhesion factors are involved in HSC

homing and binding to the osteoblast-SC niche. This binding is reversible as receptor activation/expression, shedding and enzymatic cleavage can all cause HSC to be released[21-24] (Figure 1.2.3).

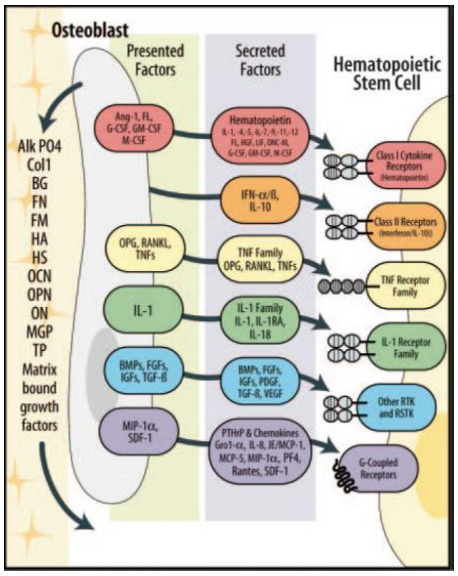

Figure 1.2.2: Osteoblasts secrete factors that control haematopoiesis. *Reprinted with permission from the American Journal of Hematology*

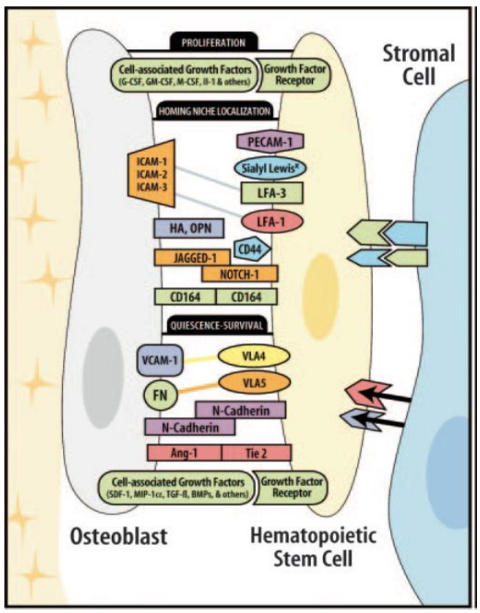

Figure 1.2.3: HSC-Ob crosstalk. *Reprinted with permission from the American Journal of Hematology.*

1.3 Bone modeling and remodeling

Bone modeling refers to the process wherein the general shape of bones changes under the influence of mechanical and physiological stresses. In

adults, bone remodeling is a more recurrent phenomenon than modeling. Bone remodeling refers to the restoration of bone in order to maintain its structural and physiological functions and prevent damage. Here, old bone is constantly replaced with new bone by the formation of protein-rich matrix. This matrix is subsequently mineralized. Bone remodeling starts before birth and persists until the death of the individual. Bone remodeling is orchestrated by osteoblasts and osteoclasts.

Bone remodeling consists of four phases: activation, resorption,reversal, and formation. During activation, monocyte-macrophage osteoclast precursors are activated from the circulation, which removes the endosteum. The endosteum consists of cells lining the bone surface. Mononuclear cells fuse with each other resulting in multinucleated preosteoclasts. These preosteoclasts then attach via RGD peptide linkages to proteins of the bone matrix and form sealing zones near sites of bone resorption below multinucleated osteoclasts.

The resorption process orchestrated by osteoclasts takes around 2-4 weeks. Osteoclast development and resorption are controlled by RANKL to OPG ratio, IL-1, IL-6, CSF, parathyroid hormone, 1, 25-dihydroxy vitamin D as well as calcitonin. Osteoclasts secrete H^+ ions into the bone resorption compartments giving rise to a low pH environment which enable mobilization of bone mineral. The organic bone matrix is digested by the release of an array of factors by osteoclasts: tartrate-resistant acid phosphatase, cathepsin K, matrix metalloproteinase 9 and gelatin, leading to the formation of Howship lacunae and Haversian canals in trabecular bone surface and cortical bone respectively. The last phase of resorption is performed by mononuclear cells after which multinuclear osteoclasts go through apoptosis.

During the reversal phase, preosteoblasts are recruited to the sites of resorption that also contain mononuclear cells, monocytes, and osteocytes released by bone matrix. Several factors secreted by the matrix: TGF-β, IGF-1, IGF-2, BMP, PDGF AND FGF are thought to play a role in reversal. Histomorphometry indicates that TGF-β concentration correlates with bone turnover, bone restricted ALP and osteocalcin. Further, the reversal phase is

thought to be influenced by a strain gradient in the lacunae with osteoclasts activated by reduced strain and osteoblasts activated by increased strain.

Bone formation occurs in approximately 4-6 months. Osteoblasts manufacture collagenous matrix and release membrane-bound matrix vesicles. These functions serve 2 purposes: (1) To produce calcium and phosphate which results in a mineralized matrix and (2) To enzymatically destroy pyrophosphate and proteoglycan matrix inhibitors. Approximately 50-70% osteoblasts go through apoptosis ,while the remaining grow into osteocytes and form an osteocyte network via gap junction connections to bone lining cells, osteoblasts as well as other osteocytes. Bone lining cells control entry and exit of mineral elements in the bone extracellular fluid, thereby acting as a bone blood barrier. Under the influence of parathyroid hormone and mechanical forces, these bone lining cells can again differentiate into osteoblasts. In advance of bone resorption, these bone lining cells detach from the endosteum and congregate into specific microenvironments that will act as the future bone remodeling sites. The net outcome of the bone remodeling process is the formation of a new osteon. The bone remodeling occurs in a similar manner in both cortical and trabecular bone. The features of the newly formed bone includes maintained bone strength, healthier revitalized new bone with conserved calcium and phosphate homeostasis[9,25-27] , (Figure 1.3.1).

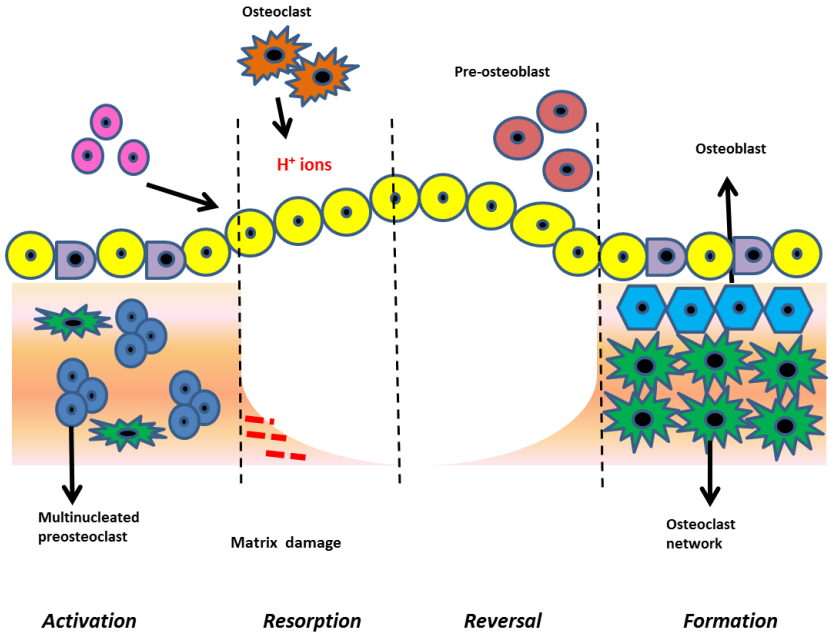

Figure 1.3.1: Different stages of Bone remodelling

1.4 Bone repair

The bone possesses an intrinsic capacity for regeneration in response to injury, as well as continuous remodeling during skeletal development and throughout adult life. Injury initiates a cascade of healing events that recapitulate some of the stages of embryonic bone formation and are described here in three biological stages: inflammation, repair, and remodeling. The initial acute inflammatory response involves the formation of a hematoma at the site of damaged blood vessels, with an increase in tissue volume. Neutrophils and macrophages arrive and ingest the cellular debris generated as a result of necrosis whilst releasing growth factors and cytokines. These biochemical signals encourage the migration and differentiation of MSCs from surrounding bone, marrow, and periosteum. Capillary growth and fibroblast activity generate fibrovascular granulation tissue at the injury site. Cartilage formation and vascularisation both occur simultaneously. The resulting increase in tissue size enables increased blood flow into this region. As chondrocyte differentiation advances with mineralisation of cartilage template and formation of osteoblast cells, a repair

blastema is produced. The relatively short inflammatory phase is followed by the repair phase, which begins as osteoblasts rapidly lay down new osteoid to form woven bone at the injury site which is now called bony callus. Progressively, the third phase of healing, remodeling, restores original tissue volume and reorganizes collagen fibers and forms mechanically strong bone with the reestablishment of marrow and haematopoiesis[7,28-30] (Figure 1.4.1).In the clinical setting, the majority of bone fractures heal without the formation of a scar tissue, and bone regeneration occurs with its pre-existing properties mostly restored. However, there are cases of fracture healing in which bone regeneration is impaired; for example, up to 13% of fractures occurring in the tibia are associated with delayed union or non-union[31]. In addition, there are other conditions (

Table1.4.1) in orthopedic surgery and in oral and maxillofacial surgery in which bone regeneration is required in large quantities (beyond the normal potential for self-healing), such as for skeletal reconstruction of large bone defects created due to trauma, infection, tumor resection and skeletal abnormalities, or cases in which the regenerative process is compromised, including avascular necrosis and osteoporosis[7,32].

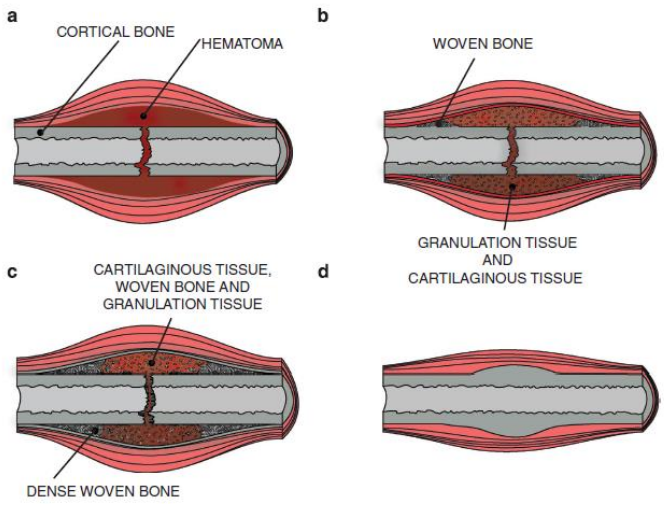

Figure 1.4.1: Schematic representing the four classical stages of fracture healing. *Reprinted with permission from Nature Publishing group.*

Table1.4.1: Overview of select bone disorders (*Source Medscape: http://www.medscape.com/)*

Disease name	Brief Description	Pathology
Avascular necrosis	Death of cells in bone due to interruption of blood supply	Aberrant blood supply, vascular coagulation and lipid metabolism, cell death.
Osteoporosis	Reduction in bone mass and architectural integrity of bone leading to reduced bone strength	Estrogen deficiency, Calcium and Vitamin deficiency, Aging and osteoporotic fractures.
Osteopetrosis	Characterised by the failure of osteoclasts to perform their bone resorption function leading to compromised bone modeling and remodeling.	Osteoclast dysfunctions, Underlying mutations that hinder with acidification at the osteoclast site.
Osteomyelitis	Inflammation of bone triggered by microorganism infection.	Trauma, Host immune status, underlying diseases, Type and vascularity of the bone
Metastatic bone disease	Occurs when cancer spreads from its original disease site to bone	Tumours produce proteolytic enzymes that breakdown basement membrane and enable them to migrate to surrounding sites, breast carcinoma cells and oat cell tumors secrete parathyroid hormone-related peptide (PTHrP) which stimulate osteoclastic bone resorption

SECTION B: AVASCULAR NECROSIS (AVN)

Avascular necrosis (AVN) also referred to as osteonecrosis of bone, is a severe incapacitating condition that occurs due to compromised blood supply to bone. It results in cell death within the bone and bone marrow and ultimately leads to bone collapse (Figure 1.7.2). Approximately 20,000 – 30,000 new cases of the disease are diagnosed each year in the USA and the condition accounts for 10% of all total hip replacement surgeries. AVN primarily affects bones with a single terminal vascular supply, which makes them susceptible to limited blood flow. These include the femoral head, carpals, talus, and humerus. The debilitating condition eventually leads to arthritis. AVN typically affects men and women between the ages of 25 and 50. A wide range of clinical and preclinical studies have shown promising results in treating osteonecrosis using Regenerative Medicine-based principles. The emerging field of Regenerative medicine and tissue

engineering promises therapies for improved healing of damaged tissue significantly eliminating the risks, limitations and drawbacks of current treatment options.[28,31,33-39].

1.5 Epidemiology

As stated previously, AVN affects people in the younger age group with Hungerford and Jones (2004) in the United Sates reporting that around 25% of patients in their institution are below the age of 25.They propose that if 10% of THA procedures are due to AVN, then the United States would have 10,000-20,000 AVN cases annually[40] . Further, reports from the 2007 Australian, Canadian and Swedish national registries indicate that around 2.8-6% of THAs performed in these countries are due to an AVN diagnosis. A lower incidence of AVN was reportedly the 2009 National joint registry for England, Wales and Northern Ireland with a 2% incidence rate in the year 2008 (Reference: National Joint Registry for England and Wales, 6th Annual Report, 2009). Nevertheless, age wise pairing of cases requiring THA indicated an 18% incidence rate in patients aged 30-39 and a 7% incidence rate in patients aged 40-49. Nordic Arthroplasty Register Association report analysis indicates that 2.2% of THR's executed in the years 1995-2011 were attributed to AVN. Fukushima *et al*. surveyed the incidence of AVN in the year 2005 in Japan. It was found that 11,400 patients were undergoing treatment for idiopathic osteonecrosis. The disease affected 27% males and 18% females in their 40s. Steroid administration (51%) and Alcoholism (31%) were thought to be the main reasons for disease initiation[41]. Kang *et al*., reported that AVN was attributed to 50-60% of total THA procedures in the years 2002-2006 in Korea, with an increasing trend:20.53 occurrences per 100,000 people in 2002 and 37.96 occurrences per 100,000 people in 2006[42]. India and Thailand lack data for AVN incidence due to the absence of national joint registries in these countries. Lai *et al*., using data obtained from the national health insurance databases (1996-2004) found that 46% of all THAs were due to AVN (79% men, Average age=50 years)[43].They suggest that these statistics could also be used to throw light on disease incidence in China, many of the subjects in the survey being Han Chinese. Tien *et al*. [32] reported

similar disease numbers in Taiwan and state increased disease incidence overtime.

Although the exact reason is unknown, abundant use of steroids probably accounts for the higher incidence of AVN in Asian populations. Research using Taiwanese pedigree subjects has shown that mutations in Type II collagen gene in chromosome 12q13 were linked to the onset of AVN.[44-46] Similar susceptibility was reported in a Japanese family[47] and in the Chinese population[48]. COL 2A1 mutations disrupt an integral gly-X-y triple helix repeat by changing an amino acid. Abnormally large collagen fibrils have been reported in the epiphyseal cartilage of patients with AVN of the femoral head[49]. Further, it has been reported that this mutation is responsible for the abnormal pathology in the hip joint, which results in hip osteoarthritis, AVN of the femoral head and Leg-Calve-Perthes disease with an increase in age. Further, a meta-analysis conducted by Lin *et al*., indicates that VEGF-634G/C polymorphism significantly predisposed the Asian population to AVN[50] (Figure 1.5.1)

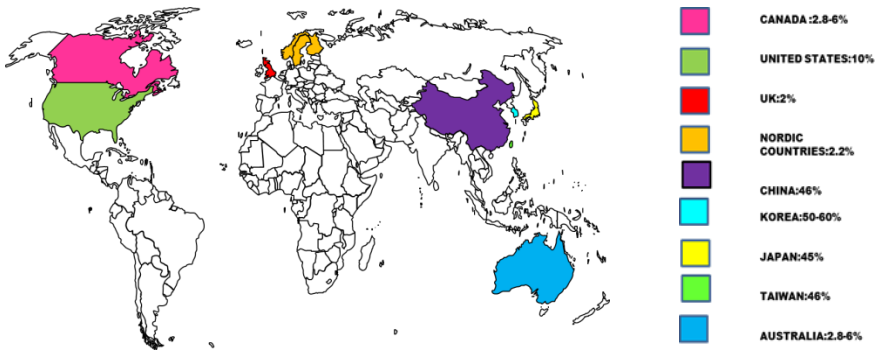

Figure 1.5.1: Percentage of THA's attributed to AVN across the world

1.6 Blood supply to the femoral head and its clinical importance

Bone is a highly vascular organ and cross-talk between blood vessels and bone cells is critical to maintaining its structure and during repair. The role of the vasculature in bone formation is well documented. As early as the 18th century, Albrecht von Haller in his book Experimentorum de ossium formatione stated that “the origin of the bone is the artery carrying the blood and in it the mineral elements”[51] .The role of blood vessels as key players in the bone formation process was identified in 1763, around the same time Hunter reiterated this hypothesis[52]. However, it was following a publication by Trueta in 1963 who proposed the presence of a ‘vascular stimulating factor’ that their vital role in bone formation was brought to attention[53]. In multiple studies, inhibition of angiogenesis in animal models has shown fibrous tissue formation[54-58]. Apart from nutrient transport and waste product removal, the vasculature plays critical roles in bone formation, remodeling and healing. The vasculature is important for both intramembranous and endochondral ossification. Endothelial cells in the vasculature secrete growth factors that direct the behaviour and function of various cell types including osteoblasts and osteoclasts. Consequently, angiogenesis occurs before osteogenesis *in vivo* and is also required for formation of bone.

1.7 Anatomy of blood supply to the femoral head

The lateral epiphyseal arteries enter the femoral head via the posterosuperior segment. Approximately, 80% of the femoral head blood supply comes from these arteries. In the cortex, these arteries are located medially and anteriorly near the anterosuperior region of the femoral head[30,59] (Figure 1.7.1). Blockage of these arteries could lead to AVN (Figure 1.7.2).

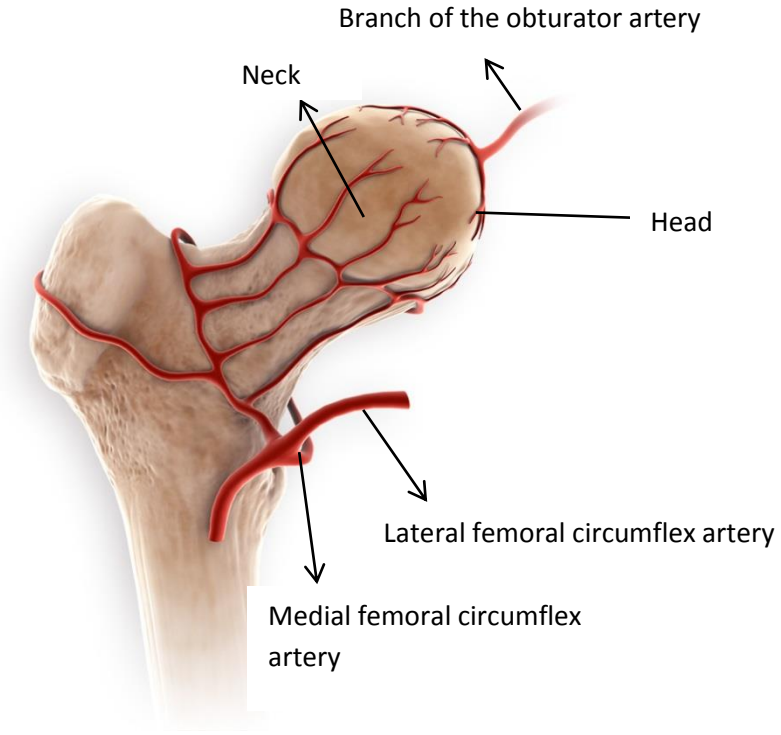

Figure 1.7.1: Blood supply to the femoral head

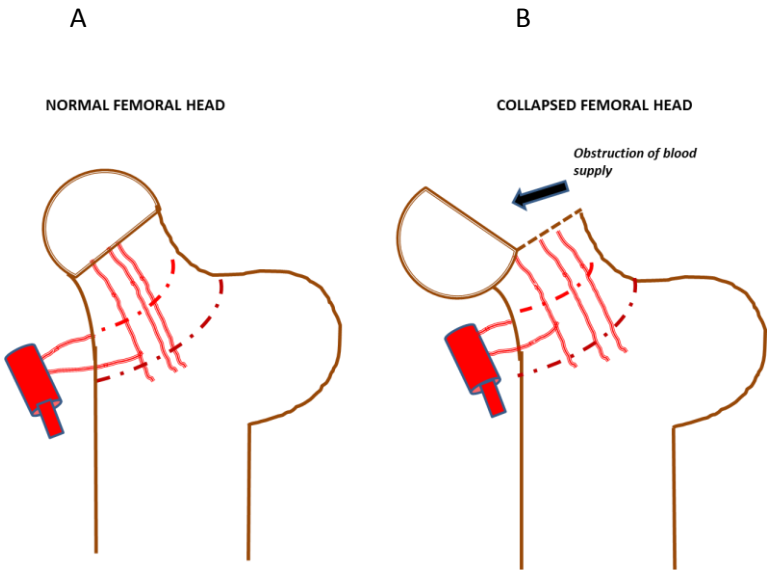

Figure 1.7.2: Schematic showing normal femoral head (A) and avascular necrotic collapsed femoral head (B).

1.8 Staging systems

Arlet-Ficat was the first system introduced for staging osteonecrosis. This system is based on radiographic changes to the femoral head (Figure 1.8.1).

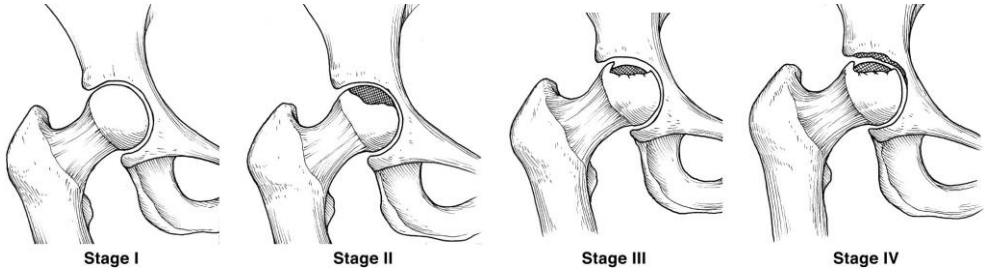

Figure 1.8.1: Ficat classification of the four radiographic stages of hip osteonecrosis. Stage I = normal radiographic appearance. Stage II =transition phase. Stage III = sequestrum with subchondral collapse. Stage IV = decreased joint space and the collapse of the femoral head. *Reprinted with permission from AAOS.*

The introduction of magnetic resonance imaging (MRI) techniques has given rise to the Steinberg or University of Pennsylvania osteonecrosis classification system which helps distinguish subchondral collapse from femoral head articular cartilage collapse. Association Research Circulation Osseous (ARCO) staging system, which was introduced in 1992, is another frequently used classification system utilizing MRI for disease staging[60].

1.9 Conventional Treatment options for Osteonecrosis

Non- operative treatment

Small lesions have the potential to heal spontaneously and therefore it may be sufficient for such cases to be kept under observation. In one study, 3 out of 13 asymptomatic hips in patients with very small lesions healed[61]. Another study on 40 patients with small lesions reported that 88% of the hips had become asymptomatic while 73 % collapsed at a follow up period of 10 years. Therefore , the authors of the study advice including a long term follow-up even in cases of very small lesions[62].

Non weight bearing

Non weight bearing has been suggested as an option to slow progression of the disease.However, a study on patients subjected to limited weight bearing showed no improvement in majority of the patients at 34 months of follow-up. Hence non-weight bearing is not an effective treatment option for managing ON[63].

Treatment options for Osteonecrosis will depend on the underlying cause (Table **1.9.1**).If the condition is diagnosed early, and the underlying cause is known, taking lipid-lowering drugs in cases of fat embolism and anticoagulants to treat coagulation abnormalities may help. Non-surgical treatment of Osteonecrosis generally slows the progression of Osteonecrosis, but most people require surgery. (Source: National Institutes of Arthritis and Musculoskeletal and Skin Diseases).

Table 1.9.1: Causes of AVN

Traumatic causes	Displaced fracture Transcervical fracture Compression fractures
Non-Traumatic causes	Corticosteroid use Alcoholism Sickle cell disease Gaucher's disease Coagulation abnormalities Caisson's disease Haemoglobinopathies

Surgical treatment options include

1. Core decompression:

Core decompression is considered the gold standard for treatment of osteonecrosis.This was first described by Ficat and arlet in 1964 and is conducted if AVN is in the early stage. The rationale behind the use of the core decompression procedure is to reduce the intraosseous pressure (increased pressure for example, can be caused due to fat infiltration as a result of steroid therapy[64]) in the femoral head and thereby provide a channel for the flow of blood enabling integration of healthy bone in the necrotic area. As a consequence , the pain experienced in the hip is ameliorated[65].

However , there is a lot of discrepancy in the success rate of this procedure. Most positive outcomes are achieved when treating osteonecrosis at its early stage (Stage I and II Ficat classification of disease)[66]. Ficat *et al.,* reported a clinical success rate of 89.5 %[67] with core decompression performed on 156

hips at stage I and II AVN., while Chan *et al.,* reported an 88% improvement in this condition while treating 32 hips with core decompression[68]. Mont *et al.,* examined 2025 hips affected with osteonecrosis and reported that 71 % of core decompression treated patients had positive outcomes in contrast to 34.5 % of patients with positive results, treated non surgically[65].

However , the literature is inconsistent on the success rate of the core decompression procedure . Smith *et al*. using a modified version of the Ficat and Arlet classification , reported a failure rate of 16% for Stage I , 53 % for Stage II A , 80% for Stage II B and 100 % Stage III[69] . Koo *et al.* conducted a randomised study on 37 hips. At a follow-up period of 2 years, 78 % of core decompression treated hips and 79 % non-operated hips progressed to collapse[70]. Inconsistent success rate of this procedure could be due to differences in stage of AVN, follow up period and sample size among research groups.

2. Nonvascularised Bone Grafting

This procedure involves removal of the necrotic bone by decompression of the necrotic lesion. A bone graft is then introduced to the femoral head via a core tract, a window or through a trapdoor[71]. However, use of autografts are limited by problems caused by donor-site morbidity and limited availability. Further, use of allografts face serious constraints due to immunocompatibility, necessitating lifelong treatment with immunosuppressives.

3. Free vascularized Fibular grafts

This technique is an extension of the above procedure except that a segment of bone, as well as the blood supply, is taken from the small bone in the leg (fibula) of the patient to enable vascularization and osteogenesis at the necrotic area[72]. However, this procedure involves considerable surgery and may present problems when harvesting the fibula. Additionally, using vascularized bone grafting may vary the bone volume in the femoral head making a future necessary hip replacement procedure difficult.

4. Osteotomy

This procedure may be used in special cases. Here, the bone near the necrotic area is rotated, so that the other portion that is not affected by AVN becomes the new weight-bearing area[73]. This procedure allows for decreased hypertension and intramedullary pressure in addition to improved mechanical stability. However, this treatment option is limited because of the complex surgery involved. Additionally, the outcomes of this procedure are inconsistent and complications arise if a later total hip surgery is carried out.

5. Femoral head resurfacing

A metal head is placed over the original femoral head in order to delay disease progression. However, over a period of time total femoral head replacement will need to be carried out [74].

6. Total hip arthroplasty – Total hip reconstruction had the highest success rate of all the treatment options discussed above. Grino and Steinberg have reported a high success rate for this procedure over a period of 10 years. However, THA is used as an end stage treatment option because of removal of large amounts of host bone. Additionally, it limits subsequent operative procedures[75],[73].

Table 1.9.2 summarises the drawbacks of the above mentioned treatment options.

Table 1.9.2: Drawbacks of current treatment procedures

Procedure	Shortcomings
Core Decompression	Inconsistent success rate
Nonvascularised bone grafting	Donor site morbidity, limited availability of allografts,immunocompatible
Free vascularised fibular grafts	Highly invasive procedure, potentially necessitating Total hip replacement in the future
Osteotomy	Invasive, inconsistent outcomes, susceptible to post-op complications
Femoral head resurfacing	Total hip replacement may need to be carried out eventually
Total hip arthroplasty	Only an end stage treatment option due to a large amount of tissue loss involved in this procedure.

SECTION C: BIOMATERIALS FOR BONE TISSUE ENGINEERING

Bone is the second most transplanted tissue following blood. Conventional treatment options to treat tissue or organ loss include transplantation of tissues and organs (by using Autografts, Allografts or Xenografts) or the use of mechanical assist devices. Although these traditional approaches have rescued countless patients and have improved a significant number of lives, they suffer from many serious limitations. Autografts, although they possess the best clinical outcome, are limited by problems caused by donor-site morbidity and limited availability. Allografts and Xenografts face serious constraints due to immunocompatibility, which makes it necessary for the patients to undergo lifelong treatment with immunosuppressives. These approaches also lead to higher risk of infection, viral disease transmission, tumor development and many other associated side effects. The use of mechanical devices also suffers from critical problems brought about by thrombo- embolisation, associated infection, and limited durability. The transplant option is further limited by the shortage of donor tissues and organs[76].

The rapidly evolving field of tissue engineering aims at solving these problems by engineering living tissues *in vitro* by using cultured cells that are coaxed to grow in a three-dimensional organization (provided by a scaffolding material) with a view of restoring functionality to the organ. Tissue Engineering as defined by Langer and Vacanti is an “interdisciplinary field of research that applies the principles of engineering and the life sciences towards the development of biological substitutes that restore, maintain, or improve tissue function”[7].

1.10 Biomaterials for bone regeneration

Given the significant clinical need, the demand for orthopedic biomaterials is rising significantly. The different biomaterials evaluated for bone repair comprise ceramics, bioactive glass, natural and synthetic polymers and a combination of these.

Osteoinductivity of a biomaterial refers to its capacity to facilitate bone formation spontaneously in the absence of osteoinductive factors. The

osteoinductivity is usually verified by implanting the material into non-osseous sites (subcutaneously implantation or into intramuscular sites) and observe the formation of ectopic bone. In 1965, Urist first demonstrated the formation of ectopic bone in muscles of different animals by demineralised bone matrix that has been decalcified by hydrochloric acid[77]. Bone formation was enabled by BMPs present in the matrix. The inconsistent osteoinductivity observed in various calcium phosphate materials is attributed to differences in composition, architecture, pore size and porosity of these materials. Table 1.10.1 gives an overview of ideal characteristics of these parameters.

Functional inorganic materials

Tricalcium phosphate, HA, bioactive glasses and their combinations are popular due to their similarity to the mineral phase of bone. Bioactive glass (silica glass comprising Ca and P) can produce a hydroxycarbonate apatite layer and can bond to tissue, when in contact with the biological fluid. These materials can also be modified to deliver Si at physiological levels capable of activating osteogenic signaling pathways[78-81]. The resorption rate of bioactive glass can be controlled by using them in combination with HA. However, other calcium phosphates possess better resorption capacities compared to HA but lesser mechanical strength. The inherent brittleness of ceramics is a major drawback when used for load- bearing applications.

Polymers

Natural polymers such as collagen and HA are good candidates for Tissue Engineering applications because they promote cellular attachment and chemotaxis. However, they possess several limitations such as immunogenicity, the risk of disease transmission and poor mechanical properties. This problem can be overcome by use of synthetic polymers such as polymerases, PLA, PGA, PLA and PGA co-polymers (PLGA) and polycaprolactone which can be fabricated using a range of available techniques[82-87]. Hydrogels such as polyethylene glycol and alginate-based are also attractive candidates that offer a three-dimensional environment with high water content[88-90]. Additionally, these materials can be functionalised and cell encapsulation and delivery of these materials are comparatively easy[91,92].

Composite materials

Composite materials combine inorganic and organic components taking advantage of the polymer toughness and the compressive strength of the inorganic phase. The alkaline nature of the inorganic component neutralises the acidic degradability of polymers like PLA[93,94]. Additionally, it is the belief that nano-sized inorganic components function better than their micro-sized counterparts. As a consequence, there is a growing interest in HA-collagen nanocomposites[95-97].

Table 1.10.1: Ideal scaffold properties[98,99]

Property	Purpose	Ideal scaffolds characteristics
Biomechanical property	To mimic mechanical properties of native bone to enable load bearing and provide mechanical signals to aid in differentiation of the cohabiting cells	Mechanical properties similar to bone (ideally). Young's modulus: Cortical bone:15-20GPa Cancellous bone: 100-200GPa.Due to high variability in mechanical properties formulation of the scaffold is difficult.
Pore size and porosity	Large pore sizes enable cell migration and vascular infiltration whereas smaller pore sizes provide the required area for cell attachment.	Optimal pore sizes: 5µm-vascular invasion; 5-15µm-fibroblast migration; 150-250µm-chondrocytes; 200-350µm-osteoblasts
Biodegradability	The scaffold should degrade at a rate proportional to new bone formation in order to create space for a fresh bone tissue.	Ideally 9 months for spinal fusion; 3-6 months for cranio-maxillofacial procedures.
Biocompatibility	To create a non-toxic environment that does not hamper normal cell activities	An ideal bone scaffold should be osteoconductive and osteoinductive.

SECTION D: CELLULAR THERAPY

1.11 Osteogenic and angiogenic cells

Bone tissue and periosteal derived cells

Primary osteogenic cells can be isolated from bone tissue and periosteal tissue. Studies have indicated expression of a range of osteogenic markers in

these cells such as increased ALP activity, expression of OP, BSP, OC and calcium deposition under osteogenic conditions[100,101].

Embryonic stem cells and induced pluripotent stem cells

ESC's have the potential to give rise to any tissue within the body and have the capacity for indefinite proliferation *in vitro*. Thomson and colleagues (1998) were the first to isolate and culture ESCs successfully. With respect to bone repair applications, ESC's could serve as a source from which osteoblasts, osteoclasts, nerve cells etc. can be derived.[102,103]. Cells with osteogenic potential have been detected in mixed progenitor cell population within embryoid bodies in 4-5 days of culture[103,104] as well as co-cultures with primary bone and periodontal ligament cells[105,106]. Additionally, MSCs derived from ESCs (MSC-like progenitors) have been induced towards the osteogenic lineage.[102,107-110].

Pioneering experiments by Takahashi and Yamanaka have given rise to the induced pluripotent (iPSC) technology[111]. The objective of the study was to genetically express a variety of transcription factors (that are highly expressed in pluripotent cells) with the hope that they will switch back to a pluripotent cells. After selection of the pluripotent population, four highly pluripotent factors were shortlisted-Klf 4, Sox 2, Oct 4, and Myc C- known as the "Yamanaka factors". Finally, these induced pluripotent cells were shown to be comparable to their embryonic stem cell counterparts in their capacity to differentiate in teratoma formation assays as well as giving rise to tissues in chimeric mice upon blastocyst injections.

Many protocols have been devised to differentiate iPSC cells into multiple cell types *in vitro*. These protocols are mostly based on ESC differentiate protocols. Osteogenic differentiation of ESC or iPSC cells is similar to MSC differentiation protocols which employ medium containing fetal bovine serum, ascorbic acid, β-glycerophospahate, and dexamethasone. Additionally, enhancing supplements such as BMP 2/4, have been used to differentiate stem cells into the osteogenic lineage. Additionally, Feng *et al*[112] show that a combination of TGF-β1, TGF-β3 and retinoic acid were more efficient in iPSC differentiate to MSC like cells which in turn, could be differentiated into

osteoblasts. Further, exogenous overexpression of osteogenic transcription factors such as Runx 2 have shown to enhance osteogenic differentiation of mouse iPSC cells. Other gene expression methods include employing micro RNAs in regulation of osteogenic differentiation. Studies have also shown the beneficial effects of scaffolds such as polyethersulfone (PES) nanofibrous scaffolds and gelatin scaffolds on iPSC osteoblast differentiation.

Mesenchymal stem cells

Alexander Friedenstein was the first to show the osteocyte differentiation capacity of fibroblastic cells from the stromal compartment of the Bone marrow[113]. These cells were capable of adhering to plastic and establish colony forming units fibroblastic (CFU-F). Building upon these early observations, a number of investigators explored the proliferative and phenotypic characteristics of CFU-F[114-116]. MSC's are traditionally derived from the bone marrow[117] although they have been derived from a number of other mostly connective tissues[118], for example adipose tissue [119], periosteum[101,120,121] and synovial membrane[122].

The widespread distribution of MSCs led to the hypothesis that MSCs could be derivatives from perivascular tissue environment. The isolation of colony progenitor populations of cells from blood vessels of numerous human tissues indicated expression of markers and multipotential differentiation capacities characteristic of MSCs. Therefore it was suggested that perivascular cells are precursors to MSCs with Arnold Caplan endorsing the viewpoint that all MSCs are pericytes[123].

The bone marrow comprises the hematopoietic, endothelial and stromal cells systems. The stromal cell system refers to nonhematopoietic cells of mesenchymal origin or mesenchymal stem cells possessing the capacity for self-renewal and differentiation into different connective tissue lineages[124,125]; inclusive of the osteogenic lineage[126].

Mesenchymal stem cells (MSCs) offer great promise as a possible cell source for cell-based therapies[127] because of their ability to self-renew and differentiate into multiple mesenchymal cell types that include osteoblasts,

chondrocytes, and adipocytes[128,129]. Hung *et al*. showed that a high amount of angiogenic factors and anti-apoptotic factors like IL-6, VEGF and MCP-1 were present in MSC conditioned medium. These factors prevented cell death of endothelial cells under hypoxia and also promoted capillary sprouting *in vitro*. Additionally, MSCs provide ECM components that act as substrates for endothelial cells[130]. Further, as MSCs transition back to pericytes located on blood vessels, they play a role in stabilising the developing vasculature *in vitro* and *in vivo*. MSCs secrete a wide range of therapeutic growth factors, cytokines, and chemokines which serve important functions during injury[131,132].

A further clinical advantage of MSCs is that they have a distinct immunophenotype characterized by the absence of HLA Class II expression and the low expression of co-stimulatory molecules. MSCs also possess the capacity for immunomodulation and suppress mixed lymphocyte reactions (MLRs) involving autologous or allogeneic T cells or dendritic cells. MSCs also inhibit T-cell proliferation and inhibit both naïve and memory T-cell responses[133,134].

Endothelial progenitor cells

Progenitor cells are primitive bone marrow (BM) cells with the potential to proliferate, migrate, and differentiate into various mature cell types. Specifically, Endothelial Progenitor cells have the capacity to mature into the cells that line the lumen of blood vessels. EPCs were first discovered in the adult circulation when mononuclear blood cells from healthy human volunteers were observed to acquire an endothelial cell–like phenotype *in vitro* and to incorporate into capillaries *in vivo*. These putative EPCs were characterized based on their expression of CD34 and vascular endothelial growth factor receptor-2 (VEGFR-2), two antigens shared by embryonic endothelial progenitors, and hematopoietic stem cells (HSCs). Studies performed subsequently[135-137] confirmed that CD 34 cells isolated from bone marrow or umbilical cord blood also had the capacity to differentiate into mature endothelial cells. However, both CD 34 and VEGFR-2 are expressed

by mature endothelial cells. Therefore, a search for unique markers was required.

EPCs are now identified through the expression of three cell surface markers. They are located primarily in the bone marrow and can be mobilized into the peripheral blood where they represent between 0.01% and 0.0001% of mononuclear cells in healthy subjects.

In culture, two distinct types of EPCs are seen. The first type, referred to as early EPCs appears after 3–5 days, is formed by spindle-shaped cells and dies after 4 weeks. The second type, called late EPCs or outgrowth endothelial cells (OECs), appears after 2–3 weeks, forms a cobblestone monolayer and remains viable for about 12 weeks. Early EPCs, which are derived from CD14+ MNCs, are myeloid cells and possess endothelial properties like stimulation of neovascularization by paracrine factors but do not get incorporated into the endothelial lining. OECs are derived from CD14- MNCs, have properties comparable to mature ECs but a higher proliferative ability and are incorporated into the endothelial lining of new blood vessels.

EPCs seem to have an enhanced ability to be incorporated into newly forming microvasculature and this property makes them therapeutically desirable for tissue engineering applications. Though their concentration in blood is low, they have been detected in the newly formed vasculature and contribute to about 5%–35% of the endothelial cells in new capillaries. In fact, EPCs are mobilized by tissue ischemia and cytokines from the bone marrow into peripheral blood and migrate to regions of neovascularization, where they then differentiate into mature endothelial cells and encourage vasculogenesis. EPCs have been shown to develop a favorable environment for fracture healing via angiogenesis and osteogenesis, through two mechanisms: One is through the osteogenic and endothelial differentiation potential of CD34+ cells, while the other one is the paracrine effect of CD34+ cells, brought about by the secretion of VEGF. These properties make EPCs especially advantageous for use in bone tissue engineering applications[138,139].

SECTION E: BIOACTIVE FACTORS AND GENE THERAPY

Delivery of pro-osteogenic genes has been explored in a number of studies as a potential therapy for bone healing[140,141]. Gene delivery offers a number of advantages over protein delivery. Firstly, it offers a more regulated delivery at the region of interest; the gene is processed in an authentic manner and may most probably need to be delivered just once. To this end, adenoviral, lentiviral and retroviral-derived vectors and non-viral vectors have been utilised. Mesenchymal stem cells are the choice for genetic modification strategies in bone repair because of their ability to differentiate into osteoblasts and capacity to home upon implantation[142,143].

Modes of gene transfer

1.12 Viral and non-viral gene transfer

In viral gene transfer, the inherent property of virus to transfer their genetic constituents into cells is exploited. When used for gene therapy, pathogenic portions of the viral genome are removed from the viral genome while keeping its ability to infect, intact. The cDNA of therapeutic genes are then cloned into these viral genomes to create a recombinant viral vector. Viral vectors, a particularly non-integrating vector such as retrovirus or lentivirus are employed when long-term expression of the transgene is the goal. Additionally, non-integrating vectors can be used in non-dividing cells as well. First generation adenoviruses express antigenic portions of the virus which would elicit an immune response resulting in eradication of the transduced cell population. However, this may not be a hindrance if long-term transgene expression is not required as the transduced cells would die eventually. Adeno-associated viruses are considered to be the safest option because their wild-type counterparts are not disease causing and are incapable of replication without a helper virus. However, this virus needs to be used at high multiplicities of infection and its production at a clinical grade remains a challenge, not to mention the associated increases in cost. Retrovirus can transduce dividing cells effectively; however, they cause insertional mutagenesis. The same problem is encountered with lentivirus but with the

development of non-integrating lentiviruses, they have come to be an excellent option given their superior transduction efficiency and capacity to transduce non-dividing cells. The safety of using adenovirus has been challenged by the death of a patient in a gene therapy trial. Although they do not pose a problem when used in moderate doses, immunogenicity, and the resulting inflammatory response are the major roadblocks associated with the use of adenovirus.

Due to the safety issues and high costs, non-viral vectors have been considered as an alternative. The efficiency of gene transfer, in this case, can be attempted to be enhanced by the use of DNA with a liposome or any polymer carrier. Gene transfer can also be enhanced by physical methods of DNA delivery such as electroporation or sonication. However, gene transfer efficiency using non-viral methods is extremely ineffective compared to viral gene transfer methods[140].

1.13 Example studies using growth factor and gene therapy approaches for Bone Repair

The most common growth factors used for tissue engineering applications are VEGF, FGF, and PDGF. VEGF, generally regarded as the key angiogenic factor, stimulates endothelial cells to migrate, proliferate, and differentiate. VEGF has been used to induce angiogenesis in a number of experiments. However, when this factor is used in isolation, vessels are most often unstable, leaky and hemorrhagic, making it necessary to use a more complex signaling strategy. FGF, like VEGF, is also known for its ability to induce the formation of the microvasculature. FGF, which represents a family of over 20 molecules, was the first angiogenic growth factor to be discovered. FGF 2 or basic FGF is the chief molecule involved in the initiation of angiogenesis. It also aids in the migration and proliferation of smooth muscle cells. Endothelial cells are stimulated to proliferate and drive capillary formation, following the release of FGF 2 from macrophages. While FGF and VEGF initiate angiogenesis, PDGFs are invaded in later stages of vessel formation which involves stabilization and remodeling. PDGF is the key protein secreted by platelets and forms homo and heterodimers of α and β polypeptide chains. Two receptors for PDGF exist and their ligand-induced dimerization initiates

receptor autophosphorylation, which in turn has widespread effects throughout the body, especially in the development of kidney, lungs and CNS and blood vessels. As regards the vascular system, endothelial cells not only produce PDGF but also display receptors for PDGF on their cell surface[144].

A range of growth factors produced by osteogenic cells, platelets, and inflammatory cells – including bone morphogenetic proteins (BMPs) , insulin-like growth factor-1 and -2, transforming growth factor-β1 (TGF-β1), platelet-derived growth factor, and fibroblast growth factor-2 –contribute importantly to bone healing. The bone matrix acts as a reservoir for these growth factors, which get activated during matrix resorption by matrix metalloproteases.

Furthermore, the acidic environment that develops during the inflammatory process leads to activation of latent growth factors; which assist in chemo-attraction, migration, proliferation, and differentiation of MSCs into osteoblasts or chondroblasts. All of these functions are driven by complex interactions between growth factors and other cytokines and are influenced by multiple regulatory factors. Thus, the use of osteogenic growth or differentiation factors for joint-preserving treatment of AVN is a promising approach[34].

SECTION F: THE EPHRINS

The erythropoietin-producing hepatocellular carcinoma (Eph) receptors and their corresponding cell surface ligands are known collectively as the “Ephrins”. They possess 14 receptors and 8 ligands, making them the largest of the receptor tyrosine kinase families. The critical role of Ephrin B2 as a promoter of osteogenesis and angiogenesis has been researched in a number of studies. Ephrin B2 and its receptor Eph B4 are known to play a critical functional role in bone remodeling.

Bone homeostasis is maintained by activities of osteoclasts that promote bone degradation and osteoblasts that promote bone degradation and osteoblasts that promote bone formation. A landmark study by Zhou *et al*., made use of gain and loss of function studies as well as osteoclast-osteoblast cocultures to demonstrate that reverse signaling from Eph B4 in osteoblasts

to Ephrin B2 in osteoclasts inhibits osteoclast differentiation[145]. Additionally, they demonstrated that the inhibitory signal is mediated through interaction with PDZ domain proteins, making these proteins promising candidates for drug targeting. Furthermore, they demonstrate that signaling between Ephrin B2 and Eph B4 promotes osteoblast differentiation and this process may be inhibited by Rho A inactivation[146-148] (Figure 1.13.1).

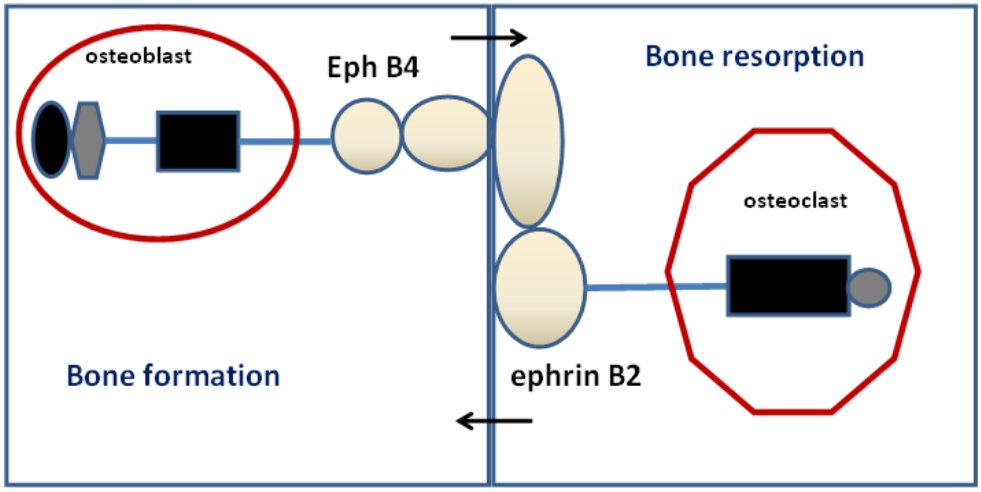

Figure 1.13.1: Schematic showing Ephrin B2-Eph B4 bidirectional signalling

With regards to the role of Ephrin B2 in angiogenesis, in the blood vasculature, Ephrin B2 is expressed on arterial angioblasts, endothelial cells (ECs) and perivascular mesenchymal cells, whereas one of its binding partners, the receptor Eph B4, is found specifically on venous ECs. Targeted inactivation of either Eph B4 or Ephrin B2 genes in mice leads to failure of embryonic vessel formation and early lethality, demonstrating their critical role during physiologic angiogenesis.

Groups of Swamiphak *et al.* and Wang *et al*. have shown the crucial association between Ephrin B2 and VEGF receptors. Swamiphak *et al*. demonstrated that Ephrin B2 leads to signaling and trafficking of VEGFR2[149] while *Wang et al*., show that bidirectional signaling by Ephrin B2 causes endocytosis of VEGF-3 and signaling once bound to VEGF-C[150]. Both these processes lead to sprouting angiogenesis and lymphangiogenesis. VEGF

influences the behavior of both osteoblasts and osteoclasts. Expression of VEGF and its receptors has been detected in both cell types[132]. VEGF plays a critical role in differentiation to the osteoblastic lineage. Mayer *et al*. showed that VEGF-A plays an autocrine role in osteoblast mineralisation[151]. Additionally; Street *et al*., showed VEGF, in a dose-dependent manner increased ALP activity and nodule formation in primary human osteoblastic cells[152]. Further, they showed increased expression of VEGF but not FGF (another critical regulator of angiogenesis) in these cells under hypoxia, thereby establishing the definitive and key role of VEGF as a potential therapeutic option in bone repair. Additionally, it has been shown that VEGF also plays a role in differentiation of chondroprogenitor cells to chondrocytes within bone tissue. Furthermore; reports have suggested that VEGF is a chemoattractant to osteoclasts[153] and may have a prominent role in osteoclast differentiation[154] (Figure 1.13.2).

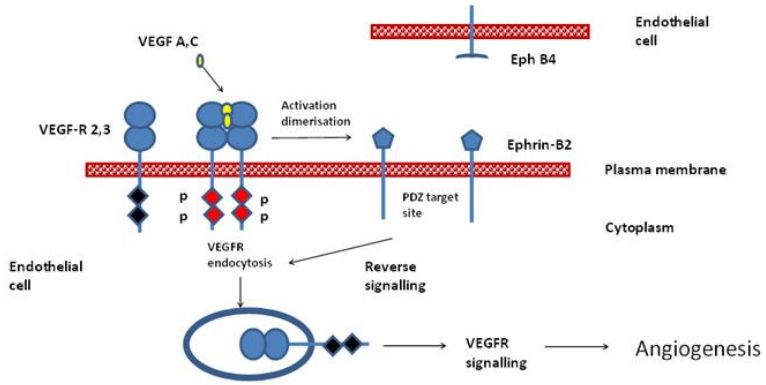

Figure 1.13.2: Role of ephrin-B2 reverse signaling in VEGFR mediated angiogenesis

SECTION G: HYPOTHESIS AND AIMS OF THESIS

AVN is a serious necrotizing condition of bone that occurs due to localized ischemia. It primarily affects the femoral head of the hip joint, leading to serious loss of bone tissue, structural failure and, ultimately, a severe and untreatable osteoarthritis. The condition generally affects people between the ages of 25-50, with 50% of cases requiring Total Hip Arthroplasty (THA) and negatively impacts the long-term quality of life in these patients. Current treatment strategies are limited because they are mostly surgical in nature and have a low success rate. A promising alternative (with the possibility of better clinical outcome) to treat AVN would be to restore the vascular supply using Tissue Engineering based principles.

The field of Regenerative medicine and tissue engineering promises therapies for improved healing of damaged tissue significantly eliminating the risks, limitations and drawbacks of current treatment options. Bone healing following fracture involves collaborative contribution between cells, growth factors, osteoconductive materials, mechanical stimuli along with good vascularization as outlined by the diamond concept[37]. The goal of tissue engineering is to restore structure and function to a defect by exploiting the body's natural healing response with the aid of one or all of the above listed key elements. Thus, necrotic bone can potentially be replaced with healthy functional bone tissue. A multipronged approach is therefore justified while employing therapeutic strategies for bone healing. Therefore this thesis has explored the following specific aims:

1. Develop a Tissue Engineered bone construct using hMSCs seeded on HA/TCP scaffold (Biosel, DePuy Synthes) and evaluate its osteogenic potential under static and dynamic conditions.

2. Compare its osteogenic potential with MBCP granules (Biomatlante)

3. Evaluate the osteogenic and angiogenic potential of MSCs modified to overexpress Ephrin B2 in comparison to MSCs transduced with a control protein, dsRED.

Aim 1 (A): Evaluation of material properties, protein adsorption and cytocompatibility of the HA/TCP Biosel scaffold (first material to be tested)

The first material to be tested was a biphasic scaffold (Biosel, DePuy Synthes) manufactured as 3mm cubes composed of 75% Hydroxyapatite (HA) and 25 % tricalcium phospahate (TCP). The Biosel has been used in a clinical and pre-clinical study. The Biosel scaffold was evaluated to assess its physical, chemical, mechanical and morphological properties. Additionally, the scaffold was functionalized with fibronectin so as to enable cell attachment in further studies and protein adsorption capabilities were evaluated. The cytocompatibility of the scaffold was evaluated using the ISO standard protocols to assess material toxicity.

Aim 1 (B) Develop protocols for appropriate cell loading and evaluate the *in vitro* viability, osteoconductivity and osteoinductivity of the Biosel scaffold.

Once the material was characterized and was deemed cytocompatible, the next step was to develop protocols for appropriate and efficient cell loading onto the Biosel scaffold. MSC attachment, matrix deposition, cell viability and osteoinductivity of the material were evaluated in comparison to monolayer controls. Enhancement of the osteoinductive capacities of the cell loaded Biosel scaffold through the application of a mechanical load using a perfusion bioreactor was also evaluated.

Aim 2: Assessment of cell viability, osteoconductivity and osteoinductivity of hMSCs loaded onto MBCP granules (second candidate material to be tested)

It was hypothesized that particle based material offer populating cells with better attachment space and a greater degree of freedom to proliferate and deposit matrix. Additionally, the open porosity would enhance nutrient and waste exchange throughout the construct. The material chosen was commercially available MBCP+, (Biomatlante, France). This material, a three dimensional interconnected material is similar to the trabecular architecture as

well as the crystalline structure of native bone. The material is osseointegrative and possesses an optimal porosity to aid in cell migration and angiogenesis (Reference: MBCP+ Biomatlante manual). The material was assessed for cell viability, matrix mineralisation and osteoinductivity as was performed with the Biosel scaffold.

Aim 3: Enhancement of the inherent osteogenic and angiogenic capacity of hMSC by lentiviral overexpression of Ephrin B2.

It was hypothesized that overexpressing Ephrin B2 in hMSCs would prove beneficial in the avascular necrotic environment by providing a novel one-step approach to treating avascular necrosis by enhancement of both angiogenesis and bone formation. Ephrin B2 was cloned into a plex backbone destination vector and characterized by a restriction digest. Lentiviral vectors of Ephrin B2-plex and a control plasmid in the same backbone (dsRED-pleX) were produced. MSCs were transduced at an MOI=5 and assessed for Ephrin B2 overexpression by qPCR and Western Blot.

The effect of Ephrin B2 overexpression on the osteogenic and angiogenic capabilities of hMSCs in comparison to controls was evaluated by assessment of ALP activity, osteogenic and angiogenic gene expression, calcium deposition, Matrigel tubule formation and VEGF ELISA assays.

CHAPTER 2: SURFACE CHARACTERISATION, CYTOTOXICITY, AND PROTEIN ADSORPTION STUDIES ON HA/TCP BIOSEL SCAFFOLD

2.1 INTRODUCTION

Ceramics have been used since ancient times and their therapeutic use has been recorded since Egyptian times. A dentistry book published in the late 1700's indicates dental implant and transplant procedures being conducted at that time[155] , while Dressman in 1892 published the application of Plaster of Paris in filling bone defects[156]. Albee and Morrison were the first to publish the use of TCP in filling of bone defects[157]. McGee *et al*., were the first to report the use of a ceramic composed of TCP and $MgAl_2O_4$ in a bone replacement dog model[158].

The apatite-like structure of hydroxyapatite is very similar to the mineral phase of bone, enamel, and dentin, making it a popular choice for hard tissue applications. HA (Ca/P ratio=1.67) possess a hexagonal structure and a chemical formula of $Ca_{10}(Po_4)_6(OH)_2$. It comprises about 69% of native bone and is the most stable form of calcium phosphates. It is stable in body fluids as well as temperatures up to 1200^0C. It is bioactive and possesses low degradability. β-tricalcium phosphate (β-TCP) (Ca/P=1.5) with a chemical formula of $Ca_3(Po_4)_2$ also possess a hexagonal structure[159].

Calcium phosphate material properties that simulate properties of bone include (Figure 2.1.2):

Protein adsorption

Chromatographic analysis has indicated that synthetic apatites enable protein adsorption[160]. Protein adsorption is required for cell attachment, proliferation, and differentiation.

Interconnected porosity

Interconnected microporosity of HA, β-TCP or BCP is attained by the use of porogen or using the foaming technique[161]. Sintering temperature affects the microporosity of a scaffold. For example; CaP material sintered at 1200^0C shows less microporosity than that sintered at 1000^0C, with a significant change in crystal size[162]. HA derived from corals or bovine sources are made to retain the porosity of the original biological bone in the course of processing.

Biodegradability

The biodegradability of a material is determined by placing the material in an acidic buffer environment and measuring Ca^{2+}ion release over time[163,164]. This acidic environment to a certain degree mimics the *in vitro* osteoclastic bone resorption activity. *In vitro* and *in vivo*, there are certain properties of CaPs that determine degradability-composition, particle, and crystal size, porosity and processing conditions. In the case of biphasic calcium phosphates, degradation rate depends on the ratio of HA to TCP, with higher ratios showing lower rates of degradation[165].

Bioactivity

Bioactivity of a material is defined as the ability of a material to bond directly to newly developing bone[166]. The newly developed bone bonds via a carbonate apatite (CHA) layer to biomaterials, the *in vitro* bioactivity of which has an electrolyte composition similar to serum. CHA formation *in vitro* occurs in the presence of proteins (serum, for example) or in the absence of proteins (SBF or mineralizing solution). *In vitro*, CA formation on CaP material occurs by the uptake of calcium and phosphate ions from the serum or SBF. However, *in vivo* CHA formation on CaP surfaces in osseous and non-osseous sites is mediated through cell dissolution /precipitation. *In vivo* (Figure 2.1.1) , the acidic environment created by the cellular activity of macrophages and osteoclasts triggers partial dissolution of CAP leading to increased supersaturation of the surrounding fluid, causing CHA precipitation integrating Ca^{2+},HPO_4^{2-},PO_4^{3-},Mg^{2+},Na^{+},CO_3^{2-} from the fluidic microenvironment. The number of CHA nanocrystals on the CHA surface is influenced by the dissolution capabilities of the material[167].

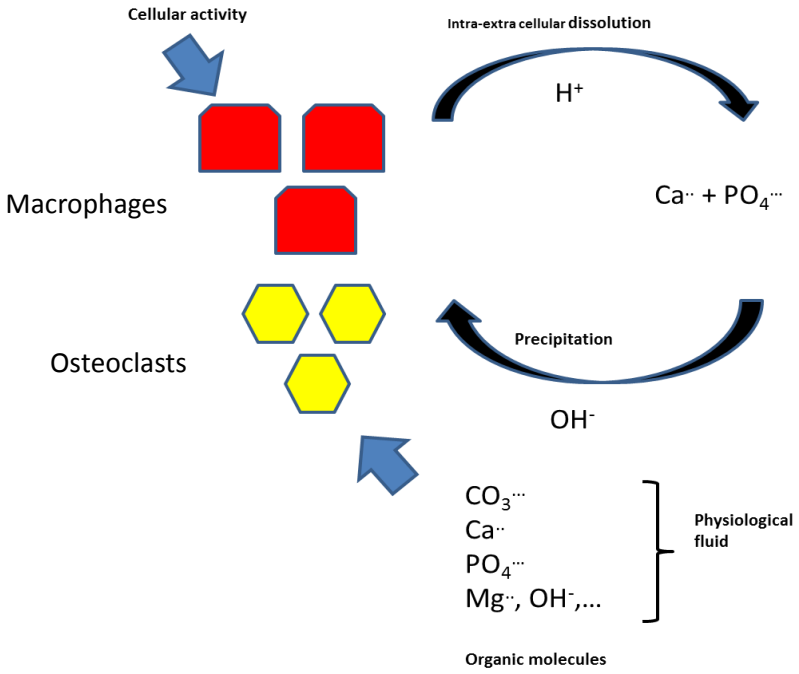

Figure 2.1.1: Representation of dissolution/precipitation processes occurring during the formation of CHA on CaP surfaces *in vivo*. Cellular activity creates an acidic environment, which in turn causes dissolution of CaP. This causes supersaturation in the fluid microenvironment, leading to precipitation of CHA, incorporating organic molecules and ions.

Osteoconductivity

Osteoconductivity refers to the property of a material to serve as a template to the newly developing bone enabling attachment, proliferation, and differentiation of the populating cells.[168]

Cellular response to CaP

Cellular response to CaPs is dependent on material surface topography (roughness), constitution and particle size.

Protein adsorption is influenced by biomaterial surface properties, the ionic milieu as well as surface chemical and structural properties of the protein itself[169-171]. Protein adsorption onto the material surface increases with the presence of micropores due to the subsequent increase in available surface area. Zhu *et al*.,[172] found that high porosity and pores greater than 20 nm showed better adsorption of proteins and fibrinogen and insulin in comparison to lower porosities[173]. A few studies have integrated nanophase calcium phosphate ceramics into hydrophobic polymer scaffolds as a means to

improve protein adsorption[174,175]. It has been proven in studies that proteins like fibronectin can be severely denatured on a hydrophobic surface[169,176].

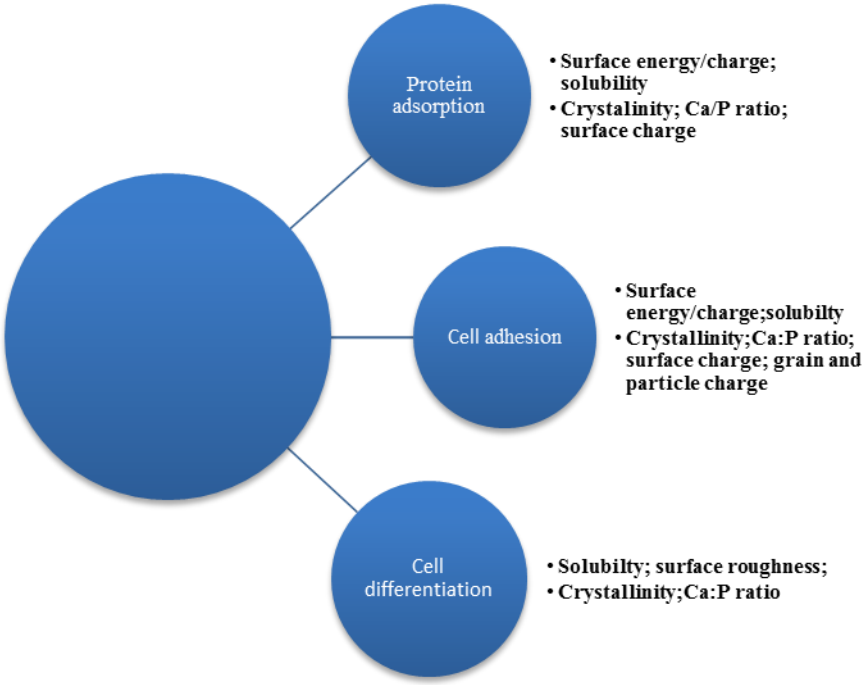

Figure 2.1.2: Specific Material properties that that affect biological function

Studies by Kandori *et al.*,[177,178] prove that cationic groups such as calcium help proteins to attach to the material surface and enable protein adsorption on even weakly soluble calcium phosphate ceramics like HA. For example, they propose that proteins like fibronectin go through a structural change in order to adsorb to calcium surfaces[173,177,178]. Additionally, protein adsorption is greater with increasing ion concentration and pH changes on the surface of soluble calcium phosphate materials. As regards osteoinductivity; Barradas *et al.*,[179,180] demonstrated higher levels of BMP2 gene expression by increased calcium levels in the medium even in the absence of osteogenic differentiation factors. Further, studies by Khoshniat *et al.*, [181]show that the presence of phosphate ions plays only an ancillary role in aiding osteogenic differentiation[182].

Adsorption of a protein to the biomaterial surface is an important parameter for testing the functionality of a biomaterial for use in tissue engineering

applications. Cell attachment to biomaterial surface is facilitated by protein adsorption. **Fibronectins** consist of a linear array of distinct domains that gives each polypeptide a modular construction. Each of the two-polypeptide chains that make up a fibronectin molecule contains:

1. Binding sites for other components of the ECM, such as collagens and proteoglycans. These binding sites facilitate interactions that link these diverse molecules into a stable, interconnected network.

2. Binding sites for receptors on the cell surface. These binding sites hold the cell in a stable attachment to the ECM[176].

Chapter specific Aims:

1. Define the morphological, chemical and mechanical properties of the Biosel scaffold.
2. To evaluate the protein adsorption capabilities of the Biosel scaffold
3. To evaluate the cytotoxic properties of the scaffold.

2.2 Materials & Methods

2.2.1 Physical characterisation of the Biosel scaffold

2.2.1.1 Scanning Electron Microscopy (SEM)

A SEM is a type of electron microscope the images a sample by scanning it using a beam of electrons in a raster scan pattern. The electrons interact with the atoms that make up the sample producing signals that contain information about the sample's surface topography, composition and other properties such as electrical conductivity. The surface characteristics of the Biosel scaffold were evaluated using a Scanning Electron Microscope (SEM) (Hitachi S-4700) at a voltage of 10kV.The material was mounted on aluminum stubs using an adhesive carbon tape. The material was then gold sputter coated using a sputter coater (EMSCOPE SC500 Gold Sputter Coater), loaded onto the instrument and imaged.

2.2.2 Chemical characterisation

2.2.2.1 Energy dispersive x-ray Spectroscopy (EDX)

EDS or EDX is an analytical technique and is used to determine elemental composition or for chemical characterization of a sample. It relies on the investigation of an interaction between the X-ray source and the material of interest. Its characterization methodology is based on the principle that each element has a unique atomic structure, which allows for unique set of peaks on its X-ray spectrum. Therefore, to enable the emission of characteristic X-rays from a specimen, a high energy beam of charged particles is focussed onto the test sample.

The elemental analysis was performed for three samples using an EDX spectrum (Hitachi Scanning Electron Microscope with EDX Analysis System) that was connected to the SEM. Measurements were done on three rectangular regions per sample.

2.2.2.2 X-ray photoelectron Spectroscopy (XPS)

X-ray photoelectron spectroscopy is a quantitative technique that helps define the elemental composition, empirical formula, chemical state and electronic state of the elements that exist within a material. An XPS spectrum is obtained when a material is irradiated with an X-ray beam while simultaneously measuring the kinetic energy of electrons that escape the top 1 to 10 nm of the material being tested.

The surface composition of the material was measured using an XPS (Kratos Axis 165 spectrometer) using a Mono Al K_2 X-ray gun, 1486.58 eV; 150 W (10 mA, 15kV).

2.2.2.3 Thermogravimetric Analysis (TGA)

TGA is a technique applied to determine the amount and rate of change in the weight of a material as a function of temperature or time in a controlled atmosphere. Measurements are used mainly to determine the composition of materials and to predict their thermal stability at temperatures up to 1000 ^{0} C. The technique can characterize materials that show weight loss or gain due to decomposition, oxidation or dehydration.

The material purity and thermal stability analysis were carried out using Thermogravimetry (TGA-7, Perkin Elmer). The sample was heated from 30 degrees C to 700 degrees C, increasing the temperature by 10 degrees C every minute. Tests were run under nitrogen to prevent degradation.

2.2.2.4 Fourier Transform Infrared Spectroscopy (FTIR)

Fourier Transform Infrared Spectroscopy (FTIR) is an analytical technique used to identify organic (and in some cases inorganic) materials. This technique measures the absorption of various infrared light wavelengths by the material of interest. These infrared absorption bands identify specific molecular components and structures. Absorption bands in the range of wave numbers 4000 -1500 are typically due to functional groups (e.g. -OH, C=O, N-H, -CH3, etc.). The region between 1500 - 400 wave numbers is referred to as the fingerprint region. Absorption bands in this region are generally due to intra-molecular phenomena, and are highly specific for each material. The specificity of these bands allows computerized data searches to be performed against reference libraries to identify a material.

Chemical characterisation of the material was carried out using a Fourier Transform Infrared (FT-IR) spectrophotometer (FTIR AIM -8800).

2.2.3 Mechanical characterisation

To measure the strength of each scaffold, force was applied to each sample with a compressor. Load was applied until the scaffold was completely crushed. Compression tests were carried out for 5 samples. Tests were carried out using a tensile tester (Lloyd Lr10K, screw-driven testing machine).

2.2.4 Isolation and characterisation of hMSCs

Bone marrow (isolated from the iliac crest) hMSCs were obtained from healthy volunteers (aged 18-30 years) with informed consent and approval from the National University of Ireland Galway and University College Hospital ethics committees. Characterisation of surface receptors was performed using CD105, CD73, CD90 (positive) and CD34, CD45 (negative). Tri-lineage differentiation capacity was determined using standard chondrogenic, adipogenic and osteogenic differentiation assays (work performed by Georgina Shaw at REMEDI).

hMSCs (at passage 3) from three separate donors, were utilised for experiments and maintained in Minimum Essential Medium Alpha Medium supplemented with 10% foetal bovine serum (FBS) and 1% penicillin/streptomycin (P/S). All cells were cultured at 37°C and 5% CO2, unless stated otherwise.

2.2.5 Cytotoxicity Evaluation

The cytotoxicity of the scaffold was evaluated using the ISO standard protocols of Elution and Direct contact (ISO standard 10993-5). Briefly; a couple of 48 well plates (one 48 well plate each for Elution and direct contact) were seeded with 15,000 hMSC's / well for 6 wells/plate. The cells were left to attach for 24 hours. In parallel, three scaffolds were incubated with 0.8ml each of hMSC growth media for 24 hours. The next day, three wells of the plate kept for the elution experiment were fed with medium incubated with the scaffolds; while the remaining three wells were fed with hMSC growth medium. Additionally, three scaffolds were placed for 3 wells each for the plate kept for direct contact. The remaining wells were left without any manipulation and all wells were refreshed with fresh medium. The following day viability analysis for all wells in both plates was performed using the cell titer blue assay. Additionally, cell number was evaluated using the quanti-iT ™ PicoGreen double stranded DNA assay (Molecular Probes) following the manufacturer's instructions. Briefly, standards (prepared by dilution) and diluted samples were added a 96- black well plate in triplicate. Picogreen reaction buffer was added to both samples and standards and incubated at RT for 3 min in the dark. Readings were performed at 538 nm with excitation at 485 nm using a Wallac Victor3TM 1420 Multilabel counter fluorescent plate reader. From the obtained triplicate readings, the mean fluorescence reading was calculated. Using the trend line equation from the standard curve, the DNA concentration/ml was obtained. This value was then corrected for dilution and DNA/well. The resulting value was converted to pictograms of DNA and then divided by 8 (assuming ~8 pg. of DNA per nucleus)[183] to obtain the cell number.

2.2.6 Protein adsorption studies

Nine 3mm cubes of Biosel scaffold (DePuy Synthes) consisting of HA (75 %)/TCP (25%) were placed in nine separate wells of a 24 well plate. 1ml of 10µl/ml Fibronectin (FC010, Millipore) in PBS was added to three scaffolds, 1ml of 50µg/ml Fibronectin in PBS was added to next set of three scaffolds and 1ml of 100 µg/ml Fibronectin in PBS was added to the remaining set of three scaffolds. The scaffolds were incubated with the respective Fibronectin concentrations for 30 minutes. At the end of 30 minutes, the scaffolds were removed and placed in a 48 well plate containing 0.5 ml PBS to remove loosely adsorbed proteins. In order to release the adsorbed protein, scaffolds were then transferred to separate wells containing 0.5 ml Triton-X in Tris-HCl and left overnight in a shaker at 4^0C. The absorbance was measured at 595 nm using a spectrophotometer (Perkin-Elmer). The absorbance data obtained was normalised to a bovine serum albumin standard. Protein adsorption onto the scaffold surface was quantified using Coomassie (Bradford) protein assay kit (Thermo Scientific, USA).

The above protein adsorption protocol was repeated in a similar manner for the different fibronectin concentrations with varying incubation time points of 1 hour and 2 hour respectively.

2.2.7 Statistical analysis

GraphPad Prism® software Inc. was used for statistical analysis. Significance was evaluated using one-way followed by Tukey post hoc analysis. Error bars represent the mean ± standard deviation. *p*-values ≤0.05 were considered statistically significant.

2.3 Results

2.3.1 Characterisation of Physical properties- SEM images revealed the morphology and porosity of the Biosel scaffold

SEM was performed to morphologically and qualitatively evaluate the HA/TCP Biosel scaffold. The SEM micrograph of HA/TCP Biosel scaffold exhibited crystals characteristic of HA. The company provided information states that the Biosel scaffold consists of pores ranging from 200-500 µm in size, and

pores of unequal size was visualised using the SEM. A representative pore size of 338.14 µm is shown in the Figure 2.3.1.B (marked by arrow), although pore diameters that appeared smaller was also exhibited throughout the scaffold.

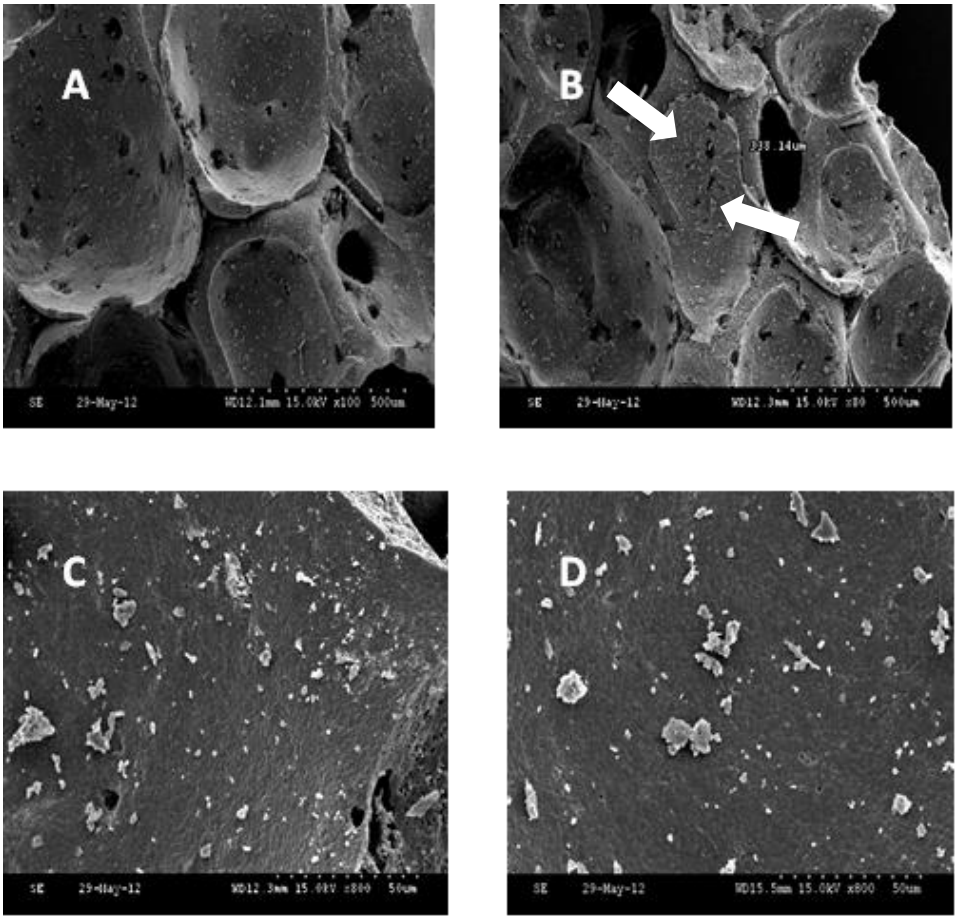

Figure 2.3.1: SEM imaging completed for three samples of the Biosel scaffold: A) Magnification:100X , Scale bar:500µm, B) Magnification 80X,Scale bar:500µm,**Displayed pore size measurement = 338.14µm**, C)Magnification:800X, Scale bar:50µm and D)Magnification:800X,Scale bar:50µm. Data are representative of 3 samples.

2.3.2 Characterisation of Chemical properties

EDX, XPS, FTIR AND TGA help characterise the identity and purity of the Biosel scaffold

2.3.2.1 Energy Dispersive X-ray Spectroscopy

As seen from the graph (Figure 2.3.2), EDX results indicate the presence of inorganic elements like Ca and P, traces of Al, as well as C & O. The EDX result, indicates that Ca/P ratio of 2.30 is higher than that of pure HA (1.67) and TCP (1.5) and in 75% HA/25% TCP (1.65).

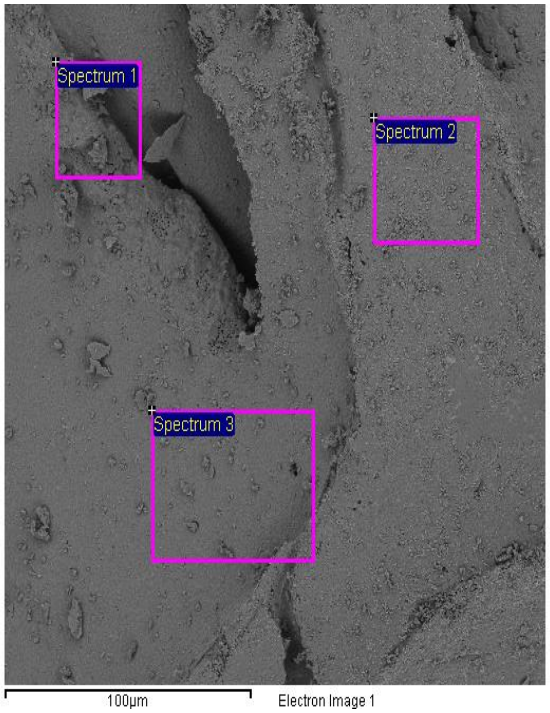

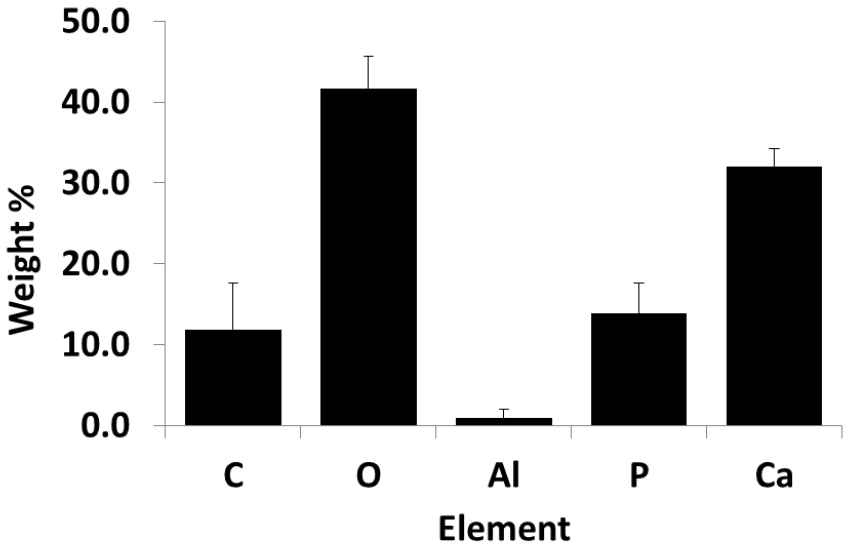

Figure 2.3.2: EDX analysis completed for three samples. A) SEM image showing rectangular areas on the sample that were selected for EDX analysis) Graph quantitatively depicting the elements detected by the EDX spectrum. Data represents mean ± SD of three independent Biosel samples. Results are expressed as percentages.

2.3.2.2 X-ray Photoelectron Spectroscopy

XPS data indicate that Ca/P ratios are higher than those expected for pure HA (1.67) and TCP (1.5) and in 75% HA / 25% TCP (1.65). The material surface is contaminated with O (mainly) as well as C. As indicated earlier (Section2.2.2.2), XPS data only measures the top 1-10 nm of the material

surface. There is relatively more Ca near the surface of the scaffold structure (compared to the whole material as indicated by EDX data- 30%) and possibly Ca terminated as oxide or hydroxide (Figure 2.3.3).

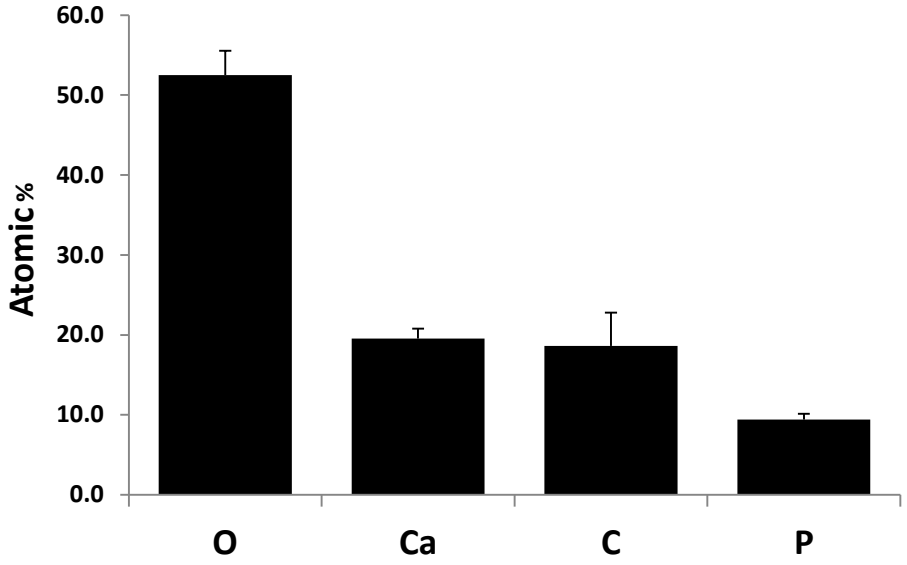

Figure 2.3.3: XPS analysis completed for three samples. Graph quantitatively depicting the elements detected by the XPS spectrum. Data represents mean ± SD of three independent Biosel samples.

2.3.2.3 FTIR

The FTIR adsorption spectrum displayed characteristic peaks of the sample and confirmed sample identity..

Absorption bands in the range of wave numbers 4000 -1500 are typically due to functional groups (e.g. -OH, C=O, N-H, $-CH_3$, etc.). The region between 1500 - 400 wave numbers is referred to as the fingerprint region. Absorption bands in this region are generally due to intra-molecular phenomena, and are highly specific for each material. The specificity of these bands allows computerized data searches to be performed against reference libraries to identify a material.

The obtained FTIR spectra obtained from three different samples are shown. The bands were observed at 3846.66 and 3740.00 cm^{-1} due to the stretching mode of hydrogen bonded OH^- ions. OH^- ions prove the presence of hydroxyapatite[184]. Additionally, PO_4^{3-} assymetric stretching mode of vibration was evaluated by the presence of a strong and complex band at 1016.66 cm^{-1}

along with a band of medium intensity (at 2306.66 cm^{-1}) showing symmetric stretching vibration[185]. Therefore, the FT-IR analysis displayed all the typical adsorption bands expected from HA, establishing the identity of the material.

A

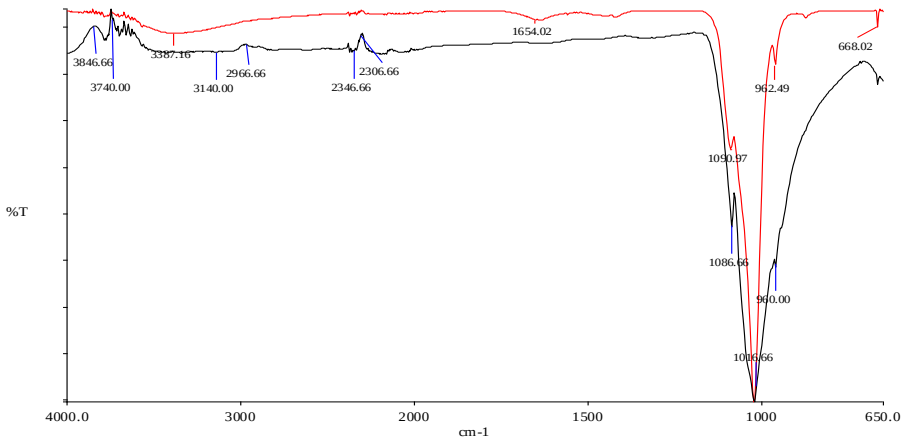

B

IR Frequency (cm^{-1})	Bond and functional group
1016.66	PO asymmetric stretching
2306.66	PO stretching
3846.66 , 3740.00	OH Bonding in water

Figure 2.3.4: FTIR analysis. A) FTIR spectrum: representative for three independent Biosel samples. B) Table representing the obtained wavelengths and their corresponding functional group.

2.3.2.4 Thermo gravimetric analysis

The sample was heated from 30 degrees C to 700 degrees C, increasing the temperature by 10 degrees C every minute. Tests were run under nitrogen to

prevent degradation. As seen from the graph (Figure 2.3.5), the sample lost almost no weight (in terms of volatile substances, like water, or inorganic materials), indicating purity of the material. These data support EDX data which exhibited only traces of contamination with inorganic aluminium.

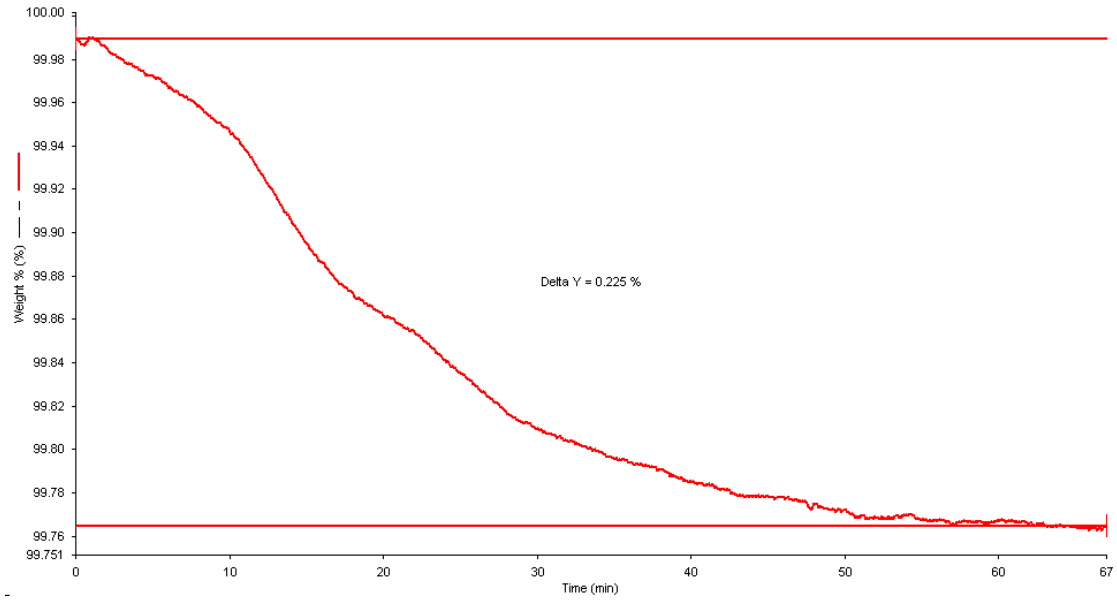

Figure 2.3.5: TGA analysis: TGA graph of the Biosel scaffold. Data are representative of 3 samples.

2.3.3 Mechanical properties

Mechanical testing was carried out for 5 specimens (Figure 2.3.6). The compressive strength value of 4.2 +/- 0.9 MPa (Figure 2.3.6 A) is consistent with reported results for such brittle HA / TCP scaffolds [186,187].The compressive strength is thus comparable to that obtained for human cancellous bone, a value in the range 2 MPa to 20 MPa. Figure 2.3.6 B and C depict the intact sample and crushed sample (after applying load) respectively.

A

Max Load (N)	37.8±8.6
Strain @ max load (%)	22.3±8.1
Max Stress (MPa)	4.2±0.9

B C

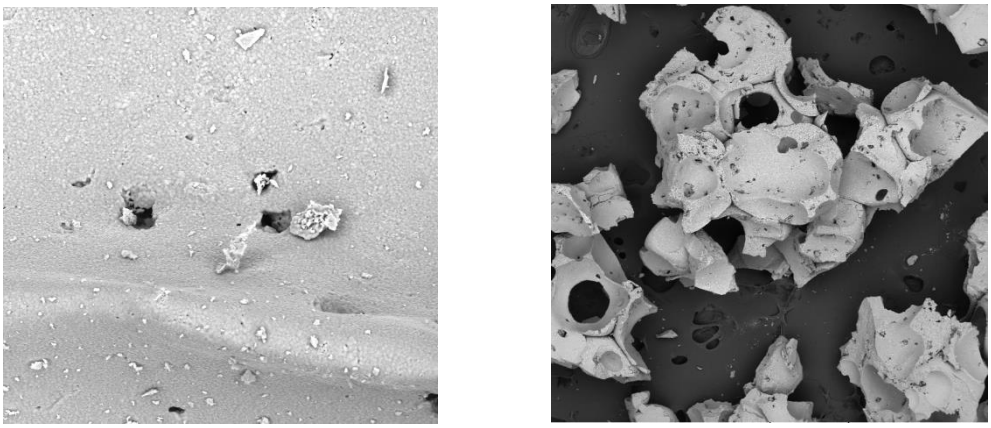

Figure 2.3.6: Compression testing values (A) and SEM images of intact (B) and crushed scaffolds (C). N=5

The Biosel scaffold proved to be non-toxic to hMSCs. Cytotoxicity of the HA/TCP Biosel scaffold was evaluated using the ISO standard protocols of material toxicity – Elution and Direct contact. The control and treated samples were then evaluated for metabolic activity using the cell titer blue assay (Figure 2.3.7) and the cell number was evaluated by measuring the DNA content of cell lysates using the picogreen assay (Figure 2.3.8).There was insignificant difference in metabolic activity and cell number between test and control samples showing the cytocompatible properties of the scaffold.

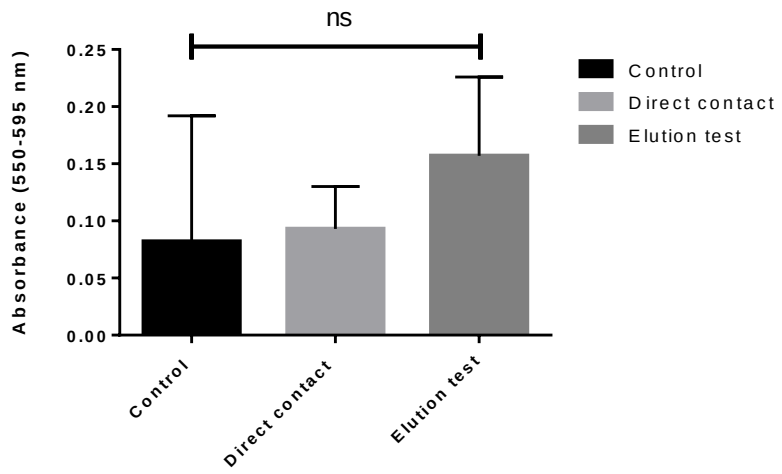

Figure 2.3.7: Cell titer blue assay. Analysis of cell viability among control, direct contact and test groups show insignificant differences in viability,-proving the cytocompatible nature of the scaffold. Data represents mean ± SD for 3 Biosel scaffolds, one-way ANOVA followed by Tukey's post hoc analysis.

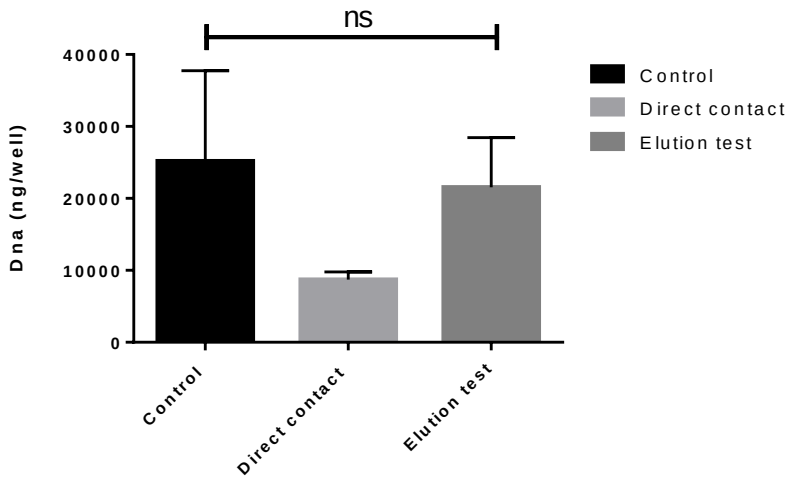

Figure 2.3.8: DNA Content. Picogreen analysis in control, direct contact and test groups show insignificant differences in DNA content, proving the cytocompatible nature of the scaffold. Data represents mean ± SD for 3 Biosel scaffolds, one-way ANOVA followed Tukey post hoc analysis.

2.3.4 Protein Adsorption studies prove the bioactivity of the Biosel scaffold

Figure 2.3.9 shows a graph of concentration of protein adsorbed on the scaffolds at varying concentrations of 10µg/ml, 50µg/ml and 100µg/ml respectively at 30 minutes, 1 hour and 2 hours incubation times. There is a

significant increase in the amount of protein adsorbed at 1 hour and 2 hour incubation compared to incubation at 30 minutes, with insignificant variation between 1 hour and 2 hour incubation time points. The highest protein concentration value among 1 hour and 2 hour incubation times (although insignificant), was obtained with 100µg/ml at 1 hour. Therefore, to achieve maximal protein adsorption at minimal time, 100µg/ml fibronectin at 1 hour incubation time was used for subsequent experiments.

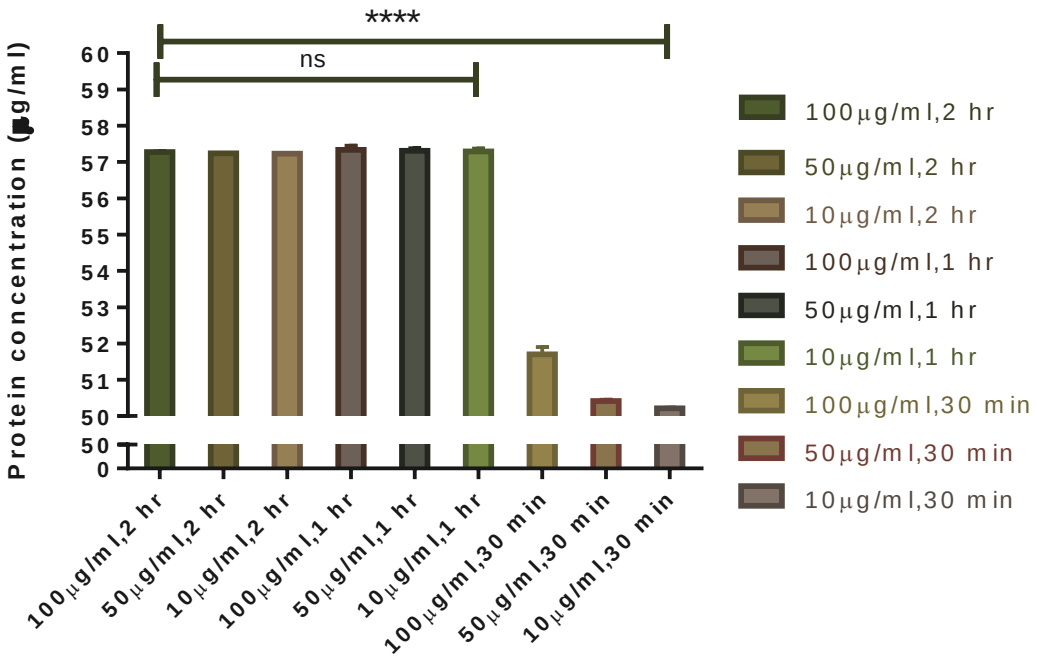

Figure 2.3.9: Protein adsorption capacity of the fibronectin-coated Biosel scaffold. Protein adsorption at a range of concentrations (100µg/ml,50µg/ml, and 10µg/ml) at incubation times of 2 hours. 1 hour. and 30 minutes. Data represents mean ± SD for 3 Biosel scaffolds per condition, one-way ANOVA and Tukey post hoc analysis, (****p<0.0001).

2.4 Discussion:

SEM was employed to study the morphology and porosity of the HA/TCP scaffold (Figure 2.3.1). The scaffold exhibited crystalline structures on its surface which were identified as hydroxyapatite. The scaffold exhibited sporadic porous architecture throughout its surface. There are contradictory reports[188-190] in the literature as regards the importance of porosity in bone tissue engineering applications. Porosity represents the percentage of void space in a solid and is a morphological entity that is independent of the

material. Pores are vital for the formation of bone tissue because they enable migration and proliferation of osteoblasts and mesenchymal stem cells, as well as vascularisation. A porous surface also enables mechanical interlocking between the biomaterial implant and the surrounding natural bone, thereby providing greater mechanical stability at this critical juncture. Porosity and pore size of a biomaterial are important parameters to be considered while fabricating a scaffold. Due to a wide range of bone features *in vivo* and diverse range of biomaterials, cells, and cytokines used, there can be no standard pore size for all bone tissue engineering applications.

However, the following features need to be given consideration:

1. Higher porosity and large pores enhance ingrowth of bone as well as osseointegration of the implant after surgery.

2. Biomaterials that possess a high degradation rate should not have high porosities, as well as this will compromise mechanical and structural properties before new bone are formed.

The Biosel scaffold has a porosity of 60%-80% as per data provided by DePuy Synthes. However, the morphologically as per SEM images (particularly at higher magnifications) the scaffold exhibited minimal pores. Although a high porosity would compromise the mechanical strength of the Biosel, its high HA content (75%) could potentially off-set the negative effects. As indicated earlier, higher HA: TCP ratios have slower rates of degradability. Further, a minimum pore size of 50-100 µm is considered appropriate to enable osteogenesis, making the Biosel scaffold (having pore sizes ranging from 200µm-500µm) a promising candidate for bone tissue engineering applications. At higher magnifications, the Biosel scaffolds exhibited greater number of crystals in its surface. The crystalline nature of the scaffold surface will influence its *in vivo* behaviour. Additionally, as indicated by EDX and XPS data, the Ca/P ratio is >1.67, which would influence its crystallinity. It has been shown that higher Ca/P ratios result in greater crystallinity and therefore lower solubility.

Material characterisation is critical to help correlate the material features and an observed cellular response. Since no single technique can provide a holistic evaluation of a material, a number of analytical characterisation methods need to be employed. XPS (Figure 2.3.3) and FTIR help identify the material while TGA analysis (Figure 2.3.5) proved the purity of the scaffold. While XPS data indicated the presence of surface contaminants, their negative effects on the behaviour of inhabiting cells is still ambiguous.

Protein adsorption onto the scaffold surface is an important parameter to consider while evaluating the bioactivity of the surface. The Biosel scaffold was coated with fibronectin (Figure 2.3.9). Garcia *et al.,*(1997)[191] demonstrated that precoating of materials with fibronectin helps in higher cell detachment strength. Additionally, fibronectin has been found to act as a survival factor for differentiated osteoblasts[192]. Following *in vivo* implantation of biomaterials, protein adsorption from the surrounding microenvironment has been found to enable attachment, proliferation, and migration of cells[193]. The importance of scaffold porosity is also critical for its protein adsorption capabilities. A scaffold with greater porosity will have greater surface area and will, therefore, enable superior protein adsorption to it surface[173]. A hydrophobic surface will usually tend to adsorb proteins better compared to hydrophilic surface[194]. Contact angle measurements have shown that β-TCP is more hydrophobic than BCP and BCP are more hydrophobic than HA[173,195,196].

Most mammalian cells are anchorage-dependent and require a substrate to perform most of their activities[197-200]. *In vivo*, tissues are made of cells and extracellular matrix. The cells secrete extracellular matrix which acts as their structural support and as a substrate to enable cellular behavior such as attachment, migration, proliferation and differentiation. Enzymatic digestion of the ECM during isolation of the cells causes a marked decrease in the synthetic and secretory activities of the cells. Therefore, in an effort to mimic the *in vivo* environment, protein absorption can be performed on a scaffold in order to improve cell attachment and survival[201].

Prior to evaluating the biological response of cells to a biomaterial, it is necessary to conduct cytotoxicity tests to rule out any potential subsequent negative effects on tissue response. The ideal in vitro test would employ cells that the Biosel scaffold would encounter in preclinical or clinical applications. Therefore, human mesenchymal stem cells were employed which represents the cell choice for our subsequent studies. There were no significant differences in the metabolic activity or DNA content of cells evaluated with direct contact or elution tests compared to the no treatment positive control groups (Figure 2.3.7, Figure 2.3.8).

2.5 Chapter summary:

The SEM micrograph of the Biosel scaffold exhibited crystals characteristic of HA and morphologically exhibited pores of unequal size. The scaffold was morphologically observed to have a porous architecture but with a high empty fraction. However a more porous structure would be beneficial to enable cells to integrate into the interior of the scaffold and would facilitate in growth of tissue. EDX, XRD and FTIR data help ascertain the identity of the material which will prove useful in subsequent studies. The TGA analysis results helped ascertain the thermal stability as well as purity of the sample. Further, the Biosel scaffold proved to be non-cytotoxic according to ISO compliant protocols, permitting its use in subsequent studies.

Evaluation of the osteoconductive and osteoinductive nature of the HA/TCP Biosel scaffold using static and dynamic cell culture systems

3.1 Introduction

HA and calcium phosphate-based materials are the most frequently studied scaffolds for bone tissue engineering applications due to their inherent osteoconductive properties and their capacity to incorporate with the host bone tissue[179,180,202,203]. The first study to effectively demonstrate new bone formation on cell scaffold ceramic implanted in a subcutaneous immunocompromised mouse model was reported by Goshima *et al*.[204] Subsequently, different groups have shown similar results using syngenic rats[204,205], immunocompromised mice[206-208] or critical sized defects[209,210], vascularized bone flaps[211,212].

HA may be coated onto bioinert scaffolds such as titanium surface in order to make them bioactive[213]. However, the disadvantage of using HA includes brittleness, slow biodegradability and shaping difficulties, limiting its clinical use[130,214]. In many cases, osteogenic differentiation (Table 3.1.1 shows various osteogenic markers and their role in differentiation) in calcium phosphate ceramics is achieved by making use of pro-osteogenic chemicals such as dexamethasone, ascorbic acid, and β-glycerophosphate[215] . Lee *et al.,* (2010) found superior gene expression of ALP, OCN, and BSP at day 14 and day 21 on electrospun scaffolds supplemented with hydroxyapatite when compared to no coating[174]. Also, they noted increased expression of these osteogenic genes with increase in HA content[175]

Table 3.1.1: Osteogenic markers and their role in differentiation[216]

Marker name	Type	Role during differentiation
RUNX2	Transcription factor	MSC differentiation into immature osteoblasts
Osterix(OSX)	Transcription factor	Required downstream of RUNX2, promotes osteogenesis, inhibits chondrogenesis
Alkaline phosphatase (ALP)	Enzyme	Acts by increasing local phosphate ion concentration by initiating mineral formation
Type I collagen	ECM protein	The junction between 2 collagen bundle fibers is the site of mineral nucleation
Osteopontin(OPN)	ECM protein	Inhibits irregular mineral crystal formation
Bone sialoprotein(BSP)	ECM protein	Binds via hydroxyl groups to $Ca^{2+}$and promotes mineral nucleation.
Osteocalcin (OCN)	ECM protein	Regulation of mineral growth, direction, size and quantity during later stages of differentiation
Osteonectin (ONN)	ECM protein	Plays a similar role as osteocalcin
Bone morphogenic protein (BMP2)	Growth factor	Secreted by immature osteoblasts; may activate a number of autocrine /paracrine pathways
Bone morphogenic protein (BMP7)	Growth factor	Plays a similar role as BMP2

Biphasic calcium phosphate scaffolds benefit from the advantages of both HA (improved mechanical strength, osteoconductivity) and TCP (improved osteoinductivity). Application of mechanical stimuli by use of spinner flask, rotating wall vessel and perfusion bioreactors[217-220] resulted in improved fluid flow and vascularisation within scaffolds. Bioreactors enrich the process of *in vitro* cell culture. Bioreactors have the potential to lead to improved *in vitro* cell culture by providing efficient and homogenous cell distribution, enhancing automation, reducing the risk of contamination and providing more uniform fluid flow through the scaffold. Most importantly, bioreactors simulate the *in vivo* environment more effectively than two-dimensional cultures[221].

Mechanotransduction refers to the process of cell regulation wherein mechanical stresses are converted into biochemical signals which modulate activity within and between cells. Ingbeger *et al*., (1994) [222] showed that application of mechanical stimuli influences gene expression and biosynthetic activities in many cell types. Additionally, in cases such as distraction

osteogenesis, surgeons make use of mechanical stimuli in order to accomplish the needed outcomes. The main objectives that need to be achieved by use of a bioreactor for tissue engineering include (a) even cell distribution throughout the scaffold, (b) maintenance of optimum concentrations of gases and nutrition in the cell culture medium and (c) presenting the cells with suitable mechanical stimuli. Also these bioreactors need to operate under aseptic conditions so as to enable tissue maturation.

The application of mechanical stimuli to hMSCs has been used as an effective means to stimulate the differentiation of these cells towards the osteogenic lineage[223]. Rubin *et al.,* have postulated that the pro-osteogenic effects could also be due to attenuated adipogenic differentiation in response to mechanical stimuli[224]. Schumacher *et al.* observed higher levels of osteogenic gene expression and homogenous cell distribution under dynamic culture conditions in comparison to static culture[225]. Similar results were obtained by Yu *et al*.[226] , Bjerre *et al*.[227] , and Wang *et al*.[214]. In addition, Xie *et al*.[228] observed improved cell proliferation of MSCs seeded on the β-TCP scaffold in flow perfusion culture compared to static culture as measured by the rate of glucose consumption.

Dynamic culture using the U-cup perfusion bioreactor (Cellec Biotek AG) was explored in this study (Figure 3.1.1). The U-cup Bioreactor offers various performance advantages including homogenous cell distribution, effective nutrition and waste exchange, enhanced reproducibility and reduced risk of contamination due to culture automation. The U-cup bioreactor can be used with different types of porous scaffolds and has been applied to many tissue engineering operations including osteogenic tissue[229,230], vascular tissue[230,231], cartilage[232,233], hematopoietic stroma[234], co-culture of different bone cell types[235], and decellularised ECM[236].

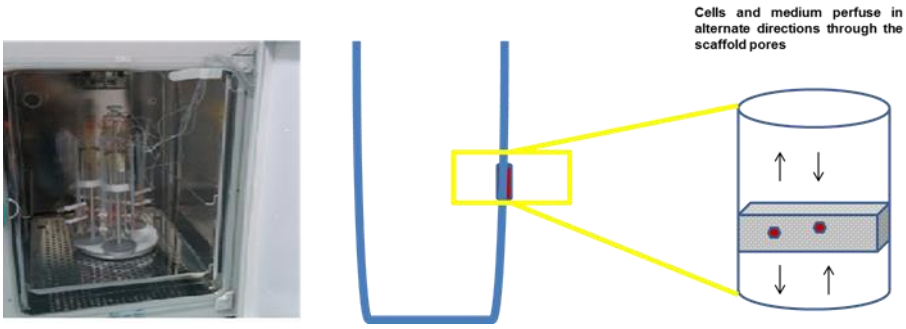

Figure 3.1.1: Schematic of the working principle of the u-cup Bioreactor.

Scherberich *et al*. (2007) cultured cells of the stromal vascular fraction (SVF) of adipose tissue on hydroxyapatite scaffold with an objective of generating constructs with osteogenic and vasculogenic potential. The constructs were cultured directly under perfusion using the U cup bioreactor. Control constructs were cultured under standard two-dimensional conditions. They observed reproducible ectopic bone formation only from dynamic cultures[237]. Additionally, they observed a depletion of the endothelial fraction of SVF cells when cultured under 2D. Further, Papadimitropoulos *et al.* (2011) developed a three-dimensional co-culture system consisting of osteoblastic-osteoclastic-endothelial cells to simulate bone turnover. They observed human origin ectopic bone formation, blood vessels and osteoclasts on implantation[238]. Further, Papadimitropoulous *et al.* (2014) demonstrated that three-dimensionally expanded stromal MSCs maintained superior clonogenicity and differentiation compared to two-dimensional cultures[239]. Additionally, reduced inter-donor variability was observed in three-dimensional cultures of 5 donors compared to 2D cultures, probably due to reduced dispersion of the cultures. Further multipotency associated gene clusters were significantly upregulated in three-dimensional cultures compared to 2D cultures.

Chapter Specific Aims:

1. Develop protocols for appropriate and efficient cell loading onto the Biosel scaffold.
2. Evaluate hMSC attachment, proliferation and viability on the Biosel scaffold.

3. Evaluate the osteoinductivity of the Biosel scaffold.

3.2 Materials and methods

3.2.1 Cell seeding density optimisation

Initially, the following hMSC cell densities were evaluated based on literature[240] : $1x10^5$, $2.5x10^5$ and $5x10^5$.The cells were seeded on a fibronectin pre-coated Biosel scaffold using a vacuum loading protocol optimized in our lab. Briefly, the Biosel scaffold was placed in a sterile BD vacutainer. hMSCs (suspended in 50µl of media) were added to the scaffold. The vacutainer was then closed and the plunger was pulled up gently so as to enable cell penetration inside the scaffold. At 24 hours post seeding, the cell-seeded scaffold was fixed and imaged in the Scanning electron microscope (Hitachi S-4700) to assess cell distribution.

3.2.2 Optimisation of cell loading method

Initially, two seeding protocols were checked for cell loading; 1) drop seeding and 2) vacuum loading.

3.2.2.1 Drop seeding

Bone marrow (isolated from the iliac crest) hMSCs were obtained from healthy volunteers with informed consent and approval from the National University of Ireland Galway and University College Hospital ethics committees. hMSCs (at passage 3) were cultured in MSC growth media consisting as described previously. Next, $0.5x10^6$ hMSCs in 10µl MSC growth media were drop seeded on top of the 3mmx3mmx3mm Biosel scaffold (precoated with 100µg/ml fibronectin in PBS) and left to incubate for 30 minutes. The scaffolds were then transferred to a screw-capped Eppendorf and 2 ml of hMSC growth media was added (Figure 3.2.1).

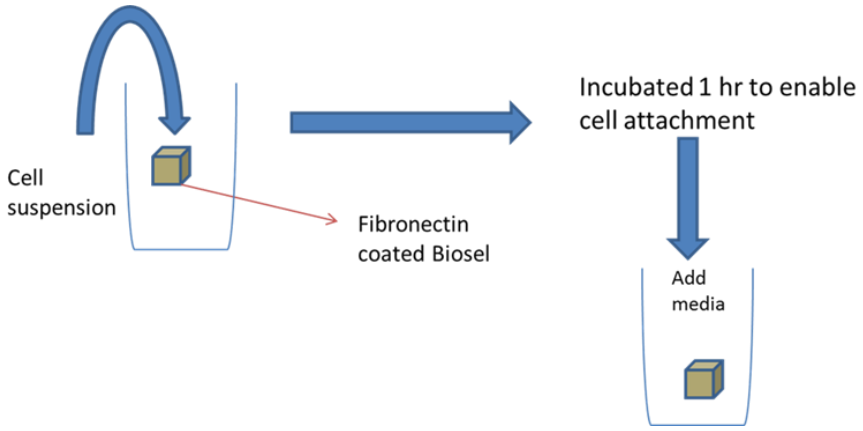

Figure 3.2.1: Schematic of steps involved in drip seeding protocol

3.2.2.2 Vacuum seeding

MSCs (not exceeding P5) were cultured in MSC growth media consisting of 10% FBS. Fibronectin (100µg/ml) coated Biosel scaffold was placed in a sterile BD vacutainer. Next, $0.5x10^6$ hMSCs resuspended in 10 µl media was applied onto the biomaterial by application of a gentle vacuum and left to incubate for half an hour in incubator. The scaffolds were then transferred to a screw-capped Eppendorf and 2ml of hMSC growth media was added (Figure 3.2.2).

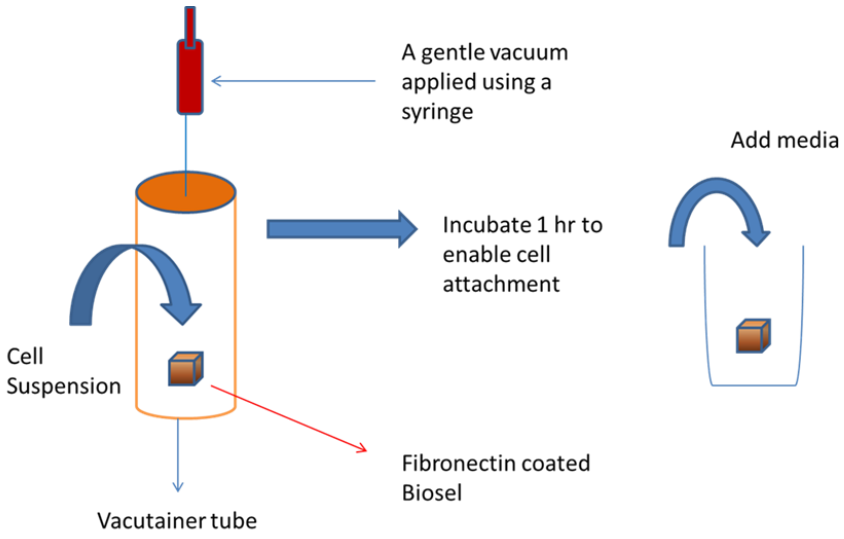

Figure 3.2.2: Schematic of steps involved in the modified vacuum seeding protocol

.

3.2.3 Cell seeding density

To evaluate cell seeding efficiency, cell seeding density was assessed by measurement of DNA content on the scaffold 24 hours post seeding. Briefly, the scaffolds were washed with PBS and 0.1% Triton-X100 in Tris HCl buffer was added and the scaffolds were left to shake overnight at 4^0 C. Next day the lysate was analysed for DNA content using the Picogreen kit (Molecular Probes).

3.2.4 Cell distribution analysis

The scaffolds were transferred to a fresh plate, washed with PBS and fixed with glutaraldehyde(Sigma-Aldrich) and after a series of alcohol (50 %, 75%, 80%, 90 % and 100 %) drying and a critical point drying step using hexamethyldisilazane (HMDS) (Sigma-Aldrich) for 30 minutes. Following overnight air drying, samples were gold sputter coated and imaged using a scanning electron microscope (Hitachi S-4700) to assess cell distribution.

3.2.5 Optimisation of cell seeding density

The fluidic capacity of the scaffold as stated previously is 10ul. Cell densities of $0.5x10^6$ and $1x10^6$ in 10ul of cell culture media were drop seeded as per the following table. Test scaffolds were induced with osteogenic medium (consisting of DMEM (low glucose) supplemented with 1mM Dexamethasone,10mM ascorbic acid, 2-phosphate,1M β-glycerophosphate,10% FBS and 1% penicillin-streptomycin) 48 hours post-seeding to check for cell distribution and matrix deposition by SEM. Cell distribution, viability and cell number were evaluated.

Table 3.2.1: Overview of experimental set-up for cell loading optimisation

Outcome	Time points	n
Viability	3,10,21	18
Cell number	10,21	24
Cell distribution	3,21	4

Following incubation for 3, 10 and 21 days post seeding the scaffolds were transferred to a fresh plate and washed twice with PBS. The scaffolds were then incubated with medium containing 10% Cell titre blue (Promega) (CTB) at 37^0C, 5% CO_2 and 90% humidity for 4 hours and absorbance measurements were performed at 550-595 nm on a Wallac Victor3™ spectrometer. Cell number was measured using the Picogreen assay (Molecular Probes) for double-stranded DNA following the manufacturer's instructions as described previously.

3.2.5.1 Modification of vacuum loading method for cell loading on scaffolds

Due to poor penetration of cells to the scaffold interior and insignificant levels of alkaline phosphatase activity, a modification of the cell loading protocol was devised as described in Table 3.2.2.

Table 3.2.2: Modifications on the earlier used vacuum protocol

Modification	Previous method	Current method	Rationale
Cleaning scaffold	No cleaning method employed	Sonication + Baking	Cleaning particulate matter from the scaffold
Vacuum applied using	Vacutainer + syringe	Snap cap + tube syringe	
Cell suspension	1 x 10^6 cells in 10 µl of culture medium	20 x 10^6 cells in 200 µl of culture media	To enable better cell penetration within the scaffold

3.2.6 Evaluation of cell viability, distribution, morphology and osteogenic differentiation on the material using the modified vacuum loading protocol

3.2.6.1 Viability of cells on the material

The viability of cells on the material was assayed by using a two colour stain to simultaneously detect live and dead cells. The live/dead stain was prepared by adding 1 µl calcein (2 µM) and 4 µl of ethidium bromide (4 µM) to 1ml of PBS. The scaffolds were taken off the plates and then 120ul of live/dead stain was added directly to the scaffold. After 30 minutes of incubation with the live

dead stain the scaffolds were imaged on a confocal microscope (Zeiss LSM 510 Axiovert inverted confocal microscope).

3.2.6.2 Cell distribution

The scaffolds were transferred to a fresh plate, washed with PBS and fixed with 2.5% SEM grade glutaraldehyde and incubated at room temperature for 5 minutes. Then a series of alcohol (50 %, 75%, 80%, 90 % and 100 %) drying and a critical point drying step was conducted using hexamethyldisilazane (HMDS) for 30 minutes. Following overnight air drying, samples were gold sputter coated and imaged using a scanning electron microscope to assess cell distribution.

3.2.6.3 Alkaline phosphatase activity

Alkaline phosphatase activity of cell lysates from the scaffolds was measured as an indicator of osteogenesis. At days 3, 7 and 10 post osteogenic induction, the scaffolds were washed with PBS and 0.1% Triton –X in Tris HCl was added and the scaffolds were left to shake overnight at 4^0C. Next day the lysate was analysed for ALP using the kit obtained from Abcam.

3.2.6.4 Calcium quantification of monolayer controls

hMSCs (40,000 cells/ well of a 24 well plate) were kept as monolayer controls for the osteogenesis assay. At 12 days post induction, the wells (2 wells per condition) were washed with PBS twice. Cells from each well were then scraped in 200µl of 0.5M HCl and collected into an appropriately labeled Eppendorf tube. The tubes were shaken at 4^0C overnight. Following shaking, the samples were spun briefly to pellet cell debris. The calcium levels in the samples were quantified using the Stanbio kit as per the manufacturer's instructions. Briefly, standards ranging from 0 to 1 µg were prepared in 0.5M HCl. Standards were set up in triplicates from 0 to 1 µg were prepared in 0.5M HCl. Standards were set up in triplicates in wells of a microplate. Additionally; 10µl of samples were added in triplicate to three different wells of a microplate. Working solution (200µl, prepared in a 1:1 ratio of binding reagent and working dye) was then added to all the standards and samples. The absorbance was then read at 595 nm (Wallac Victor3™).

3.2.6.5 Alizarin red staining for monolayer controls

Additionally, 1 well per condition was stained for alizarin red to check for the presence of calcium. The wells were washed a couple of times with PBS and fixed in ice-cold 95% methanol for 10 minutes. The methanol was aspirated off and the wells were washed twice in dH_2O and then stained with 2% Alizarin Red S Solution for 5 minutes. Alizarin Red S solution was prepared by dissolving 2g Alizarin /red in 100 ml of dH_2O with pH adjusted to 4.1-4.3.The wells were then washed in dH_2O and later imaged using an Olympus BX51 upright microscope.

3.2.7 Bioreactor culture strategy

A dynamic culture system was employed to enhance fluid flow throughout the scaffold so as to allow for sufficient nutrient and waste exchange. Additionally, application of mechanical stimulation has been shown to enhance bone tissue formation.

3.2.8 Optimisation of cell seeding density

Firstly, $1x10^6$ hMSCs, $2x10^6$ hMSCs, and $5x10^6$ hMSCs were evaluated to determine the optimum seeding density under dynamic culture. Cell seeding efficiency was evaluated using the Picogreen assay by counting the number of cells remaining in the supernatant after seeding.

3.2.9 Seeding of cells on the scaffold using perfusion and assessment of cell loading

The culture medium was removed from the bioreactor and kept in a Falcon tube. Collagenase type II (0.3%) (8ml, Thermo Fisher Scientific) was then added and perfusion was started at a rate of 0.4ml/min. The collagenase was removed and kept in a separate Falcon tube. Trypsin (8 ml) was then added and perfusion was again started at a flow rate of 0.4ml/min for 10 minutes. Trypsin was then removed and kept in the same tube were collagenase was collected. The cell suspension was spun down at 1500 rpm for 4 minutes. The cells suspension was then resuspended in papain and left in a 60^0 C oven for a couple of hours. The lysate was then assayed using Picogreen kit for DNA analysis.

3.2.10 Evaluation of osteogenesis

Scaffolds were kept in proliferation medium for 1-week post seeding and then osteogenically induced as described in Section 3.2.5.

3.2.11 RNA isolation and QPCR

RNA Isolation

RNA was isolated from the lysed cells using an RNA Aqueous for PCR kit (Ambion, USA). Briefly, hMSCs were harvested by scraping in 200µl lysis/binding solution and vortexed. An equal volume of 64% ethanol was added and the solution was mixed gently by pipetting and then added to a filter cartridge and spun at 13,000rpm, 1min, RT and the eluent was discarded. Wash solution #1 was added (700µl) to the filter cartridge, spun at 13,000rpm, 1min, RT and the eluent was discarded. Wash solution #2/3 (500µl) was then added to the filter cartridge, spun at 13,000rpm, 1minutes, RT and the eluent was discarded. The above step was repeated twice. The empty filter cartridge was then spun at 13,000 rpm, 30 sec, RT. The filter cartridge was then transferred to a fresh collection tube and 50µl of heated elution solution was applied to the center of the filter and spun at 13,000rpm, 30s, RT. The eluent was retained. The above procedure was performed twice. To the eluent, 0.1 volume 10x DNAse Buffer and 1µl DNAse/100µl RNA solution was added and incubated at 37ºC for 15-30minutes.Following incubation, 0.1 volume DNAse inactivation reagent was added and incubated for 2 minutes at RT. The solution was mixed thoroughly throughout incubation and then spun at 13,000rpm, 1 minute, RT. The supernatant was then aliquoted into a freshly labeled tube and the concentration was measured using a Nanodrop (Thermo Scientific, NanoDrop 2000, and spectrophotometer). The RNA was stored at -80ºC until further use.

cDNA Synthesis

cDNA synthesis was achieved using the Improm II Reverse Transcription System (Promega).Briefly, 400 ng of RNA stock (concentrated if required using an RNA concentrator, in case of insufficient yield) and 1µl of random primers were made up to a final volume of 5µl using nuclease-free water.

Samples were heated in a thermocycler pre-heated to 70 °C for 5 minutes and then chilled to 4 °C for 5 minutes. To enable reverse transcription, the following components were added to each sample to a final volume of 20 µl: 4 µl of ImProm-II™ 5X Reaction Buffer, 0.16 µl of Recombinant RNasin® Ribonuclease Inhibitor (20 U/ml), 1 µl dNTPs (0.5 mM), 3.8µl of $MgCl_2$ (3 mM), 1 µl ImProm-II™ Reverse Transcriptase enzyme (200U/µl) and 5.06 µl of nuclease free water. For cDNA synthesis, samples were placed in a thermocycler set at 25 ^{0}C for 5 minutes, 42 ^{0}C for 60 minutes, 70 ^{0}C for 15 minutes and cooling to 4 ^{0}C. The resulting cDNA was stored at -20 ^{0}C until further use.

RT-PCR

qRT-PCR was performed in 10µl reactions. Master mix consisting of 5µl FG, Fast SYBR Master mix (Applied Biosystems), 0.3µl of Forward Primer (10 µM), 0.3µl of Reverse Primer (10 µM) and 2.4µl nuclease free water was made for each of the genes of interest(Table 3.2.4). The 8µl master mix was added to respective wells of a 96 well PCR plate. A 1:5 dilution of the cDNA was made of which 2µl was added to wells of the 96 well PCR plate. MicroAmp® Optical Adhesive Film (Applied Biosystems) was taped on top of the PCR plate and the plate was spun briefly. The PCR reaction was performed as per the following steps (Table 3.2.3) using the Applied Biosystems StepOne Plus PCR machine.

Table 3.2.3: PCR Reaction stages.

Stage	Temperature (^{0}C)	Duration	Cycle
Holding	95^{0}C	20 sec	
Cycling	95^{0}C	3 sec	40
	60^{0}C	30 sec	
Melt curve	95^{0}C	15sec	
	60^{0}C	1 minute	
	95^{0}C	15 sec	

Gene expression was calculated using the $2^{-\Delta\Delta Ct}$ method[241,242]. Average Ct was calculated for the genes of interest as well as the normalising gene (GAPDH). The ΔCT (Ct value for the gene of interest–Ct value for GAPDH) and $2^{-\Delta\Delta ct}$ were calculated for each sample. Gene expression was depicted as fold change with respect to monolayer controls on growth media.

Table 3.2.4: Primers used for qPCR

Primer name	Forward primer	Reverse primer
GAPDH	TGGGTGTGAACCATGAGAAGTATG	GGTGCAGGAGGCATTGCT
ALP	AACACCACCCAGGGGAAC	GTAGCTGTACTCATCTTCATAGGC
Runx2	GTGCCTAGGCGCATTTCA	GCTCTTCTTACTGAGAGTGGAAGG
BMP 2	AGGACCTGGGGAGCAGCAA	CACACGGCAGGCATACTCATC
COL1A1	CTGGACCTAAAGGTGCTGCT	GCTCCAGCCTCTCCATCTTT
IBSP	CGAATACACGGGCGTCAATG	GTAGCTGTACTCATCTTCATAGGC
Osteocalcin	GGCGCTACCTGTATCAATGG	TCAGCCAACTCGTCACAGTC

3.2.12 Calcium quantification for monolayer controls

Calcium quantification of monolayer controls was performed quantitatively using the Stanbio kit as described in section 3.2.11 and qualitatively using the alizarin red staining protocol as described in section 3.2.12.

3.2.13 Statistical analysis

GraphPad Prism® software Inc. was used for statistical analysis. Significance was evaluated using one-way or two-way ANOVA followed by Tukey post hoc analysis or an unpaired T-test. Error bars represent the mean ± standard deviation. *p*-values ≤0.05 were considered statistically significant.

3.3 RESULTS

3.3.1 Drop seeding enables better cell seeding efficiency and morphology compared to vacuum loading

Cells on the scaffolds were fixed and assessed for cell distribution by visualizing in the scanning electron microscope. Figure 3.3.1 shows cell attachment but poor distribution. Additionally, the cells appear stressed, indicating the need for a revised seeding strategy and cell seeding density.

While comparing the efficacy of the drip and vacuum loading protocols, the drip method enabled a significantly enhanced cellular retention (Figure 3.3.2 A) as well as distribution (Figure 3.3.2 B).

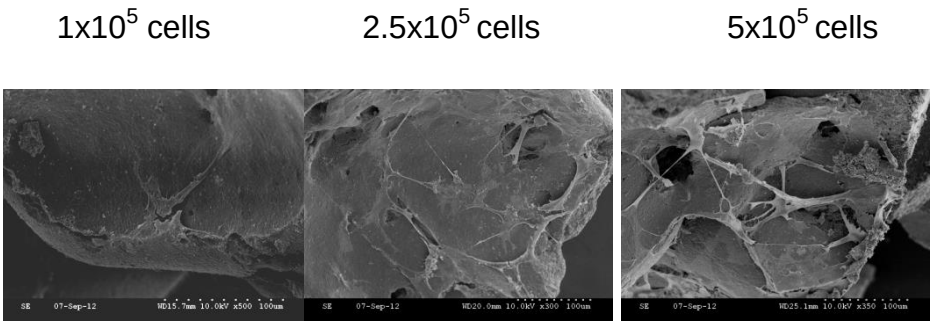

Figure 3.3.1: Morphological assessment of Cell loading efficacy by vacuum loading protocol by SEM imaging.

A

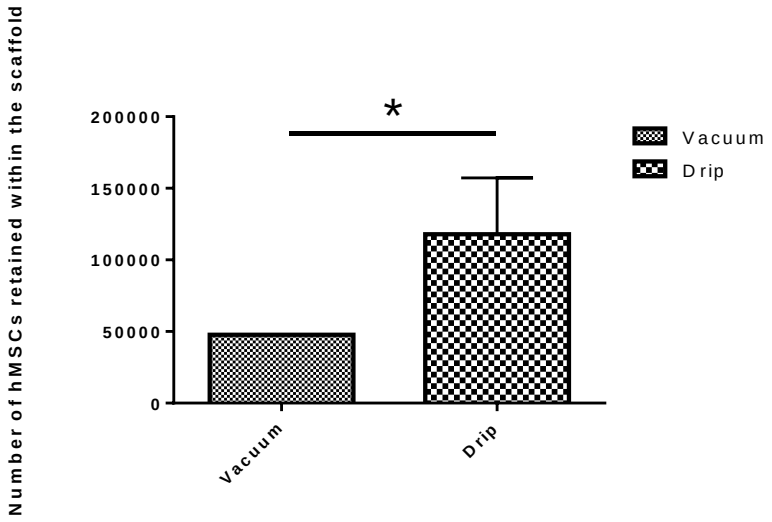

B

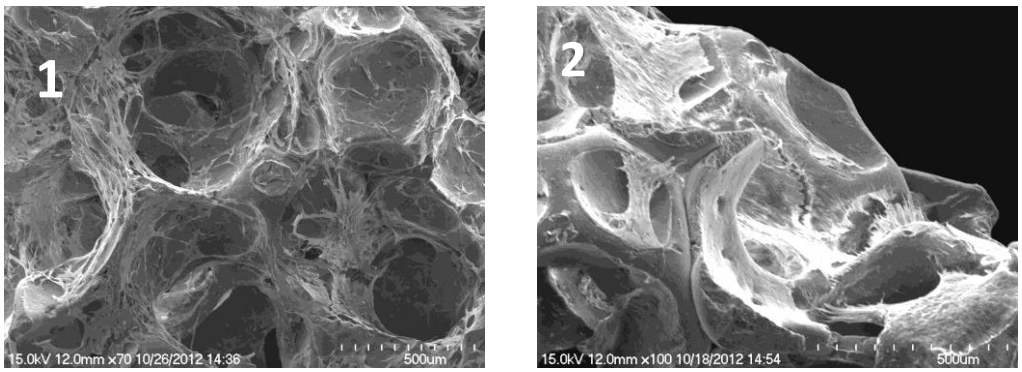

Figure 3.3.2: Cell loading efficacy comparison between drip and vacuum protocols. (A) A number of cells loaded onto the scaffold by assessment of DNA content of the cell lysates. Data represents mean ± SD for 3 Biosel scaffolds, Unpaired T-test analysis, ($^{*}p<0.05$).B) SEM images of scaffolds culture using drip protocol (1), 70X, Scale bar: 500µm and vacuum protocol (2), 100 X, Scale bar: 500µm.

3.3.2 Optimisation of cell seeding density

Outcomes tested

1. Cell distribution and osteogenic differentiation using scanning electron microscopy

2. Number of cells retained within the scaffold

3. Analysis of cell viability

Cell distribution

Cell distribution and osteogenic differentiation 21 days post osteogenic differentiation was used as the first outcome to determine optimum cell seeding density. As seen from the above images cell distribution is superior in scaffolds seeded with $1x10^6$ hMSCs compared to $0.5x10^6$ hMSCs. A thick deposit of extracellular matrix is seen in scaffolds induced with osteogenic media (Figure 3.3.3 A). The number of hMSCs retained with the scaffold was significantly increased in scaffolds seeded with $1x10^6$ hMSCs versus $0.5x10^6$ hMSCs at days 3 and 21 post-seeding (Figure 3.3.3 B).However, there were insignificant differences in cell viability in scaffolds seeded with $1x10^6$ hMSCs over $0.5x10^6$ hMSCs(Figure 3.3.3 C). However, only a maximum of 5% of the seeded hMSCs was retained with the scaffold and therefore the cell loading protocol needed to be revised again.

A

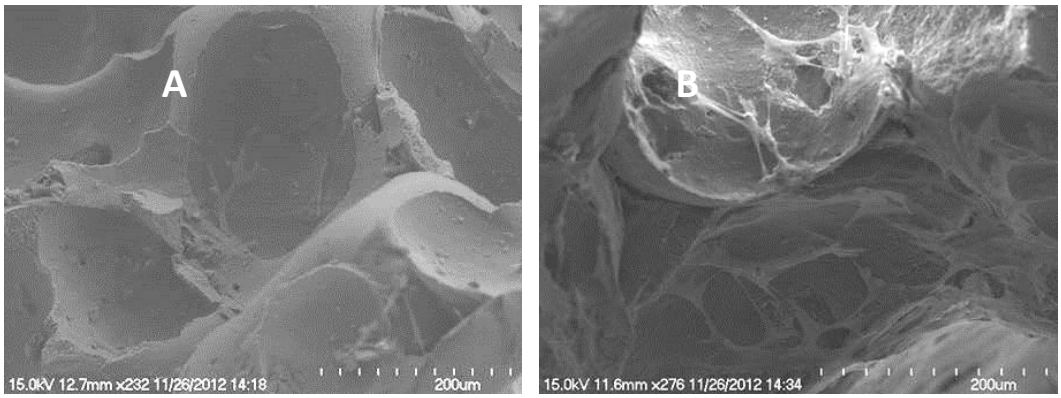

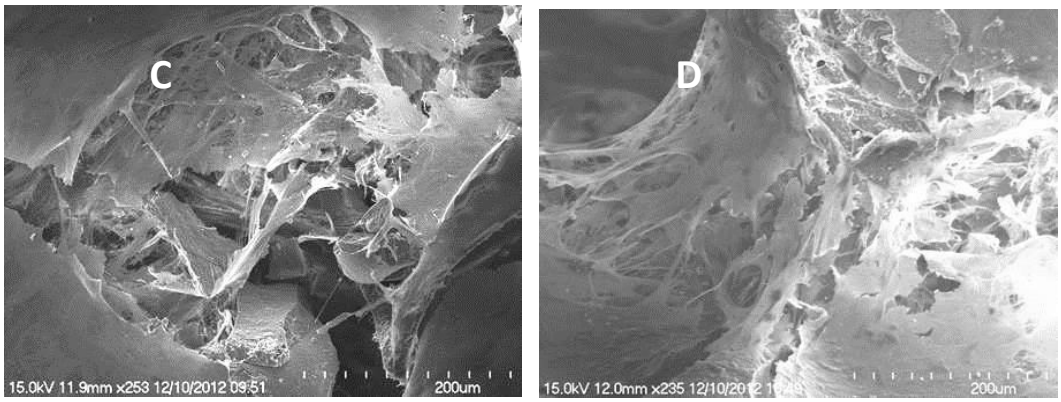

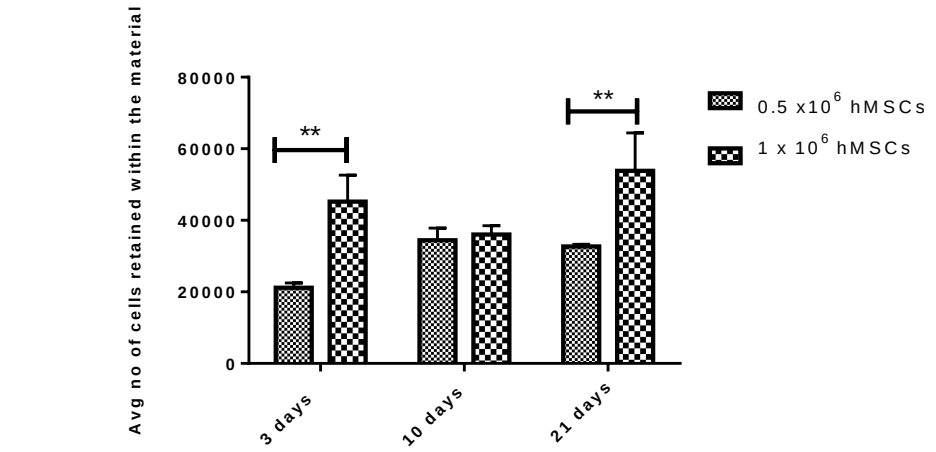

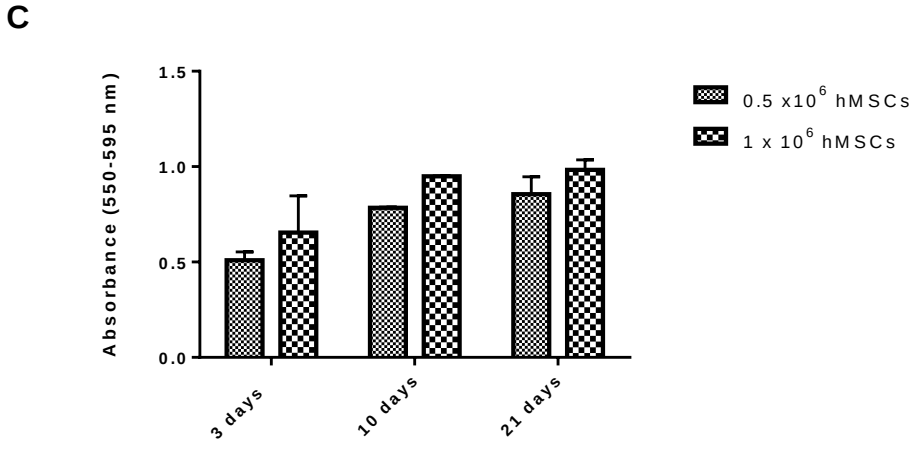

Figure 3.3.3: Optimal cell seeding density comparison between $0.5x10^6$and $1x10^6$ hMSCs (A) SEM images of scaffolds in culture 24 hours post seeding using $0.5x10^6$ (A) and $1x10^6$ hMSCs(B) and $0.5x10^6$ (C) and $1x10^6$ hMSCs (D) day 21 post osteogenic differentiation ,Scale bar, 200µm. (B) A number of cells loaded onto the scaffold by assessment of DNA content of the cell lysates.(C) The viability of loaded cells as determined by cell titer blue assay day 3,10 and 21 posts osteogenic differentiation. Data represents mean ± SD for 3 Biosel scaffolds, two-way ANOVA followed Tukey post hoc analysis,), ($^{**}p<0.05$).

3.3.3 Vacuum modified protocol

3.3.3.1 The modified vacuum protocol enabled superior cell distribution

As seen from the SEM images (Figure 3.3.4) there was a significant increase in the number of hMSCs using the modified protocol over the previous (Figure 3.3.2 B) drip protocol.

C

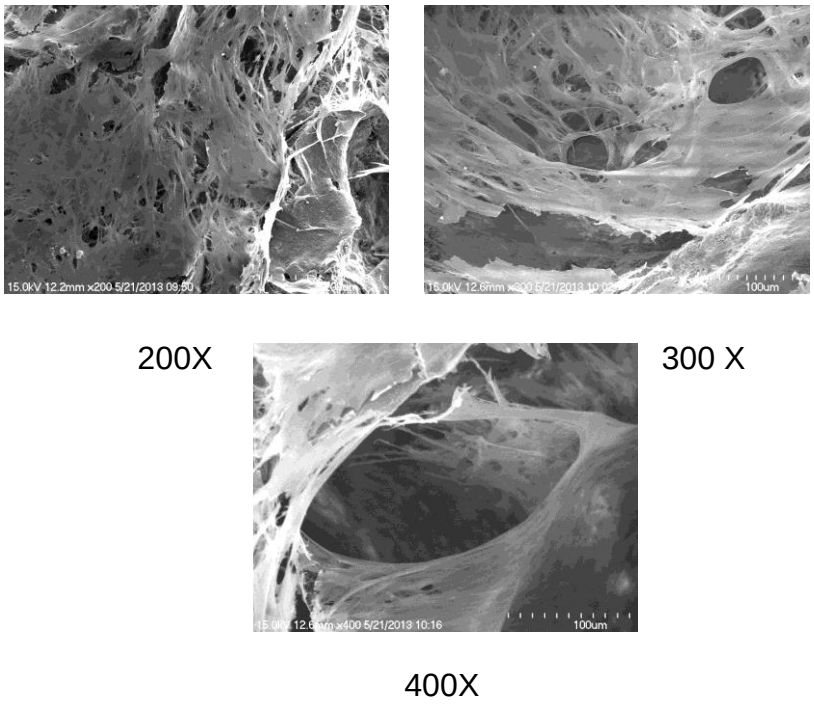

Figure 3.3.4: Analysis of cell distribution. SEM imaging 24 hours post seeding using the modified vacuum protocol. Scale bars, 100µm.

3.3.3.2 Viable cells prove the osteoconductivity of the Biosel scaffold

Imaging of scaffolds 10 days post osteogenic differentiation revealed apparent morphological differences between cells grown in growth media (GM) (Figure 3.3.5 A) and cells grown in osteogenic media (OM) (Figure 3.3.5 B). This qualitative analysis revealed mostly viable cells (representing the green cells) on the scaffold surface. Cells grown in GM showed the characteristic spindle shaped morphology of hMSCs, while cells that were osteogenically differentiated where characteristically cuboidal.

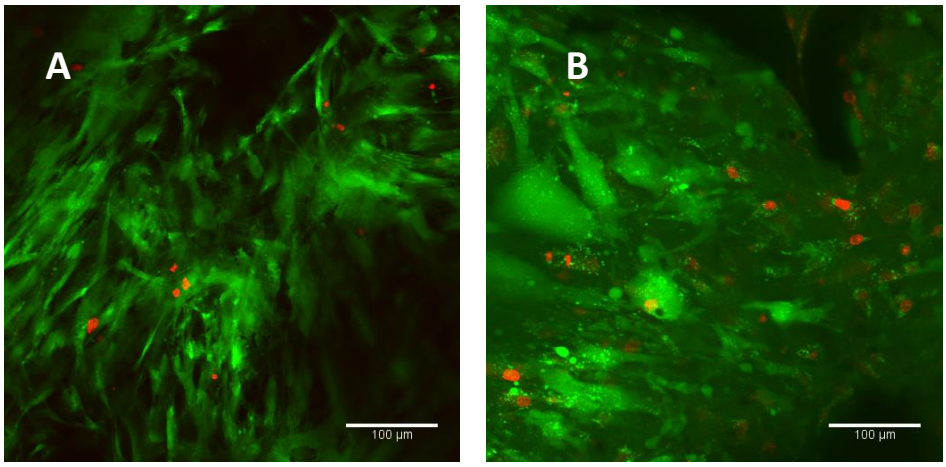

Figure 3.3.5: Cell viability and morphology assessment. A) Cells in GM and B) in OM 10 days post osteogenic differentiation. Green represents viable cells; Red represents dead cells. Scale bars, 100µm.

3.3.3.3 The Biosel scaffold did not significantly enhance ALP activity

Analysis of Alkaline phosphatase (ALP) activity, an early marker of bone formation, did not a show a significant increase in the scaffold groups (Figure 3.3.6). This is unexpected as the Biosel scaffold consists of constituents that are similar to native bone (HA and TCP, which drive osteogenic differentiation). A pilot study to evaluate ALP activity was performed using SaoS2 cell line as a positive control in order to demonstrate the efficacy of the ALP assay. Results indicate significantly increased ALP activity in scaffolds seeded with SaoS2 cells compared to hMSCs in either growth media or osteogenic media (Figure 3.3.7).

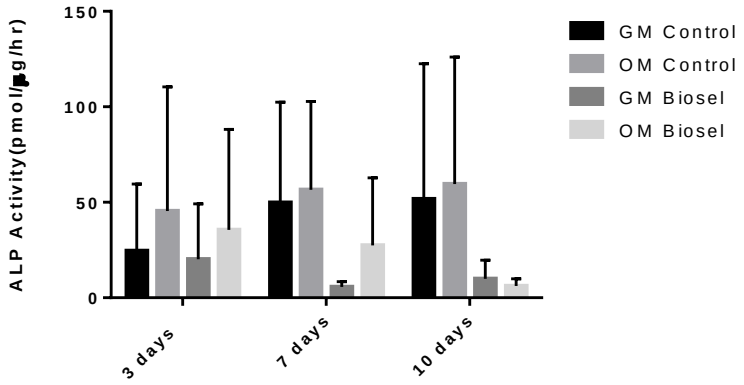

Figure 3.3.6: ALP quantification at 3, 7 and 10 days post osteogenic induction. Data represents mean ± SD for 3 hMSC donors per condition , Two-way ANOVA followed by Tukey post hoc analysis,($p>0.05$).

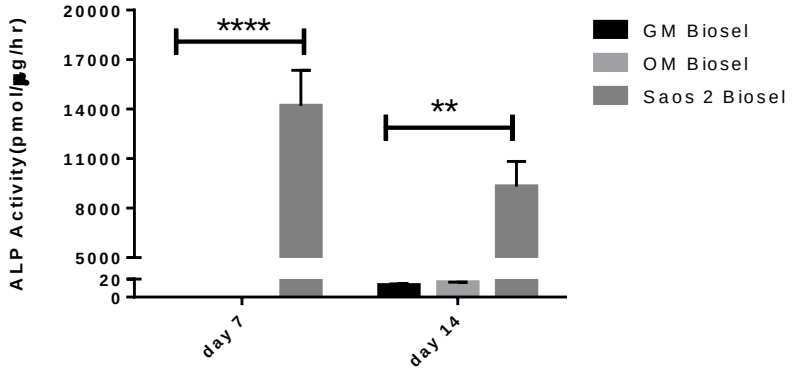

Figure 3.3.7: ALP quantification at day 7 and day 14 post osteogenic induction. Data represents mean ± SD for 3 hMSC donors per condition, two-way ANOVA and Tukey post hoc analysis, (**p<0.05), (****p<0.0001).

3.3.3.4 The Biosel supported cell proliferation and matrix production

Protein production over time was taken an indicator of growth and matrix production. Matrix production increased significantly from day 10 to day 14 in both osteogenic and growth media.

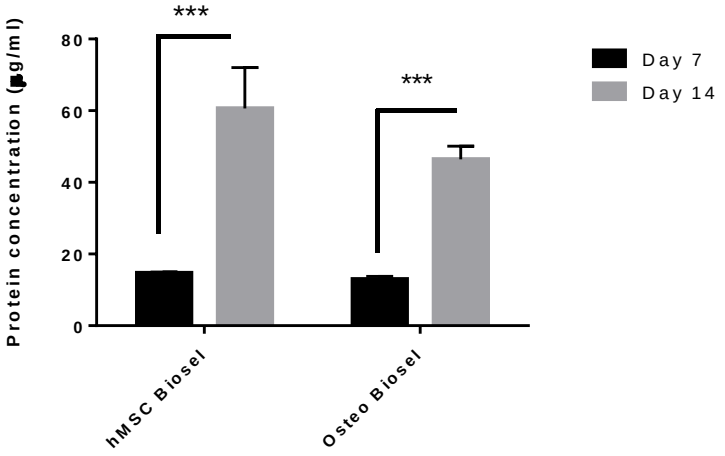

Figure 3.3.8: Protein production and matrix deposition at 7 and 14 days post osteogenic induction. A significant increase in protein production was observed from day 7 to day 14 under both growth and osteogenic medium. Data represents mean ± SD for 3 hMSC donors per condition , two--way ANOVA and Tukey post hoc analysis, p<0.001.

3.3.4 Calcium quantification and alizarin red staining demonstrate efficacy of the osteogenic induction protocol

Efficacy of osteogenic differentiation of monolayer controls demonstrated significant mineralization in test wells compared to controls, demonstrating the functionality of the osteogenic induction (Figure 3.3.9).

A

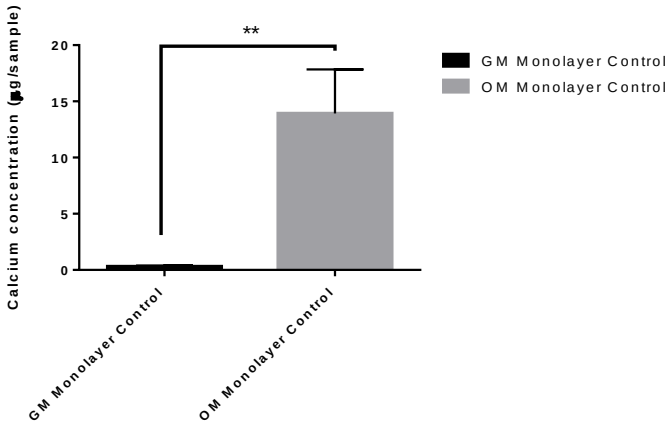

B

Alizarin red staining

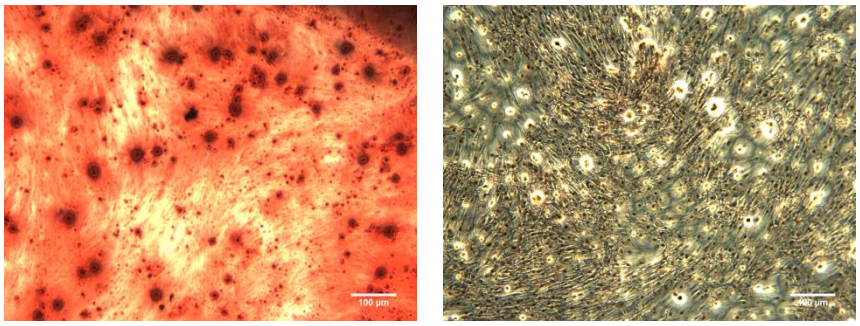

Figure 3.3.9: Calcium quantification of monolayer controls 14 days post osteogenic induction. A) A significant increase in calcium production was observed in cells cultured in the osteogenic medium compared to controls. Data represents mean ± SD for 3 hMSC donors per condition, Unpaired T-test analysis, ($^{**}p<0.05$).B) Qualitative staining of calcium using Alizarin red. Cells with osteogenic medium (left), Growth medium controls (right). Scale bars, 100µm.

3.3.5 **Cell loading efficiency under dynamic culture**

The cell loading efficiency of the Biosel scaffold was assayed by the picogreen DNA assay.Piccinini *et al* (2010)[243] reported the inadequacy of commonly used cell lysis methods with ceramic materials which invariably lead to their underestimation in standard quantitative assays. They show that ceramic materials bind to nucleic acids through polar interactions. However, this binding is reversible when a phosphate buffer containing a high phosphate concentration (800mM) along with an enzymatic extraction protocol is used to accomplish this. This method was shown to retrieve 95% DNA from the scaffolds. Therefore, the medium collected initially was also spun down at 1500 rpm for 4 minutes. The pellet was resuspended in papain and left in a 60^0 C oven for a couple of hours. The pellet was then assayed using the Picogreen DNA kit to quantify cells remaining in the medium. The highest cell retention was achieved using $5x10^6$ cells as indicated in (Figure 3.3.10). Additionally the scaffold exhibited plenty of viable cells on its surface. However, there were fewer cells in the scaffold centre as depicted by confocal images (Figure 3.3.11).

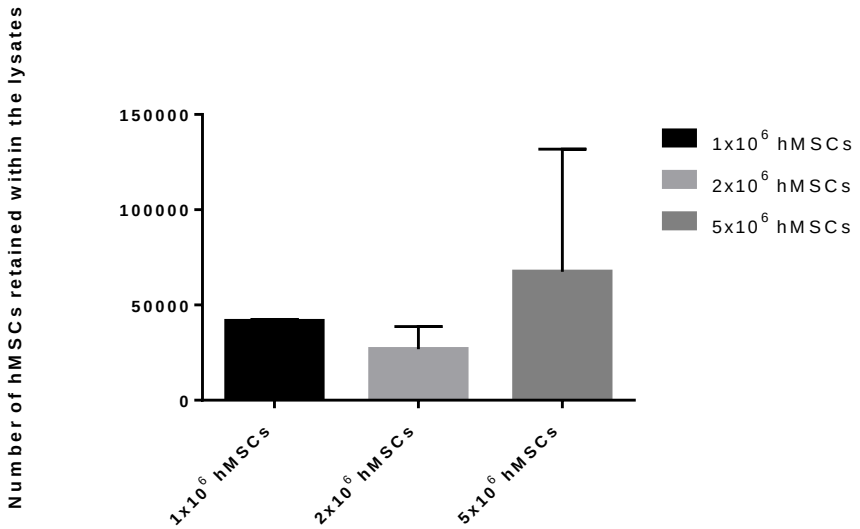

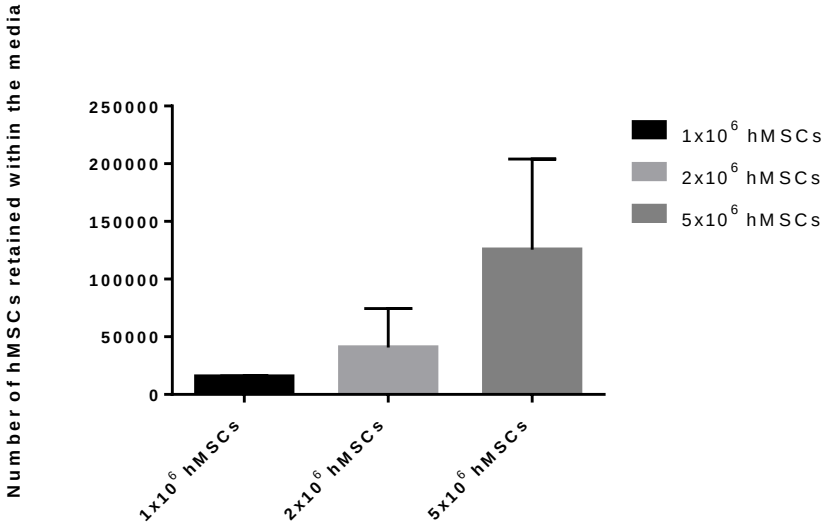

Figure 3.3.10: Cell loading efficacy under dynamic culture (A) Number of cells loaded onto the scaffold by assessment of DNA content of the cell lysates (B) Number of cells remaining in the media by cell count of media aliquots.

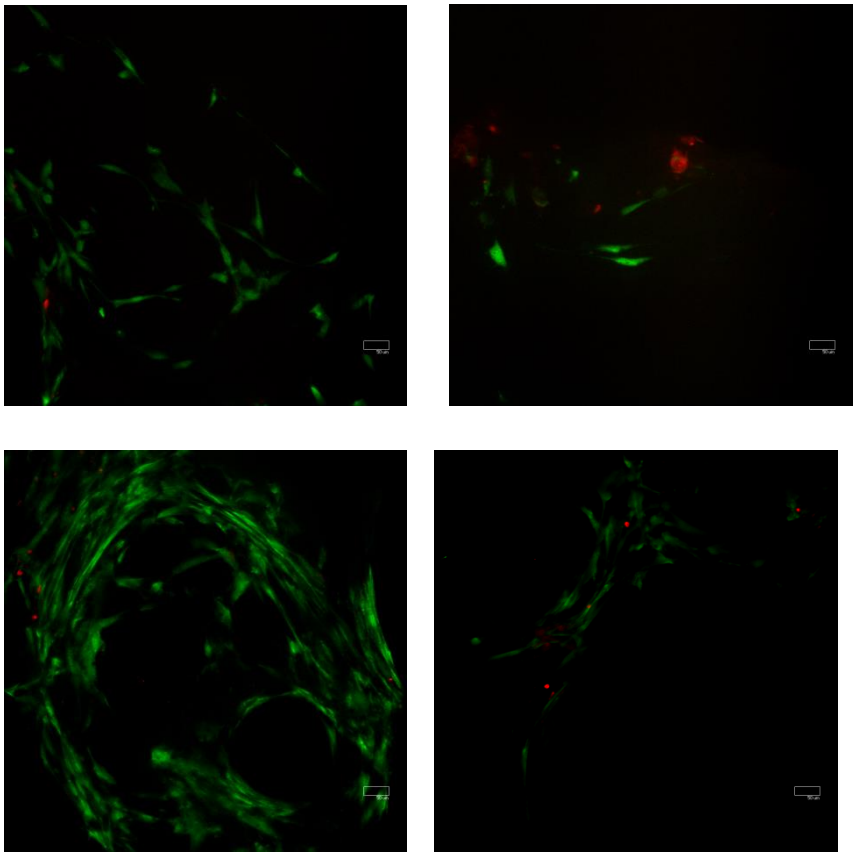

Figure 3.3.11: Cell viability and morphology assessment on the Biosel scaffold. Clockwise from left: Control (GM) Biosel surface, Control (GM) Biosel cut at the center, Test (OM) Biosel scaffold cut at the center, Test (OM) Biosel surface 10 days post osteogenic differentiation Green represents viable cells; Red represents dead cells.

3.3.6 Dynamic culture conditions did not enhance osteogenic gene expression

Gene expression of key osteogenic markers- RUNX 2, COL1A1 and IBSP was significantly upregulated only in the control samples. Although the osteogenically differentiated constructs displayed an increase in gene expression of ALP, RUNX 2 AND BMP 2, the increases were not significant (Figure 3.3.12).

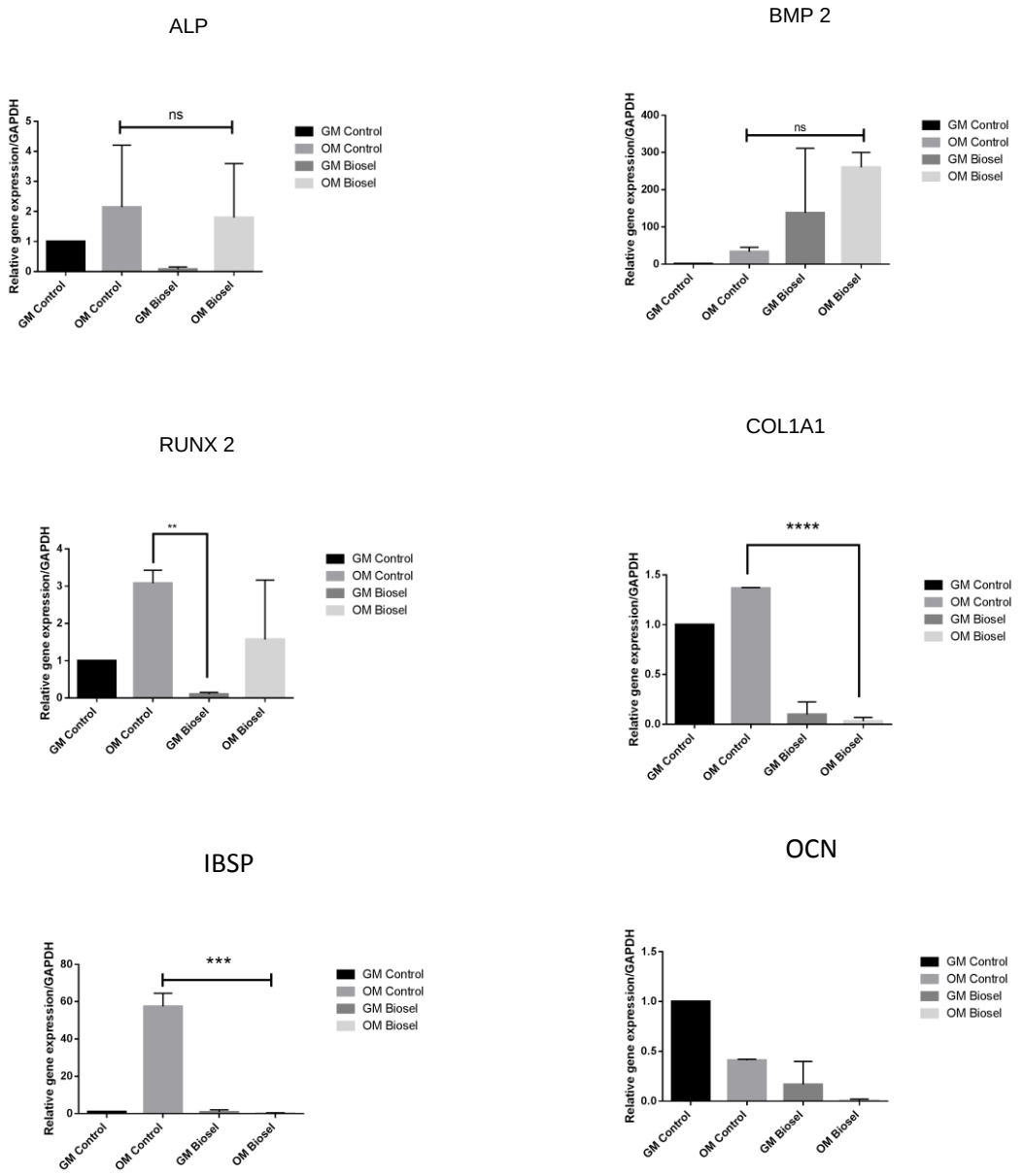

Figure 3.3.12: Effect of Perfusion culture on the expression of osteogenic gene expression: hMScs in Biosel and monolayer culture were differentiated along the osteogenic lineage. The cells were harvested, RNA was isolated and gene expression of ALP, COL1A1, IBSP, OCN (Osteocalcin) was assessed by real -time PCR. Expression levels were normalised to the corresponding GAPDH transcript levels and then normalised to GM Controls. Data represents mean ± SD for 3 hMSC donors per condition, one-way ANOVA and Tukey post hoc analysis, (*p<0.05), (**p<0.05), (****p<0.0001)

3.3.7 Calcium quantification and alizarin red staining prove the efficacy of the osteogenic induction protocol

Efficacy of osteogenic differentiation of monolayer controls demonstrated significant mineralization in test wells compared to controls, demonstrating the functionality of the osteogenic induction (Figure 3.3.13).

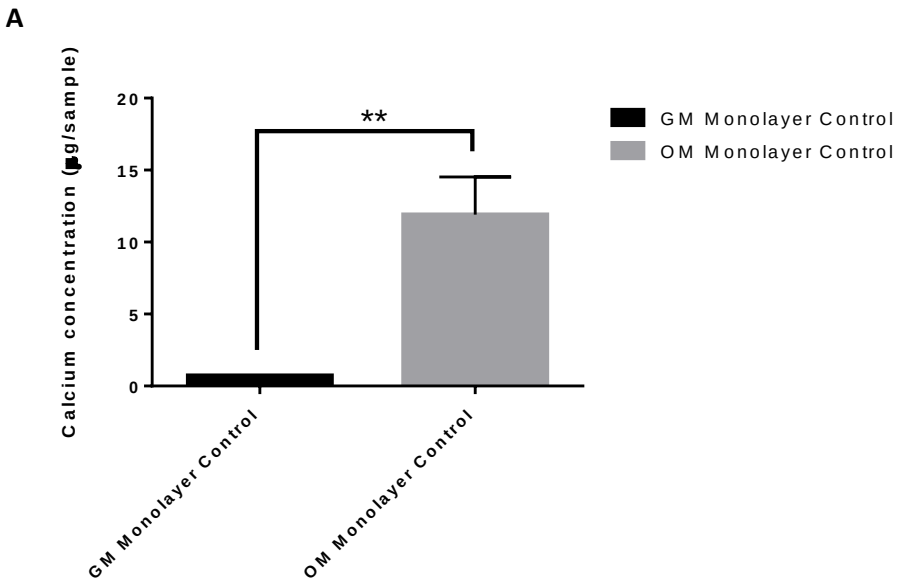

B

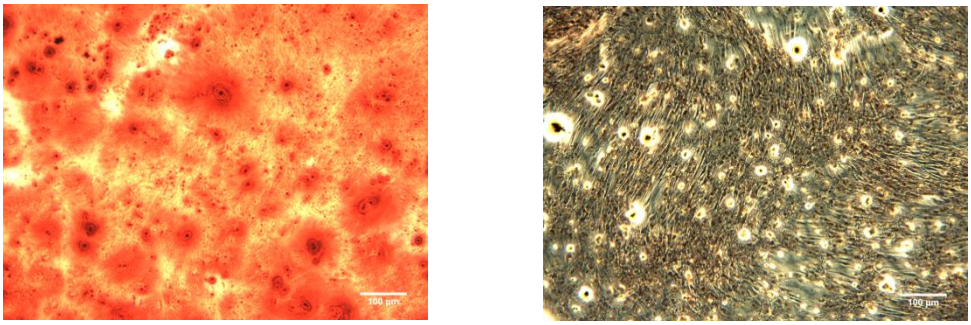

Figure 3.3.13: Calcium quantification of monolayer controls 14 days post osteogenic induction. A) A significant increase in calcium production was observed in cells cultured in osteogenic medium compared to controls. Data represents mean ± SD for 3 hMSC donors per condition, Unpaired T-test analysis, ($^{**}p<0.05$).B) Qualitative staining of calcium us using Alizarin red. Cells with osteogenic medium (left), Growth medium controls (right). Scale bars, 100µm.

3.4 DISCUSSION

Biosel was selected as the first candidate material of study due to the company collaboration of DePuy in this project. Further, Biosel has been used clinically[244] as well as animal models[245] with some success.

In the early phase of the study, the seeding protocol was optimized together with the cell seeding density. Based on literature search for scaffolds made of same materials, the following cell densities were tested: $1x10^5$ hMSCs/scaffold, $2.5x10^5$ hMSCs/scaffold and $5x10^5$ hMSCs/scaffold[240](Figure 3.3.1). A previously used vacuum loading protocol was used to load cells. However, the cells appeared stressed and were sparsely distributed throughout the scaffold (Figure 3.3.1). Therefore both the cell loading strategy and cell seeding density needed to be re-optimised. The vacuum loading protocol was compared against a drip seeding strategy. It was found that there was significant cell retention using the drip seeding strategy compared to the vacuum loading strategy as assessed by the Picogreen assay (Figure 3.3.2) .

Cell seeding densities of $0.5x10^6$ and $1x10^6$ hMSCs / scaffold were analysed per scaffold. As expected there was superior cell distribution and significant cell retention over time on scaffolds seeded with $1x10^6$ hMSCs compared to $0.5x10^6$ hMSCs (Figure 3.3.3). However, there was only 5% cell retention on the scaffold. Therefore, the vacuum loading protocol had to be revised. The vacuum modified protocol involved seeding $5x10^6$ hMSCs in 200µl to enable $1x10^6$ hMSCs in 10µl media to penetrate the scaffold. The cell number and distribution compared to the earlier vacuum protocol and drip protocol was significantly enhanced as observed by SEM images. Analysis of cell viability and morphology using live/dead staining 10 days post osteogenic differentiation revealed significant viable cells throughout the scaffold surface. Additionally, morphological differences between hMSCs and differentiated hMSC scaffold groups were apparent. While hMSCs exhibited the classic fibroblastic, the differentiated group exhibited cuboidal structures characteristic of osteoblasts (Figure 3.3.5). ALP activity analysis was used to quantitatively determine osteogenic differentiation[246] (Figure 3.3.6) . Although

there was an increased expression in ALP in the osteogenically differentiated groups, differences between groups was insignificant.

To determine the efficacy of the ALP assay, Saos 2 cells of the same density were also seeded onto the Biosel scaffold and activity was compared to osteogenically differentiated and undifferentiated hMSCs. SaoS 2 cells exhibited significant increases in ALP activity at day 7 and day 14 compared to the other groups, indicating assay efficacy (Figure 3.3.7). Protein production was taken as a read out to measure cell proliferation and matrix production on the Biosel scaffold. An increased protein production was observed over time in both differentiated and osteogenically differentiated groups, showing the ability of the Biosel scaffold to support cell proliferation (Figure 3.3.8).

Osteoinductivity of the material refers to the property of the material that is able to bring about recruitment and osteogenic differentiation of cells seeded on to it. A study by Ogata *et al*.,[247] using an MC3T3-E1 osteoblastic cell line observed a greater level of osteogenesis on HA/soluble calcium phosphate (a novel material with improved solubility).However, Osteoinductivity of a material can be more stringently analysed by use of mesenchymal stem cells as used in our study rather than osteoblastic cell lines like MC3T3-E1 and MG63.

As a means to enhance cell penetration and osteogenic differentiation of the Biosel scaffold, application of mechanical stimulation by use of dynamic cell culture using a bioreactor was explored. Yang *et al*., (2014) [248]evaluated the potential of four candidate scaffolds: HA/TCP composites, porous PU foam, PLGA/PCL electrospun fibers and collagen I gel. They observed different efficiencies in cell seeding among the various tested scaffolds, with the HA/TCP scaffolds displaying the least efficacy. Interestingly, the HA/TCP composites used in their study had similar dimensions and composition as the Biosel scaffold. They circumvent this problem by culturing MSCs for a week in proliferation medium and then switch to differentiation medium. Consequently, for the bioreactor study we cultured the scaffolds in hMSC growth medium before changing to osteogenic medium.

The scaffold surface contained viable cells on the surface, however, viable but reduced number of cells was present on the scaffold interior (Figure 3.3.11). Additionally, osteogenic gene expression of most genes was significantly higher in monolayer controls compared to the scaffolds (Figure 3.3.13). Overall, the u-cup bioreactor provided effective cell loading as noted by a negligible number of cells in the media. However, it was observed that there was low cell penetration at the scaffold interior in comparison to the well-distributed exterior. In both static and dynamic culture, high cell viability was observed, validating the suitability of the scaffold for cell growth. In this chapter the ability of the HA/TCP biphasic scaffold to support attachment, proliferation and osteogenic differentiation of hMSCs was evaluated. For perfusion cultures to work effectively, the scaffolds need to possess mechanical stability and porosity. Holtorf *et al*., (2005)[249] showed that scaffolds with larger pore sizes displayed early differentiation towards the osteogenic lineage while smaller pore sizes showed delayed differentiation. The Biosel scaffold exhibited pore sizes of unequal size which could result in altered fluid flow to the interior of the scaffold and could have impacted their osteogenic differentiation capabilities. Barrades *et al*., [179]compared the osteoconductive potential of HA and β-TCP and demonstrated greater bone formation with β-TCP. Their data was in agreement with *in vitro* conditions wherein greater expression of osteopontin, osteocalcin, and bone sialoprotein was observed when cultured on β-TCP over HA. Additionally, they observed differences in morphology of cells 24 hours post seeding with more prominent attachment and spreading on β-TCP than on HA. A study by Bancroft *et al*., (2002)[250] tested the effects of different flow rates on the differentiation capacity of marrow stromal osteoblasts, seeded on 3D scaffolds. They found improved mineralization under the different flow rates compared to static controls. Additionally, they found increased calcium content with increase in flow rate. Fluid flow also encouraged homogenous cell and matrix distribution throughout the scaffold.

The insufficient cell penetration at the scaffold interior as depicted by confocal imaging raises questions about the scaffold porosity. Additionally proliferating cells on the scaffold surface could have limited oxygen diffusion to cells at the

interior of the scaffold. It is well known that a hypoxic environment favours chondrogenesis by stimulating Sox-9 [251]through an HIF-1α dependent mechanism. However, hypoxia limits osteognesis and this could explain the downregulation of all osteogenic markers on cells cultured on the Biosel scaffold.

3.5 Chapter summary:

In this study we evaluated the osteoconductive and osteoinductive properties of the Biosel scaffold. These properties were evaluated in both static and dynamic cell culture conditions. The Biosel scaffold supported cellular attachment (as depicted by SEM imaging) and proliferation (as depicted by SEM imaging, DNA analysis and protein production).The Biosel scaffold supported hMSC osteogenesis- as depicted qualitatively by morphological differences in confocal imaging. However, the scaffold did not significantly drive osteogenesis in quantitative assays evaluating ALP activity or osteogenic gene expression. The material displayed insufficient cell penetration at its interior (even under dynamic cell culture conditions) – raising doubts about its porosity. Therefore the use of the Biosel as an osteoinductive material was brought into question.

The subsequent study was conducted on hMSCs seeded on HA/TCP particles as the second candidate material for evaluation of osteogenesis.

CHAPTER 4: ANALYSIS OF CELL VIABILITY, OSTEOCONDUCTIVITY AND OSTEOINDUCTIVITY OF hMSCs LOADED ONTO HA/TCP MBCP GRANULES AND FIBRIN SEALANT

4.1 INTRODUCTION

Fibrin sealants are cytocompatible and resorbable materials. The fibrinogen when mixed with thrombin (containing human thrombin plus a solution of calcium chloride), is converted to fibrin (this process is felicitated by calcium ions in the thrombin). The combination of ceramic and sealant may have greater mechanical strength than ceramic alone[252]. Additionally, the sealant encourages cell attachment and growth.[253,254]

Further, the sealant plays a role in vascularisation and ingrowth of blood vessels which positively influence bone growth[255]. As mentioned earlier, vascularisation is critical to bone formation. A range of biomaterials such as coral, bone-derived materials, glass ceramics and calcium phosphate have been combined with fibrin sealant to take advantage of biological characteristics of both constituents. Although this combination has produced variable results, they are routinely used in orthopedic surgery because of their ease in handling[252]. Bluteau *et al*.[256] in order to clarify discrepancies with the use of fibrin in osteogenic differentiation, studied the effects of the concentration of the thrombin component on osteogenic differentiation. They propose that thrombin concentrations of 0.5-5 U/ml increased ALP gene expression whereas concentrations of 50-100U/ml decreased ALP gene expression and PTH/PTHrP receptor, while increasing expression of OPG (an osteoclastogenesis inhibitor). However, higher thrombin concentrations increased expression of VEGF-A and VEGF-B and their respective receptors while low thrombin concentrations increased expression of VEGF-B and its receptor. The authors suggest the use of thrombin at lower concentrations as a means to benefit from the effects of both osteogenesis and angiogenesis.

In this study we evaluated the use of $MBCP^+$ granules (Biomatlante, France) of a HA/TCP ratio of 20/80 in contrast to the Biosel (DePuy Synthes) which had a higher content of the HA component. Arinzeh *et al*., (2004)[257] compared the osteoinductive potential of different HA/TCP ratios in order to determine the ideal ratio of HA/TCP necessary to achieve bone formation and complete degradability. In an ectopic mouse model, fastest hMSC bone

formation was observed when cultured with 20% HA/ 80% TCP in comparison to 100% HA, HA/TCP ratios of 76/24, 63/37, 56/44 and 100% TCP. Additionally, they found superior osteoinductivity *in vitro* on 20/80 HA/TCP over 60/40 HA/TCP in the absence of osteoinductive media as measured by osteocalcin production.

Chapter specific aims:

1. Evaluate MSC loading efficacy, proliferation and viability on the MBCP+ scaffold.
2. Evaluate the osteoconductive and osteoinductive properties of the MBCP+ scaffold.

4.2 MATERIALS AND METHODS

4.2.1 Loading of hMSCs into MBCP+ microporous scaffolds

The MBCP+ particles (Biomatlante, France) (HA: TCP ratio of 20:80) were divided into 50 mg fractions in microcentrifuge tubes. Following cell enumeration, 1 x 10^6 cells was resuspended in 400 µL culture medium (α-MEM, 10% FBS and 1% penicillin/streptomycin).hMSCs were added to the microcentrifuge tubes containing MBCP+ granules. The cell-loaded constructs were centrifuged at 200xg for 1 minute. The hMSC/scaffold particle mixture was incubated for 90 minutes at 37°C, while slowly rotating every 15 minutes. The supernatant was removed and assessed for unbound cells prior to encapsulation. Fibrin sealant (Tisseel Lyo, Baxter) was prepared according to the manufacturer's directions. Briefly, components (fibrinogen and thrombin) were pipetted out and stored at -20 until use. Just before use, the components were heated for 3minutes at 37 degrees C before adding to the hMSC/MBCP mixture. To the microcentrifuge tubes containing the mixture of MSCs and MBCP+ granules, 15 µL of fibrinogen, followed immediately by 15 µL of thrombin was added. The hMSC/Sealant/Scaffold mixture was left to solidify for 1 h in a 37^0C, 5% CO_2 incubator, after which the constructs were inverted 180° and 10 µL of fibrinogen and 10 µL of thrombin were added and again allowed to incubate for 1 hour 37^0C, 5% CO_2.The scaffolds were then transferred to a non-adherent plate containing hMSC media. In parallel, to demonstrate the efficiency of osteogenic induction, 40,000 hMSC's were

plated per well of a 24 well plate for a total of 6 wells (Figure 4.2.1). Following 48 hour post cell seeding on scaffolds, test scaffolds were induced with osteogenic media. Additionally test wells in the monolayer were also induced with osteogenic media.

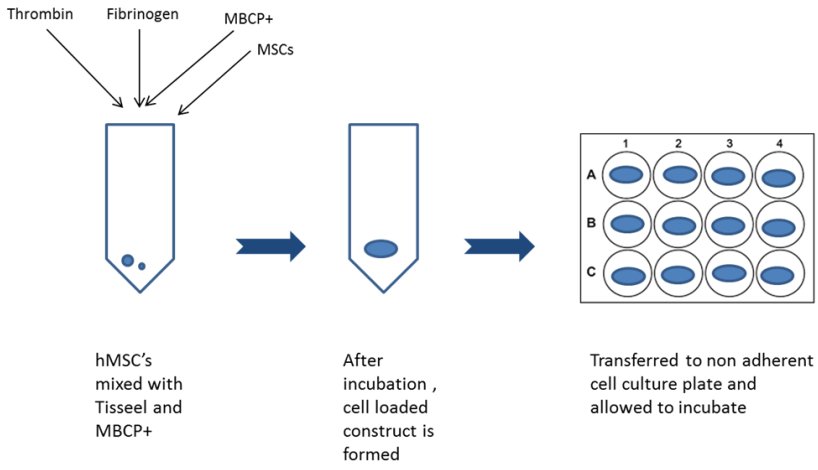

Figure 4.2.1: Overview of procedure involved in loading hMSCs on MBCP +/fibrin construct

4.2.2 Cell viability assessment

The viability of cells on the material was assayed by using a Live/Dead viability/cytotoxicity kit (Molecular Probes) to simultaneously detect live and dead cells. The live/dead stain was prepared by adding 1µl calcein (2 µM) and 4 µl of ethidium bromide (4 µM) to 1ml of PBS. The scaffolds were taken off the plates and then 120 µl of live/dead stain was added directly to the scaffold. Following 30 minutes incubation with the live dead stain, the scaffolds were imaged on a confocal microscope (Olympus Fluoview 1000 confocal microscope).

4.2.3 Alkaline phosphatase activity

Alkaline phosphatase activity of cell lysates from the scaffolds was used as an indicator of osteogenesis. At day 7 post osteogenic induction, the scaffolds were washed with PBS and 0.1% Triton –X in Tris HCL was added and the scaffolds were left to shake overnight at 4^0 C. Next day the lysate was analysed from ALP kit using the kit obtained from Abcam. Briefly, 10 µl of ALP enzyme was added to 1mM pNPP standard wells in a microplate. Alongside, 50µl of 5mM pNPP solution was added to test samples. The reactions were incubated for 60 minutes at 25^0C in the dark, following which 20µl of stop

solution was added to test and standard wells. The OD was measured at 405 nm using a Wallac Victor3™ 1420 Multilabel Counter spectrophotometer and a standard curve was used to quantify the levels of ALP. The obtained values were normalised to total protein quantified from the same lysates using Coomassie (Bradford) protein assay kit (Thermo Scientific, USA) as described previously.

4.2.4 RNA isolation and QPCR

RNA Isolation

RNA was isolated from the lysed cells using an RNA Aqueous for PCR kit (Ambion, USA). Briefly, hMSCs were harvested by scraping in 200µl lysis/binding solution and vortexed. An equal volume of 64% ethanol was added and the solution was mixed gently by pipetting and then added to a filter cartridge and spun at 13,000rpm, 1 minute, RT and the eluent was discarded. Wash solution #1 was added (700 µl) to the filter cartridge, spun at 13,000rpm, 1minute, RT and the eluent was discarded. Wash solution #2/3 (500µl) was then added to the filter cartridge, spun at 13,000rpm, 1minute, RT and the eluent was discarded. The above step was repeated twice. The empty filter cartridge was then spun at 13,000rpm, 30 sec, RT. The filter cartridge was then transferred to a fresh collection tube and 50µl of heated elution solution was applied to the center of the filter and spun at 13,000rpm, 30 sec, RT. The eluent was retained. The above procedure was performed for a total of two times. To the eluent, 0.1 volume 10x DNAse Buffer and 1µl DNAse/100µl RNA solution was added and incubated at 37ºC for 15-30minutes.Following incubation, 0.1 volume DNAse inactivation reagent was added and incubated for 2 minutes at RT. The solution was mixed thoroughly throughout incubation and then spun at 13,000rpm, 1minute, RT. The supernatant was then aliquoted into a freshly labeled tube and the concentration was measured using a Nanodrop (Thermo Scientific, NanoDrop 2000, and spectrophotometer). The RNA was stored at -80ºC until further use.

cDNA Synthesis

cDNA synthesis was achieved using the Improm II Reverse Transcription System (Promega).Briefly, 400 ng of RNA stock (concentrated if required

using an RNA isolation) and 1µl of random primers were made up to a final volume of 5µl using nuclease-free water. Samples were placed in a thermocycler pre-heated to 70 °C for 5 minutes and then chilled to 4 °C for 5 minutes. To enable reverse transcription, the following components were added to each sample to a final volume of 20 µl: 4 µl of ImProm-II™ 5X Reaction Buffer, 0.16 µl of Recombinant RNasin® Ribonuclease Inhibitor (20 U/ml), 1 µl dNTPs (0.5 mM), 3.8µl of $MgCl_2$ (3 mM), 1 µl ImProm-II™ Reverse Transcriptase enzyme (200U/µl) and 5.06 µl of nuclease free water. For cDNA synthesis, samples were placed in a thermocycler set at 25 ^{0}C for 5 minutes, 42 ^{0}C for 60 minutes, and 70 ^{0}C for 15 minutes and cooling to 4 ^{0}C. The resulting cDNA was stored at -20 ^{0}C until further use.

RT-PCR

qRT-PCR was performed in 10µl reactions. Master mix consisting of 5µl FG, Fast SYBR Master mix (Applied Biosystems), 0.3µl of Forward Primer (10 µM), 0.3µl of Reverse Primer (10 µM) and 2.4µl nuclease free water was made for each of the genes of interest.The 8µl master mix was added to respective wells of a 96 well PCR plate.A 1:5 dilution of the cDNA was made of which 2µl was added to wells of the 96 well PCR plate. MicroAmp® Optical Adhesive Film (Applied Biosystems) was taped on top of the PCR plate and the plate was spun briefly. The PCR reaction was performed as per the following steps (**machine.**

Table 4.2.1) using the Applied Biosystems StepOne Plus PCR machine.

Table 4.2.1: PCR Reaction stages

Stage	Temperature (^{0}C)	Duration	Cycle
Holding	95^{0}C	20 sec	
Cycling	95^{0}C	3 sec	40
	60^{0}C	30 sec	
Melt curve	95^{0}C	15 sec	
	60^{0}C	1 minute	
	95^{0}C	15 sec	

Gene expression was calculated using the The $2^{-\Delta\Delta Ct}$ method[241,242]. Average Ct was calculated for the genes of interest as well as the normalising gene (GAPDH). The ΔCT (Ct value for the gene of interest–Ct value for GAPDH) and $2^{-\Delta\Delta ct}$ were calculated for each sample .Gene expression was depicted as fold change with respect to monolayer controls in growth media.

Table 4.2.2 Primers used for qPCR

Primer name	Forward primer	Reverse primer
GAPDH	TGGGTGTGAACCATGAGAAGTATG	GGTGCAGGAGGCATTGCT
ALP	AACACCACCCAGGGGAAC	GTAGCTGTACTCATCTTCATAGGC
Runx2	GTGCCTAGGCGCATTTCA	GCTCTTCTTACTGAGAGTGGAAGG
BMP 2	AGGACCTGGGGAGCAGCAA	CACACGGCAGGCATACTCATC
COL1A1	CTGGACCTAAAGGTGCTGCT	GCTCCAGCCTCTCCATCTTT
IBSP	CGAATACACGGGCGTCAATG	GTAGCTGTACTCATCTTCATAGGC
Osteocalcin	GGCGCTACCTGTATCAATGG	TCAGCCAACTCGTCACAGTC

Calcium quantification

Two weeks post induction; the wells (2 wells each condition) were washed with PBS (twice). Cells from each well were then scraped in 200µl of 0.5M HCl and collected into an appropriately labeled Eppendorf tube. The tubes were shaken at 4^0C overnight. Following shaking, the samples were spun briefly to pellet cell debris. The calcium levels in the samples were quantified using the Stanbio kit as per the manufacturer's instructions. Briefly, standards ranging from 0 to 1 µg were prepared in 0.5M HCl. Standards were set up in triplicates in wells of a microplate. Additionally, 10µl of samples were added in triplicate to three different wells of a microplate. Working solution (200µl) (Prepared in a 1:1 ratio of binding reagent and working dye) was then added to all the standards and samples. The absorbance was then read at 595 nm (Wallac Victor3™).

Alizarin red staining

One well per condition was stained for alizarin red to check for the presence of calcium. The wells were washed a couple of times with PBS and fixed in ice-cold 95% methanol for 10 min. The methanol was aspirated off and the wells were washed twice in dH_2O and then stained with 2% Alizarin Red S

Solution for 5 minutes. Alizarin Red S solution was prepared by dissolving 2g Alizarin /red in 100 ml of dH_2O with pH adjusted to 4.1-4.The wells were the washed in dH_2O and later imaged in using an Olympus BX51 upright microscope.

Statistical analysis

GraphPad Prism® software Inc. was used for statistical analysis. Significance was evaluated using one-way or two-way ANOVA followed by Tukey post hoc analysis or unpaired T test analysis. Error bars represent the mean ± standard deviation. *p*-values ≤0.05 were considered statistically significant.

RESULTS

Efficiency of cell loading on the MBCP/Tisseel construct

Cell loading efficiency was determined by cell enumeration in the media sample prior to encapsulation. Cell loading efficiency was close to 100% across all donors. Additionally it was noted that scaffolds cultured in GM (hMSC growth media) began to disintegrate in culture while scaffolds in OM (Osteogenic differentiation media) remained intact in three independent experiments (Figure 4.2.2).

A

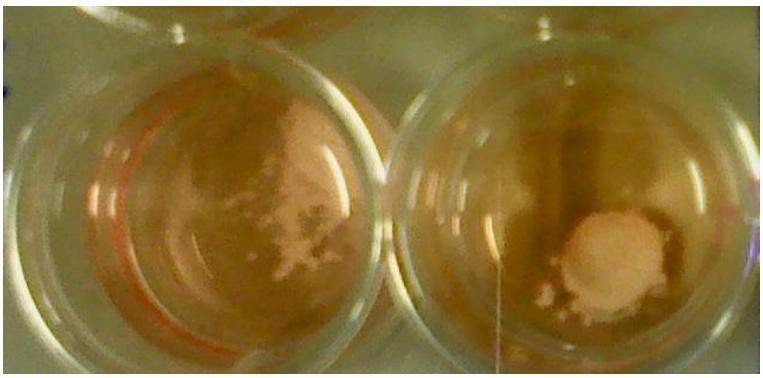

B

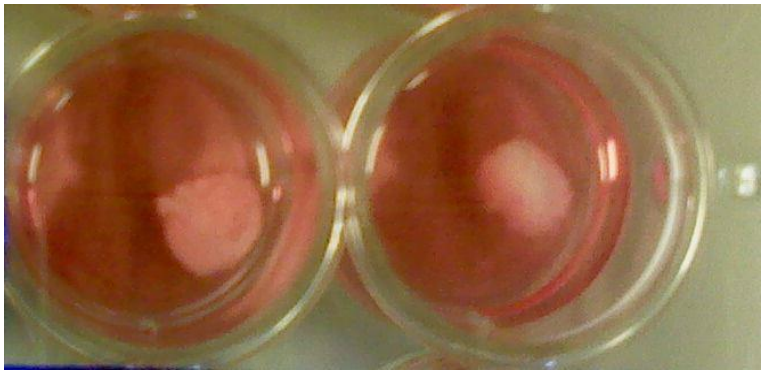

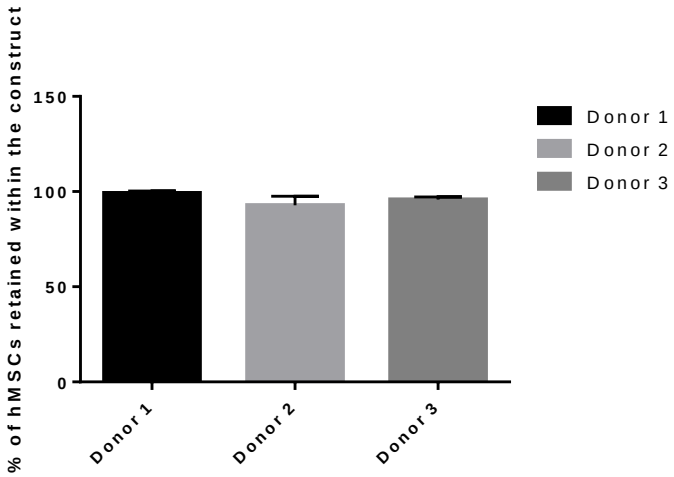

Figure 4.2.2: Cell loading efficiency. 1A) Scaffolds cultured in GM (above). Scaffolds cultured in OM (below).1B) Percentage of hMSCs retained within the construct as measured by subtracting the number of cells in the media from the number of loaded cells. Error bars represent mean± SD for 3 replicates per donor.

Viable cells prove the osteoconductivity of the MBCP+ construct

Confocal images 10 days post osteogenic induction showed a significant number of viable cells. Additionally, morphological differences between undifferentiated hMSCs and osteoblasts were noted. The scaffolds that were cultured in osteogenic medium were relatively more densely populated (Figure 4.2.3).

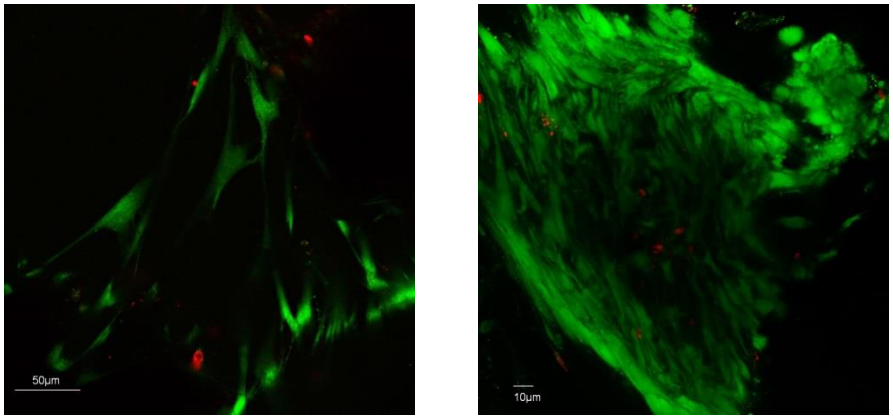

Figure 4.2.3: Cell viability and morphology assessment on the MBCP scaffold. A) Shows cells in GM (Scale bar: 50µm and OM (Scale bar: 10µm) 10 days post osteogenic differentiation. Green represents viable cells; Red represents dead cells.

The MBCP$^+$ supports matrix production in the prescence of osteogenic medium

Protein production and matrix production was significantly enhanced in MBCP-hMSC constructs cultured in osteogenic media compared to MBCP-hMSCs constructs cultured in growth media across all times, explaining the probable reason why these scaffolds did not degrade in culture compared to scaffolds in growth media (Figure 4.2.4).

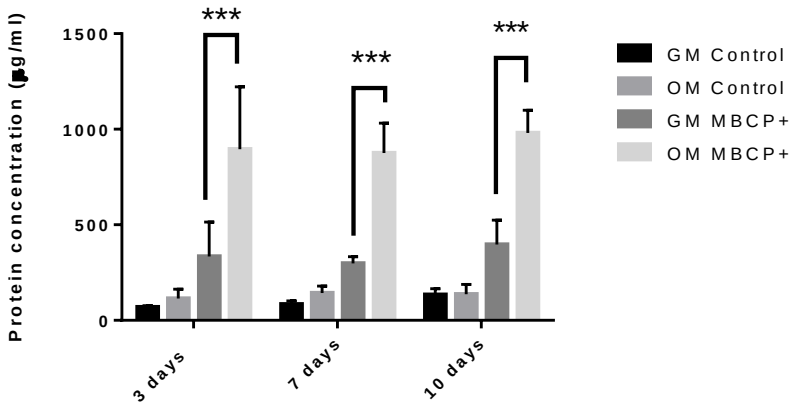

Figure 4.2.4: Protein production and matrix deposition at 3, 7 and 10 days post osteogenic induction. A significant increase in protein production was observed in scaffolds cultured under OM compared to GM at all time points. Data represents mean ± SD for 3 hMSC donors per condition, two-way ANOVA and Tukey post hoc analysis, $p<0.001$.

Analysis of osteoinductivity of the Biosel scaffold

ALP activity

ALP activity was reduced in the MBCP constructs compared to monolayer controls. Interestingly it was noted that although insignificant, there was increased ALP activity in hMSCs cultured in growth media compared to their osteogenic counterparts (when cultured on the MBCP constructs), demonstrating the osteoinductive capacity of the scaffolds (Figure 4.2.5).

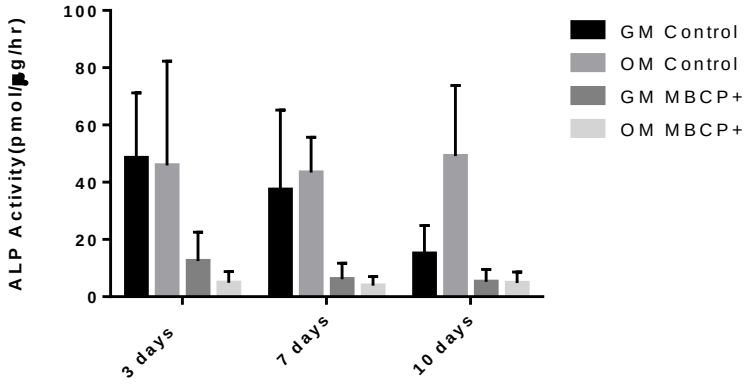

Figure 4.2.5:ALP quantification at 3, 7 and 10 days post osteogenic induction. Data represents mean ± SD for 3 hMSC donors per condition, two-way ANOVA and Tukey post hoc analysis, ($p>0.05$).

qPCR to assess osteogenic gene expression

Real time RT-PCR revealed an upregulation of ALP,BMP 2,RUNX 2, IBSP and OCN. Interestingly BMP 2 was significantly upregulated in the non-differentiated (GM) MBCP$^+$ constructs at day 7 and the late osteogenic differentiation marker, OCN was significantly upregulated as early as day 3 in the non-differentiated (GM) MBCP$^+$ constructs (Figure 4.3.5).

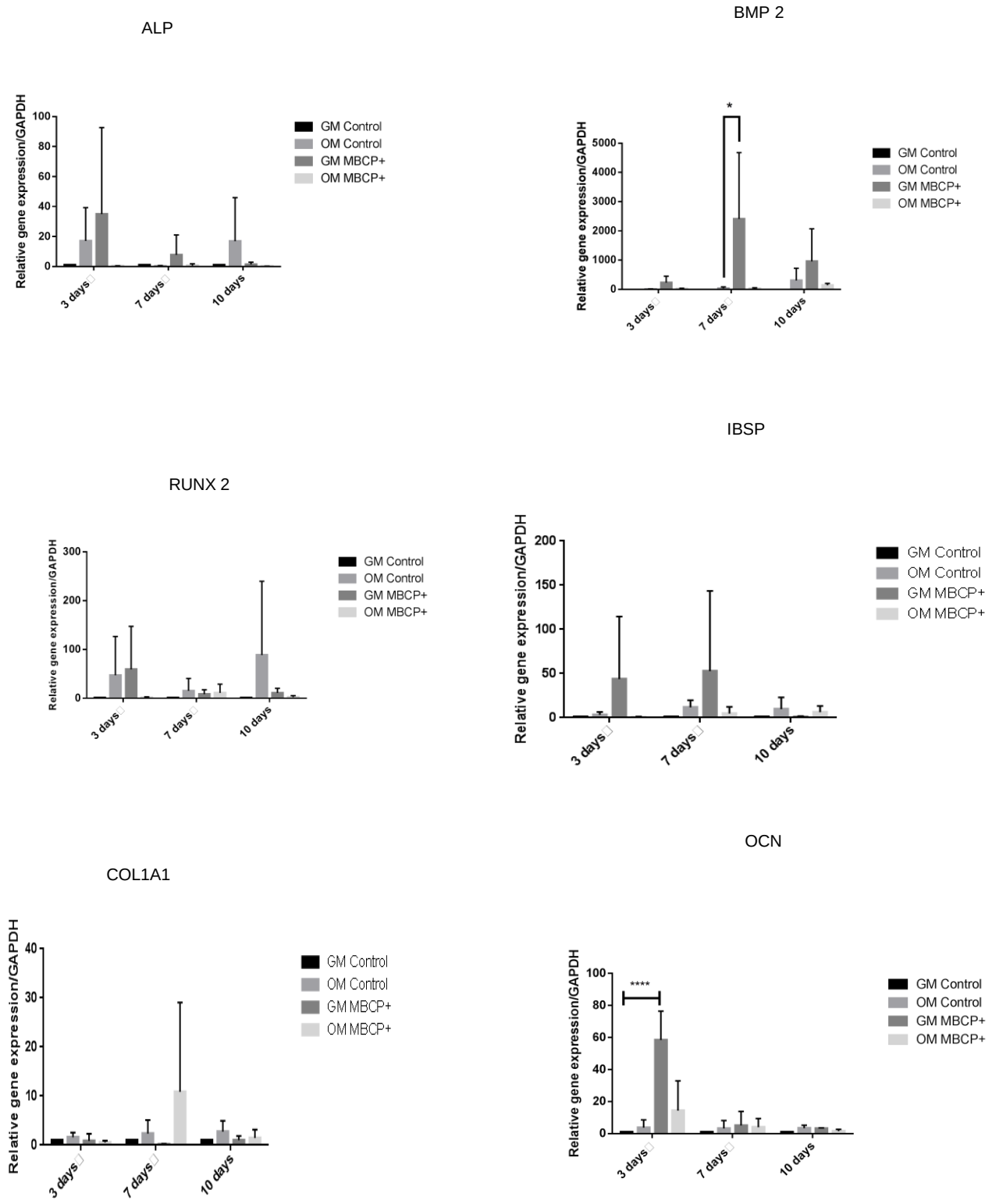

Figure 4.2.6 :QPCR Evaluation of osteogenic gene expression: hMSCs in MBCP and monolayer culture were differentiated along the osteogenic lineage. The cells were harvested, RNA was isolated and gene expression of ALP, COL1A1, IBSP, OCN (Osteocalcin) was assessed by real -time PCR. Expression levels were normalised to the corresponding GAPDH transcript levels and then normalised to GM Controls. Data represents mean ± SD for 3 hMSC donors per condition, two-way ANOVA and Tukey post hoc analysis, (**p<0.05), (****p<0.0001)

4.2.5 Calcium quantification and alizarin red staining demonstrate the efficacy of the osteogenic induction protocol

Efficacy of osteogenic differentiation of monolayer controls demonstrated significant mineralization in test wells compared to controls, demonstrating the functionality of the osteogenic induction (Figure 4.2.7). However, the test samples did not show significant upregulation of osteogenic markers as per gene expression data (Figure 4.3.5)

A

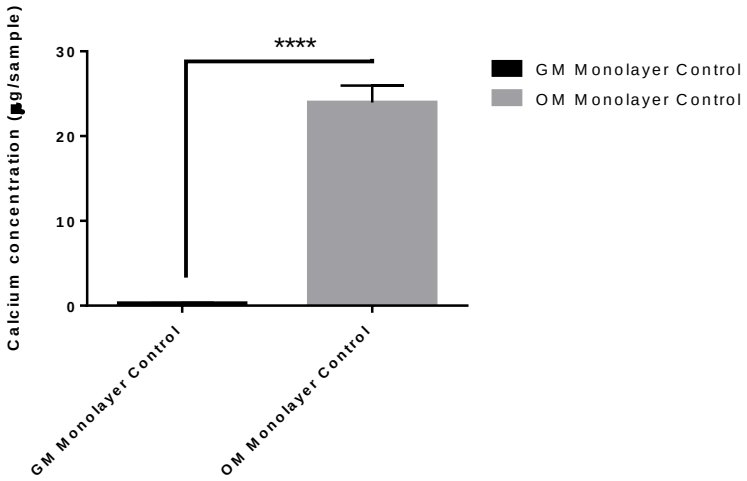

Alizarin red staining

B

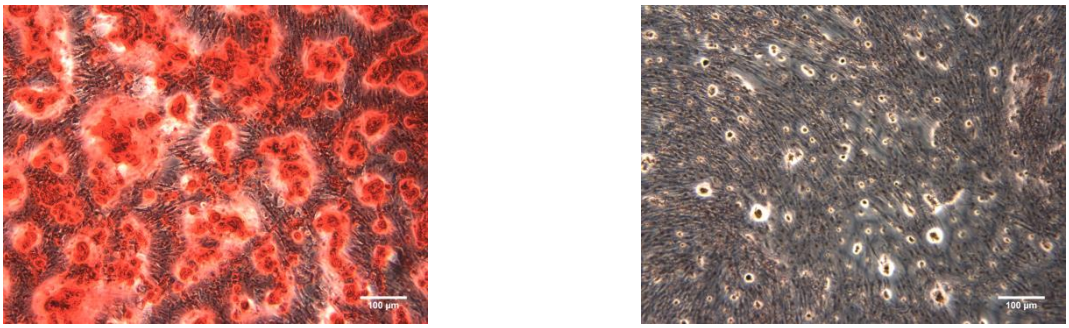

Figure 4.2.7: Calcium quantification of monolayer controls 14 days post osteogenic induction. A) A significant increase in calcium production was observed in cells cultured in the osteogenic medium compared to controls. Data represents mean ± SD for 3 hMSC donors per condition, Unpaired T-test analysis, .B) Qualitative staining of calcium using Alizarin red.Cells with osteogenic medium (left), Growth medium controls (right). Scale bars, 100µm. (****p<0.0001).

4.3 DISCUSSION

In the previous chapter, the ability of HA/TCP solid scaffolds to support *in vitro* hMSC proliferation, matrix production, viability and osteogenic differentiation was assessed. These same parameters were evaluated using the MBCP HA/TCP particles.

Cell viability and morphology were assessed 10 days post osteogenic differentiation as in the case of Biosel scaffold using live/dead viability assay (Figure 4.3.2). Morphological differences between differentiated and non-differentiated scaffolds were apparent. Interestingly, ECM-like formation was more evident in osteogenically differentiated scaffolds compared to non-differentiated controls. BMP-2, a key osteogenic gene expression marker was significantly higher in GM-MBCP compared to monolayer at day 7(Figure 4.3.5).

An additional interesting observation made during culture was that in all constructs that were osteogenically differentiated, the scaffolds remained intact whereas the undifferentiated constructs begin to break-down over time in culture (Figure 4.3.1 A). Significant protein production was observed at all the time points in differentiated constructs compared to undifferentiated constructs, to account for this observation (Figure 4.3.4).

A few studies have focussed on the spontaneous osteoinductive capacity of calcium phosphate ceramics. Muller *et al*., (2008) found increased gene expression of OCN and BSP of hMSCs cultured on BONIT matrix (BCP comprised of an HA/TCP ratio of 60/40)[258]. A study by Polini *et al*[259], demonstrated greater gene expression of Runx-2 and BSP in polycaprolactone nanofibers supplemented with TCP in comparison to nanofibers alone- despite the lack of osteogenic supplements.Guha *et al*., (2009)[260] showed increased expression in mRNA levels of OCN in cells cultured on HA/TCP compared to HA alone. Interestingly, we observed an upregulation of several osteogenic markers in the undifferentiated constructs (ALP, BMP2, RUNX 2, IBSP and OCN); with significant increases in BMP 2 and OCN. In fact the osteogenic differentiation proved to be superior in the undifferentiated constructs when compared to their differentiated counterparts

as per ALP assays and RT-PCR (Figure 4.3.5). Arinzeh *et al*., (2004) showed expression of ALP and OCN (in the absence of dexamethasone) in hMSCs cultured on HA/TCP ratio of 20/80. However, no such expression was detected on cells cultured on pure TCP or 60/40 HA/TCP. Higher osteogenic gene expression in 20/80 HA/TCP has been attributed to high degradability due to a higher percentage of the TCP component[257]. Of note, the scaffolds in our study degraded faster in culture in growth media while they remained intact in osteogenic medium, which could explain higher standard deviations[261] (Figure 4.3.1 A). More osteogenic gene and protein expression in the undifferentiated MBCP$^+$ constructs could be due to the release of calcium and phosphate into the culture medium, creating and environment primed for osteogenesis[262-264]. Although Arinzeh *et al*., observed higher bone formation with an increase in the TCP component of HA/TCP, they found the least bone formation with 100% TCP. Few studies[263,265] have shown that a slower degradation rate helps preserve the porous micro and macro-architecture of the scaffold, assisting in enhanced bone formation. Additionally the surface chemistry of the material is also at play during hMSC differentiation. Although TCP possess increased apatite precipitation, it lacks well-developed lattice structure and crystal shape in comparison to HA/TCP ceramic[203] . Arinzeh *et al*., further show increased expression of osteocalcin in hMSCs cultured in the absence of osteogenic media. In our study, significant osteocalcin mRNA was produced with decreased expression of the marker at day 7 and day 10. Giachelli *et al*., (2001)[266] and Nielsen *et al*., (2001) [267] have shown that increased phosphate levels led to increased expression of osteocalcin in human aortic smooth muscle cells and osteoblasts respectively. The repeated changes in media could have reduced the levels of phosphate overtime in our study.

The spontaneous differentiation observed in 3D culture in our study could be due to heightened cell-cell contact in comparison to 2D controls. Further, Li *et al*., (1999)[268] and Schiller *et al*., (2001)[269] reported that greater number of cell-cell interactions favour osteoblastic differentiation of hBMSC. Additionally, a number of studies have indicated that an abundant ECM supports hMSCs proliferation and differentiation[270-273].

The open porosity and resulting high degree of freedom offers cells a higher surface area to proliferate and synthesise ECM. When hMSCs are mixed with BCP particles, the cells adhere to the particle surface and make cell-cell contact producing a three-dimensional structure based on its own ECM, which would be more representative of the *in vivo* scenario rather than solid scaffolds (such as the Biosel)[274-276]

4.4 Chapter Summary:

The MBCP$^+$ scaffold supports cell attachment and proliferation and maintains cell viability. Additionally spontaneous differentiation (in the absence of ostegenic differentiation) was observed in the undifferentiated hMSC/MBCP$^+$ constructs. The study highlights the effects of two important parameters: scaffold composition and form in supporting osteogenesis. The specific composition of the MBCP$^+$ (20% HA and 80% TCP) has been shown in a number of studies[277-280] to be soluble and dissolves over time in the body-releasing calcium and phosphate in a controlled manner, favouring bone formation. Further, the MBCP$^+$, being particulate, offers an open porosity to help cells obtain oxygen and nutrients.

Therefore particulate scaffolds like the MBCP$^+$ simulates an *in vivo* environment better compared to a solid scaffold like the Biosel.

CHAPTER 5: EVALUATION OF THE OSTEOGENIC AND ANGIOGENIC POTENTIAL OF hMSCs MODIFIED TO OVEREXPRESS EPHRIN B2

5.1 INTRODUCTION

Vascularisation is critical for the success of any of the above discussed bone tissue engineering strategies. At the cellular level, this means that the crosstalk between osteoblasts (Obs) and endothelial cells (ECs) is responsible for bone formation. An appropriate source of blood supply is widely acknowledged as being critical to fracture healing.[57,281,282] Apart from AVN, numerous diseases of the bone and joint are characterised or caused by abnormal angiogenesis including Arthritis, osteomyelitis, osteophyte formation, synovitis, Paget's disease, osteoporosis, osteopetrosis and bone loss due to inflammation.

Bone, composed of an external hard cortical (or compact) layer and an internal spongy/ cancellous tissue is a highly vascular tissue and requires a blood supply to facilitate its function and structure. The inclusion of a vascularisation strategy for tissue engineered bone enables supply of nutrients, oxygen, cytokines and hormones; break-down of waste products and has a key role in development and remodelling of bone. A number of studies have focussed on various methods to improve vascularisation in Bone tissue Engineered constructs[217]. This entails (a) use of angiogenic growth factors like VEGF along with osteogenic growth factors such as BMP-2 to enhance vascularised bone formation[283-285] b) Co-culturing osteoblasts and endothelial cells in order to enable cellular cross-talk and take advantage of the important association between osteogenesis and angiogenesis. Several investigators have shown superior bone formation in coculture systems compared to monoculture systems[286-288] . (c) Application of mechanical stimulation aids in even distribution of cells within the scaffold and also assists adequate and homogenous nutrient supply and waste removal. Studies have shown endothelial cell migration , proliferation and vascular tube formation as well as enhanced VEGF release from scaffolds in response to a mechanical stimulus[289-293].(d) Employment of an appropriate biomaterial with desirable properties: Materials with greater porosity, larger pore sizes, and greater degree of pore interconnectivity [294] enable better infiltration and vascularisation of TE Scaffolds[295,296]. Treatment of AVN using hypoxia treated

hMSCs for enhanced VEGF secretion [297] and the use of bone marrow buffy coat as a source of pro-angiogenic cells [298] have highlighted the potential of using pro-angiogenic therapies for the treatment of Avascular necrosis. MSCs have been reported to be a source of angiogenic growth factors such as VEGF, FGF-2, Ang-1, and EGF, making them ideal therapeutic candidates for orthopaedic repair[118]. The strategy chosen to improve vascularisation in this study is to lentivirally modify human mesenchymal stem cells to overexpress Ephrin B2 –to evaluate its osteogenic and angiogenic potential.

The erythropoietin-producing-hepatocellular carcinoma (Eph) family and their corresponding ligands known collectively as the “ephrins” are a sub-type of the receptor tyrosine kinases. The Eph receptors are subclassed into ‘A’ and ‘B’ subfamilies and bind class wise to their corresponding ‘A’ or ‘B’ ligands on the cell surface,(with a few exceptions to this rule wherein cross class binding does occur)[299]. The Ephrins possess many known functional roles such as aiding in cell migration during embryonic development. Additionally, with respect to the nervous system they have been credited for playing important roles in axon guidance, synapse formation as well as help guiding migrating neural crest signals[300,301].

Of interest to this project, are the known roles of Ephrins in the context of angiogenesis and bone formation. In the angiogenic context, Wang *et al*.[302] recognised Ephrin B2 as an arterial endothelial marker and its receptor EphB4 as a venous endothelial marker; thereby enabling discrimination between arteries and veins in embryonic vascular development. Experiments performing knockouts of Ephrin B2 or Eph B4 in the mouse have exhibited various cardiological anomalies and the embryonic lethality at day 11[303,304].

A study by Foo *et al*.[305] suggests that Ephrin B2 is critical for mural cells to interact with microvessels. Abengozar *et al*.,[306] demonstrated inhibition of migration in endothelial cells and tubule formation *in vitro* in response to VEGF by using specific antibodies against Ephrin B2. Additionally, VEGF-induced vascularisation was inhibited in a mouse matrigel plug assay. Furthermore; primary findings by Takyar *et al.,*[307] have shown that Ephrin B2 is mandatory for osteoblast and osteoclast maturation and differentiation *in*

vivo. Subsequent to mechanical loading to the tibia in a murine model, Xing *et al*.,[308] observed up-regulation of Ephrin B2. Additionally, Ephrin B2 overexpressing murine osteoblast cell lines displayed increased osteogenesis *in vitro*[145]. Broqueres-You *et al*.[309] observed improved pro-angiogenic response to diabetes-induced ischemia by use of Ephrin B2/Fc and Katsu *et al*.,[310] showed that ex-vivo delivery of Ephrin B2 led to the development of functional vessels in hind limb ischemia by promoting angiogenesis and arteriogenesis. Salvucci *et al*. [311] showed that inhibiting Ephrin B2 activity suppresses normal pericyte and endothelial cell assembly and vascular structures. Bochenek *et al*., [312] demonstrate that the ephrins, in both receptor-dependent and independent ways, regulate endothelial cell migration and angiogenesis. Additionally, Foo *et al*.,[305] postulate the Ephrin B2 is responsible for cell motility and adhesion and blood vessel wall assembly.

Wang *et al*.[302] demonstrated that in global IGF-1 knockout mice, there was a significant decrease in expression of Ephrin B2 in osteoblasts, osteoclasts, and osteocytes. Additionally, they found that blocking Eph B4 – Ephrin B2 interaction led to decreased TRAP+ cells and reduced expression of osteoblastic differentiation markers in osteoblast-osteoclast cocultures and decreased response to IGF-1 signaling. Further, by blocking Eph B4 and Ephrin B2 in ATDC5 cells (using Eph B4 specific for TANYL-RAW) decreased baseline and IGF-1 catalysed markers. Overall, they propose that IGF-1/IGF-1R signaling mediates Ephrin B2/Eph B4 communication and thereby promote differentiation of osteoblast, osteoclasts, and chondrocytes. Arthur *et al*.,[313] demonstrate that forward Eph B signaling aids in MSC migration and activation of Ephrin B2/B1 molecules enhanced osteogenic differentiation of MSCs. Additionally, studies by Tonna *et al*., [314] suggest that Ephrin B2 signaling stimulates bone mineralisation by preventing apoptosis within the osteoblast lineage.

Chapter specific aims

1. To lentivirally overexpress Ephrin B2 in human MSCs so as to achieve long-term expression of the transgene.

2. To determine the osteogenic and angiogenic potential of Ephrin B2 overexpressing hMSCs.

3. Transduce hMSCs with a control protein (dsRED) so as to validate the outcomes observed from Ephrin B2 overexpressed hMSCs.

5.2 MATERIALS AND METHODS

5.2.1 LR Clonase reaction and transformation

Gateway®LR Clonase™II enzyme Mix (Invitrogen™ Life Technologies) facilitates the transfer of a gene of interest from an entry vector to a destination vector resulting in the creation of an expression clone (Figure 5.2.1). The entry clone (Gateway® pDONR™221 Vector containing the Ephrin B2 coding sequence; 50-150ng) (1µl), 0.5µl of Destination vector (plex_307 vector; 150ng/µl) and 2.5µl of TE Buffer (pH=8) were added to a 1.5 ml microcentrifuge tube and mixed. Additionally; 0.5 µl of Destination vector and 3.5 µl of TE Buffer (pH=8) served as the negative control. LR Clonase™II enzyme mix (1µl) was added to each of the above reactions and mixed well by brief vortexing twice. The reactions were incubated at 25^0C overnight. Proteinase K (1µl) solution was then added to each sample to terminate the reaction and vortexed briefly. The samples were then incubated at 37^0C for 10 minutes.

Figure 5.2.1: Gateway Technology

5.2.2 Transformation

One Shot® TOP10 Chemically Competent *E. coli* (50 µl) were added to each of the reaction tubes and incubated on ice for 30 minutes. The cells were heat-shocked by incubating at 42°C for 30 seconds and followed by incubation on ice for 2 minutes. S.O.C medium (Invitrogen) (200 µl) was then added to each of the tubes and plated onto a couple of agar plates, 2 plates per condition. The plates were incubated overnight at 37^0C overnight. The next day colonies were picked from the positive plate and dropped in LB broth (Sigma) containing 100 µg/ml ampicillin and shaken at 150 rpm overnight (Kuhner Shaker).

5.2.3 DNA isolation

Once glycerol stock was made from a small amount of bacterial culture (stored at -80^0C), the remaining bacterial culture was used to isolate plasmid DNA. Plasmid DNA was isolated from the cultures using the Gene Elute plasmid isolation kit (Sigma, USA) as per the manufacturer's instructions. Briefly, the cells were pelleted at maximum speed for 1 minute and the supernatant was discarded. Resuspension solution (200 µl) was added to the pellet and vortexed to dislodge the pellet and mix the suspension. Lysis solution (200 µl) was then added and left to clear for 5 minutes. Resuspension solution (350 µl) was added and inverted 4-6 times to mix. The cell debris was pelleted by mixing for 10 minutes at maximum speed. Meanwhile, 500 µl of Column Preparation solution was added to the binding column in the kit provided collection tube and spun at ≥12,000 x g for 1 minute and the flow –through was discarded. The cleared cell lysate was then added to the prepared columns and spun for 1 minute and the flow –through was discarded. Optional Wash Solution (500µl) was added and spun for 1 minute and the flow –through was discarded. Wash Solution (750µl) was added to the column and spun for 1 minute and the flow –through was discarded. The dry column was spun for 1 minute and then transferred to a fresh collection tube. Elution Solution (100 µl) was added and spun for 1 minute. The eluted DNA concentration was measured using a Nanodrop (Thermo Scientific,

NanoDrop 2000, and spectrophotometer) by measuring the A260nm / A280nm absorbances.

5.2.4 Restriction digest and Agarose gel Electrophoresis

The Eluted DNA was then diagnosed by performing a restriction digest using a reaction mix consisting of 6µl of DNA(~750 ng) , 1µl of the enzyme(EcoRI OR EcoRV OR HindIII) (New England BioLabs), 1.5µl of buffer and was made up to a total reaction volume of 15µl using distilled water. The reaction mix was incubated at 37^0C for 1 hour and then run on a 1% agarose gel for 1 hour. The bands obtained were visualised on a UV trans-illuminator (Bio-Rad, Quantity One 4.5.0 1-C analysis software). Additionally, another restriction digest was performed to diagnose packaging plasmids (psPAX2.2, pMD2.G and pRSV-Rev), provided by Martina Harte at REMEDI and plex-307 dsRED, provided by Dr.Linda Howard at REMEDI

The packaging plasmids were digested as above using the following enzymes for each plasmid (Table 5.2.1).

Table 5.2.1: Packaging plasmids and the respective enzymes used for their digestion

Packaging plasmid	Enzymes
psPAX2.2	Bam HI, EcoRI
pMD2.G	Bam HI, EcoRI
pRSV-Rev	EcoRI,PvuII

The enzymes used to digest plex-307 dsRED (control plasmid) were EcoRI, HindIII, and XhoI.

Following incubation at 37^0C for 1 hour, they were run on a 1% agarose gel and visualised as above on a UV trans-illuminator (Bio-Rad, Quantity One 4.5.0 1-C analysis software). Once the plasmid was identified to be correct, they were maxi prepped from bacterial cultures from their respective glycerol stocks. Plasmid DNA was isolated using the Pure Yield™ Plasmid Maxi prep System (Promega, USA).

5.2.5 Virus production

HEK 293T were cultured in high glucose medium containing high glucose DMEM, 10% serum and 1% penicillin/streptomycin in a 37°C, 5% CO_2, 90% humidity incubator. Once sufficient numbers of cells were grown for the experiment, they were seeded at a density of $4.5x10^6$cells/plate in 15 cm diameter cell culture dishes.

The next day, when the cells were ~70% confluent, the cells were ready to be transfected using jetPEI transfection reagent (Polyplus transfection™). In a sterile 1.5 ml polypropylene tube; the following mix of plasmids were added:

13µg of transgene (plex-307 Ephrin OR plex-307 dsRED)

13µg of psPAX2.2

5.6µg of pMD2.G

5.6µg of pRSV-Rev

The above mix of plasmids was vortexed and centrifuged at 400xg for 1 minute. In a separate tube, 41µl of jetPEI transfection reagent was added to 500µl of 150mM NaCl, vortexed and centrifuged at 400xg for 1 minute. The jetPEI mix was added to the plasmid solution and the mixture was vortexed and centrifuged at 400xg for 1 minute and incubated for 30 min. The respective mixtures were then added to the plates in a drop-wise fashion directly onto the medium. The following day, the medium was replaced and the accumulating virus in the medium was filtered using a 0.45µm filter collected at 48 hours and 72 hours post transfection. The respective viruses were pooled (5 plates for plex-307 Ephrin B2 and 5 plates for plex-307 dsRED), aliquoted, appropriately labeled and stored in -80^0C until use (

Figure 5.2.2).

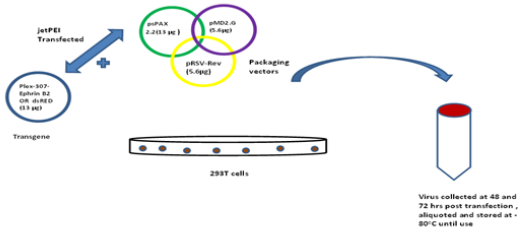

Figure 5.2.2: Steps involved in virus production

5.2.6 Virus titration

The virus titration protocol was based on the methods of Kutner *et al*., (2009)[315] and Sastry *et al*., (2002)[316]. Briefly, 293T cells were seeded at a density of 100,000 cells/well in two 6-well plates, 1 plate for each construct. Next, 1ml and 3ml of the respective viruses were added to the corresponding wells, while two wells were kept as untransduced controls. The next day the medium was replaced and the cells were incubated for an additional 48 hours.

Genomic DNA was then isolated and quantified using the picogreen assay. Quantitative PCR was used to determine the number of GAG integrations into the genomic DNA.

Primer sequences for GAG

Forward primer (3µM) GGA GCT AGA ACG ATT CGC AGT TA

Reverse primer (3µM) : GGT TGT AGC TGT CCC AGT ATT TGT C

5.2.7 Establishment of an MOI of 5 for lentiviral transduction of hMSCs.

An MOI of 5 was evaluated for transduction efficacy as per Lin *et al*., [317]. Briefly, cells were plated at a density of $1x10^5$ /well of a 6 well plate along with protamine sulphate (100µg/ml). Next day, virus appropriate for an MOI of 5 was added along with protamine sulphate (100µg/ml). An additional 2 wells were left untransduced. The following day, the virus was replaced with

medium containing 100µg/ml protamine sulphate. Following 72 hours after adding virus, puromycin selection (1µg/ml) was started.

5.2.8 Verification of Ephrin gene overexpression in genetically modified hMSCs

5.2.8.1 QPCR

RNA was isolated from the lysed cells using an RNA Aqueous for PCR kit (Ambion,). 400 ng of RNA was reverse transcribed into cDNA using Promega 2-step RT System (Promega,) as described previously. A 1 in 5 dilution of PCR Primers (Table 5.2.2) was used as described previously. All samples were normalized to GAPDH housekeeping gene.

Table 5.2.2: Primers used for qPCR

Primer name	Forward primer	Reverse primer
GAPDH	TGGGTGTGAACCATGAGAAGTATG	GGTGCAGGAGGCATTGCT
ALP	AACACCACCCAGGGGAAC	GTAGCTGTACTCATCTTCATAGGC
Runx2	GTGCCTAGGCGCATTTCA	GCTCTTCTTACTGAGAGTGGAAGG
BMP 2	AGGACCTGGGGAGCAGCAA	CACACGGCAGGCATACTCATC
COL1A1	CTGGACCTAAAGGTGCTGCT	GCTCCAGCCTCTCCATCTTT
IBSP	CGAATACACGGGCGTCAATG	GTAGCTGTACTCATCTTCATAGGC
Osteocalcin	GGCGCTACCTGTATCAATGG	TCAGCCAACTCGTCACAGTC
VEGF	GGGCAGAATCATCACGAAGT	TGGTGATGTTGGACTCCTCA

5.2.8.2 Western Blotting

For analysis of Ephrin B2 overexpression at the protein level, western blotting was performed on cell lysates. The culture media was removed and cells were washed once with ice-cold PBS.A commercially available whole cell lists buffer was used for the experiment (Pierce IP lysis buffer, Thermo Scientific,

USA). Protease inhibitor cocktail (Santa Cruz, sc-29131) was added to the buffer just before use. Briefly, 400 µl of ice-cold lysis buffer was added per well of a 6 well plate of Ephrin-B2 overexpressed hMSCs, dsRED and untransduced controls. The plate was placed on ice during lysis and periodically mixed for 5 minutes. The lysate was then transferred to a microcentrifuge tube and spun at ~13,000 × *g* for 10 minutes at 4^0C to pellet cell debris. The supernatant was transferred to a fresh microcentrifuge tube and stored at -80^0C until further analysis. Protein concentration was determined using a Coomassie Bradford protein assay (Thermo Scientific). Briefly, 5µl of standard or lysate samples were added to microplate wells followed by 250µl of the Coomassie Reagent was added to each of the wells containing samples or lysates, and mixed for 30 sec on a plate shaker. The plate was incubated for 10minutes at RT and read at 595nm on a Wallac Victor3TM 1420 Multilabel counter fluorescent plate reader. A standard curve obtained using the blank corrected 595 nm value of each standard versus its corresponding protein concentration in µg/ml was used to determine the concentration of the protein lysates.

SDS polyacrylamide gel electrophoresis

SDS gels (10%) were prepared using separating gel containing 30% bis acrylamide,1.5M Tris(pH=8.8),10%APS,10%SDS,TEMED and dH_2O and stacking gel containing 30% bis acrylamide, 1.0 M Tris (pH=6.8), 10% APS, 10% SDS, TEMED and dH_2O.

Protein preparation & Electrophoresis

Protein lysates (20µg) were mixed with loading buffer (made up of DTT, 1, 4-Dithiothreitol, Sigma-Aldrich) and made up to a total volume of 30µl with dH_2O.The protein mixtures were then denatured by incubating at 95^0C for 5 minutes. The running apparatus was set up, the protein samples were loaded appropriately along with a protein standard ladder and run at a voltage of 150V for 90 minutes until the until dye front had traveled completely through the gel.

Protein Transfer & Immunoblotting

Proteins were transferred to nitrocellulose membrane (Whatman GmbH). The Mini Trans-Blot Cell transfer system (Bio-Rad, Hercules) was used to perform wet transfer for 90minutes at 250 mA. Gel and membrane were sandwiched between sponge pads and filter papers (Whatman GmbH). Care was taken to remove any air bubbles between the gel and the membrane. The cassettes were assembled such that the nitrocellulose membrane was on the cathode side and the gel was on the anode side. An ice-pack was placed in the tank and 1 x transfer buffer was filled in the transfer apparatus. The entire set up was placed in an ice box and run. Following transfer to the nitrocellulose membrane, the membrane was blocked with 5% non-fat milk in PBS-T (Phosphate Buffered saline with Tween 20) for 1hr at RT under agitation and then washed once with PBS-T to remove the excess milk. The membrane was probed with primary antibodies for Ephrin B2 (1:200) (sc-15397, Santa Cruz) overnight at 4^0C, diluted in 5% non-fat milk in PBS-T. The following day the membrane was washed with PBS-T three times at 5 minutes intervals and then incubated with secondary antibody (1:3000) (Goat Anti-Rabbit IgG H&L (HRP); polycolonal-ab6721, Abcam). The membrane was then washed thrice at five-minute intervals in PBS-T and then incubated with Western Blotting Detection Reagents (GE Healthcare) for 1minute. Imaging of the blot was performed using AlphaInnotech FluorChem Chemiluminescent Imaging System. To membrane was then washed three times in PBS-T and stripped using 10 ml of Western blot stripping Buffer (Santa Cruz) with shaking for 30 minutes. The membrane was washed three times in PBS-T at 5-minute intervals and then incubated with GAPDH primary antibody (1:1000) for 1 hour, washed three times in PBS-T at 5 minutes intervals and then probed with anti-mouse secondary antibody at a concentration of 1:2000 for 1 hour. The membrane was then washed thrice at five-minute intervals in PBS-T and then incubated with Western Blotting Detection Reagents (GE Healthcare) for 1minute. Imaging of the blot was performed using AlphaInnotech FluorChem Chemiluminescent system.

5.2.9 Evaluation of the osteogenic and angiogenic potential of Ephrin-b2 overexpressing hMSCs

5.2.9.1 Evaluation of osteogenic potential

Following a week in puromycin (1µg/ml) selection; Ephrin B2 overexpressed hMSC and dsRED hMSCs were seeded at 40,000 cells /well of a 24 well plate. Untransduced hMSCs were also seeded alongside. MSCs from three different donors were used for the experiment. Around 48 hour post seeding, test wells were induced with osteogenic media consisting of low glucose DMEM made up with Dexamethasone (1mM), Ascorbic acid 2-Phosphate (10mM), β glycerophosphate (1M), 10% FBS and 1% Penicillin/Streptomycin. Controls were fed with hMSC growth media consisting of 10 % FBS Media was refreshed every three days.

Calcium quantification

At 14 days post osteogenic induction, media was collected for matrigel assay and stored at -80^{0}C. The wells were washed with PBS twice. Cells from each well were then scraped in 200µl of 0.5M HCl and collected into an appropriately labeled Eppendorf tube. The tubes were shaken at 4^{0}C overnight. Following shaking, the samples were spun briefly to pellet cell debris. The calcium levels in the samples were quantified using the Stanbio kit as per the manufacturer's instructions. Briefly, standards ranging from 0 to 1 µg were prepared in 0.5M HCl. Standards were set up in triplicates in wells of a microplate. HCl (0.5M, 10µl) was then added to each of the standard wells. Additionally, 10µl of samples were added in triplicate to three different wells of a microplate. Working solution (200µl) (Prepared in a 1:1 ratio of binding reagent and working dye) was then added to all the standards and samples. The absorbance was then read at 595 nm Wallac Victor3™ 1420 Multilabel Counter spectrophotometer and a standard curve was used to quantify the levels.

Alp assay

Alkaline phosphatase activity of cell lysates from the scaffolds was used as an indicator of osteogenesis. At day 7 post osteogenic induction, the scaffolds were washed with PBS and 0.1% Triton –X in Tris HCL was added and the scaffolds were left to shake overnight at 4^0 C. Next day the lysate was analyzed from ALP kit using the kit obtained from Abcam. Briefly 10 µl of ALP enzyme was added to 1mM pNPP standard wells in a microplate. Alongside, 50µl of 5mM pNPP solution was added to test samples. The reactions were incubated for 60 minutes at 25^0C in the dark, following which 20µl of stop solution was added to test and standard wells. The OD was measured at 405 nm using a Wallac Victor3™ 1420 Multilabel Counter spectrophotometer and a standard curve was used to quantify the levels of ALP.

The obtained values were normalised to total protein quantified from the same lysates using Coomassie (Bradford) protein assay kit (Thermo Scientific, USA) as described previously.

qPCR for osteogenic gene expression

RNA Isolation

RNA was isolated from the lysed cells using an RNA Aqueous for PCR kit (Ambion,). Briefly, hMSCs were harvested by scraping in 200µl lysis/binding solution and vortexed. An equal volume of 64% ethanol was added and the solution was mixed gently by pipetting and then added to a filter cartridge and spun at 13,000rpm, 1minute, RT and the eluent was discarded. Wash solution #1 was added (700µl) to the filter cartridge, spun at 13,000rpm, 1minute, RT and the eluent was discarded. Wash solution #2/3 (500µl) was then added to the filter cartridge, spun at 13,000rpm, 1minute, RT and the eluent was discarded. The above step was repeated twice. The empty filter cartridge was then spun at 13,000rpm, 30s, RT. The filter cartridge was then transferred to a fresh collection tube and 50µl of heated elution solution was applied to the center of the filter and spun at 13,000rpm, 30 sec, RT. The eluent was retained. The above procedure was performed for a total of two times. To the eluent, 0.1 volume 10x DNAse Buffer and 1µl DNAse/100µl RNA solution was

added and incubated at 37ºC for 15-30minutes. Following incubation, 0.1 volume DNAse inactivation reagent was added and incubated for 2 minutes at RT. The solution was mixed thoroughly throughout incubation and then spun at 13,000rpm, 1minute, RT. The supernatant was then aliquoted into a freshly labeled tube and the concentration was measured using a Nanodrop (Thermo Scientific, NanoDrop 2000, and spectrophotometer). The RNA was stored at -80ºC until further use. CDNA Synthesis

cDNA synthesis was achieved using the Improm II Reverse Transcription System (Promega).Briefly, 400 ng of RNA stock (concentrated if required using an RNA concentrator) and 1µl of random primers were made up to a final volume of 5µl using nuclease-free water . Samples were heated to in a thermocycler pre-heated to 70 °C for 5 minutes and then chilled to 4 °C for 5 minutes by placing on ice. To enable reverse transcription, the following components were added to each sample to a final volume of 20 µl: 4 µl of ImProm-II™ 5X Reaction Buffer, 0.16 µl of Recombinant RNasin® Ribonuclease Inhibitor (20 U/ml), 1 µl dNTPs (0.5 mM), 3.8µl of $MgCl_2$ (3 mM), 1 µl ImProm-II™ Reverse Transcriptase enzyme (200U/µl) and 5.06 µl of nuclease free water. For cDNA synthesis, samples were placed in a thermocycler set at 25 ^{0}C for 5 minutes, 42 ^{0}C for 60 minutes, 70 ^{0}C for 15 minutes and cooling to 4 ^{0}C. The resulting cDNA was stored at -20 ^{0}C until further use.

RT-PCR

qRT-PCR was performed in 10µl reactions. Master mix consisting of 5µl FG, Fast SYBR Master mix (Applied Biosystems), 0.3µl of Forward Primer, 0.3µl of Reverse Primer and 2.4µl nuclease free water was made for each of the genes of interest. The 8µl master mix was added to respective wells of a 96 well PCR plate. A 1:5 dilution of the cDNA was made of which 2µl was added to wells of the 96 well PCR plate. MicroAmp® Optical Adhesive Film (Applied Biosystems) was taped on top of the PCR plate and the plate was spun briefly. The PCR reaction was performed as per the following steps (Table 5.2.3) using the Applied Biosystems StepOne plus PCR machine.

Table 5.2.3: PCR reaction steps

Stage	Temperature (^{0}C)	Duration	Cycle
Holding	95^{0}C	20 sec	
Cycling	95^{0}C	3 sec	40
	60^{0}C	30 sec	
Melt curve	95^{0}C	15 sec	
	60^{0}C	1 minute	
	95^{0}C	15 sec	

Gene expression was calculated using The $2^{-\Delta\Delta Ct}$ method[241,242].

Average Ct was calculated for the genes of interest as well as the normalising gene (GAPDH). The ΔCT (Ct value for the gene of interest–Ct value for GAPDH) and $2^{-\Delta\Delta ct}$ were calculated for each sample. Gene expression was depicted as fold change with respect to dsRED hMSC control.

5.2.9.2 Angiogenic evaluation

Matrigel tubule formation assay

Growth factor reduced matrigel (110µl; BD Biosciences) was placed into required number of wells per well of a 48 well plate. The matrigel was incubated at 37^{0}C for 1 hour. Meanwhile , HUVEC (obtained from Lonza and cultured using EBM---2 basal media (Lonza) containing EGM™---*2* Bulletkit™ (serum and growth factors) (Lonza))were trypsinised , counted and seeded at 25,000 cells/well in 500µl of the respective day 14 conditioned medium (in triplicates) and incubated at 37°C, 5% CO_2, 90% humidity. Endothelial growth medium served as positive controls while non-conditioned hMSC and non-conditioned osteogenic media served as negative controls. The wells were imaged to assess tubule formation at 12-18 hours post seeding.

VEGF ELISA

ELISA was performed to check the amount of secreted VEGF on day 7 conditioned medium. VEGF ELISA was quantified using Human VEGF Quantikine ELISA kit (R&D Systems) according to the manufacturer's instructions. Briefly, 50µl of assay diluent was added to each well of the provided microplate, followed by 200µl of standard, control or sample to each well and covered with a plate sealer and incubated for 2 hours. After incubation, each well was aspirated and washed three times. Then, 200µl of the conjugate was added to each well, covered with a fresh plate sealed and incubated for further 2 hours. The wells were aspirated a before and washed three times and 200µl of the substrate was added and the plate was incubated at room temperature for 20 minutes protected from light. The reactions were then stopped by adding 50µl of stop solution optical density was determined using a Wallac Victor3™ 1420 Multilabel Counter spectrophotometer set to 450nm.

5.2.12 Statistical analysis

GraphPad Prism® software Inc. was used for statistical analysis. Significance was evaluated using one-way or two-way ANOVA followed by Tukey post hoc analysis. Error bars represent the mean ± standard deviation. *p*-values ≤0.05 were considered statistically significant.

5.3 RESULTS

5.3.1 Cloning and restriction digest

Restriction Digest was performed to evaluate Ephrin B2 –plex 307.It was observed that the Ephrin B2 coding sequence was successfully moved from the Entry clone to the destination vector. Additionally, the vector mapped correctly, as shown by the obtainment of expected pDRAW predicted fragment sizes (Figure 5.3.1).

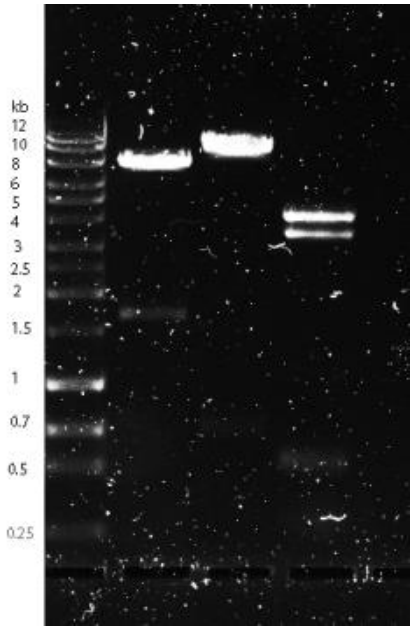

Enzyme	Expected bands	Obtained bands
Eco R1	241,7551,1625	7500,1600
Eco RV	713,8704	700,8000
Hind III	3350,312,556,584,540,4075	4000,3500,550

B

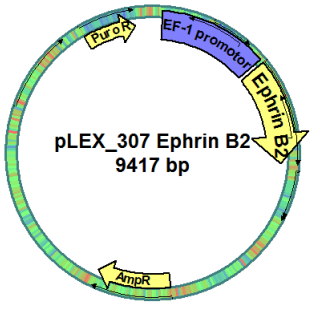

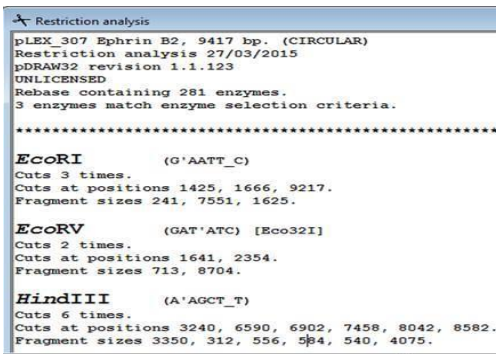

Figure 5.3.1: A) Restriction digest of Ephrin B2 in the plex-307 destination vector. Lane 1 depicts the DNA standard ladder, Lane 2 depicts sample digested with Eco R1 restriction enzyme, Lane 3 depicts sample digested with Eco RV restriction enzyme and Lane 4 depicts sample digested with Hind III restriction enzyme. The expected and obtained bands (shown in table) are matching and therefore the Ephrin B2 coding sequence was shown to be successfully moved into the plex-307 destination vector. B) Map of the vector along with predicted restriction sites.

5.3.2 Virus production

As described in section 5.2.6; HEK 293Ts were transduced at 70% confluence in 15 cm diameter cell culture dishes. Virus accumulating in the medium was collected at 48 and 72 hours post transfection. Cells, transfected with the control protein, dsRED, displayed red fluorescence 72 hours post transfection as shown in Figure 5.3.2.

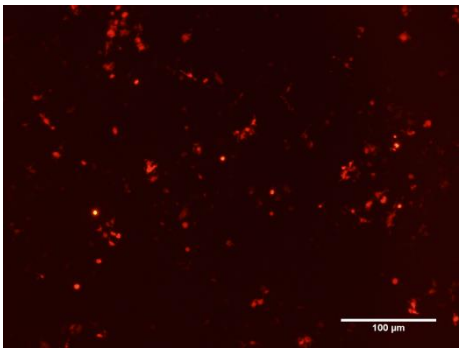

Figure 5.3.2: dsRED positive cells as seen at 72 hours post JET-PEI transfection. Scale bar, 100µm.The accumulating virus was collected at 48 and 72 hours post transfection for both dsREd and Ephrin plates.

5.3.3 Virus titration

qPCR was used to detect an increase in GAG sequence within HEK293T cells. A graph with log # GAG DNA copies per reaction for the standards on the x-axis and the Ct of the standard on the y-axis was plotted. A linear regression line was plotted and the R^2value and the line equation were determined. The line equation was used to determine the number of GAG copies in the untransduced cells and in the unknowns. The increase in GAG for each sample was calculated by subtracting the mean value for untransduced cells from the value for the transduced samples.

The increase in GAG per genome was calculated by dividing the value for the increase in GAG by the number of genomes in the PCR reaction. Based on the assumption that the 293Ts are ~triploid, 1 genome = 9.75 pg. Thereby,

200 ng= 20000 cells. The value of GAG per genome was then multiplied by the number of cells used per well for transduction=100000 cells. The obtained value gives the number of integrations/well. As seen from Figure 5.3.3, the ephrin virus had 194460.2 integrations /well of 293Ts whereas there were ~170163.37 integrations obtained with the dsRED virus.

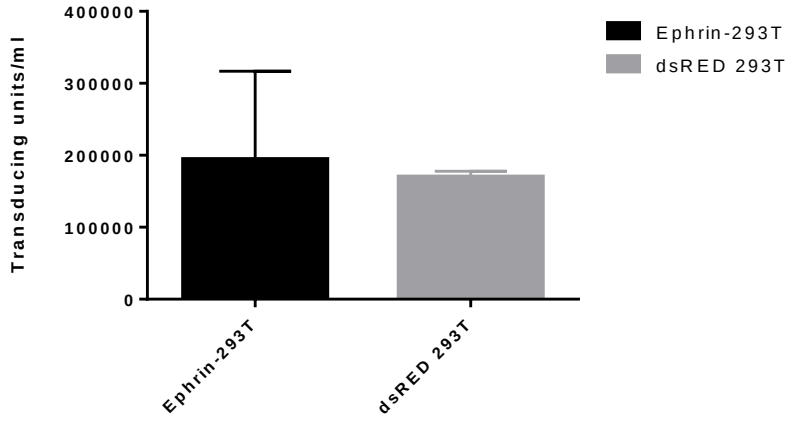

Figure 5.3.3: Number of viral integrations per well for the test plasmid (Ephrin-plex 307) and control plasmid (dsRED-pleX 307). Error bars represent mean ± SD.

5.3.4 Ephrin B2 was overexpressed successfully at the gene and protein levels

An MOI of 5 was selected to infect hMSCs as per the protocol described by Lin *et al*.[318]. Protamine sulphate was used to enhance transduction efficiency as per Lin *et al.*[318]. As described earlier, puromycin selection was started 72 hours after transduction. After a week in selections RNA was isolated, reverse transcribed and qPCR (Figure 5.3.4) was performed on the resulting cDNA samples to detect overexpression of Ephrin B2 gene. Additionally, western blot (Figure 5.3.5) was performed to evaluate for overexpression at a protein level. Ephrin B2 was visibly overexpressed in the Ephrin B2 overexpressed hMSC cell lysates compared to dsRED and untransduced controls. The protein was detected at the expected molecular weight of 37KDa.

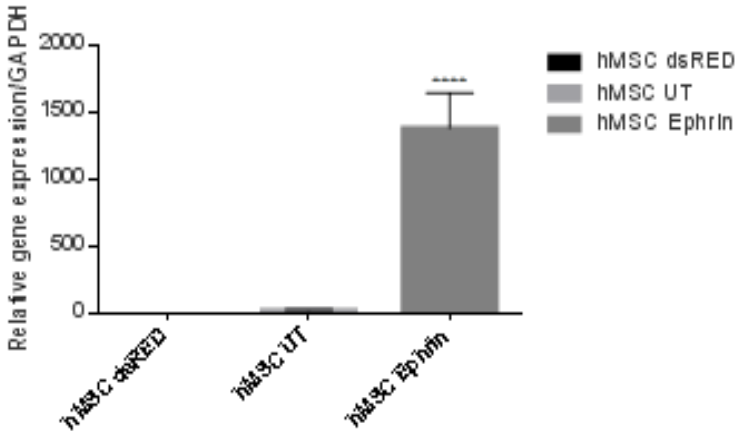

Figure 5.3.4: Effect of ephrinB2 overexpression in comparison to dsREd and untransduced controls. Ephrin B2 gene expression was significantly increased in EphrinB2-plex 307 transduced populations compared to dsRED-pleX 307 and Untransduced controls. Data represents mean ± SD for 3 hMSC donors per condition, one-way ANOVA and Tukey post hoc analysis, (**** p<0.0001).

A

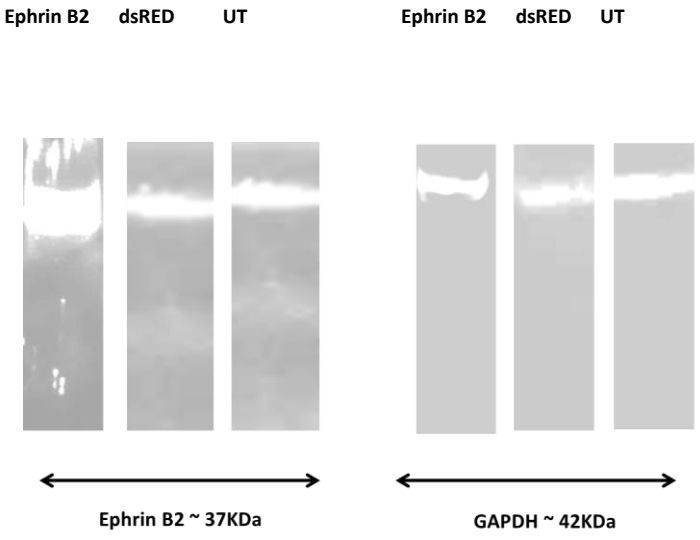

B

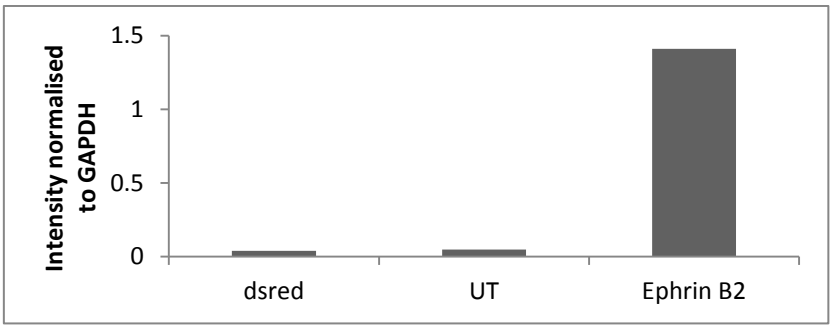

Figure 5.3.5: A) Western blot to detect overexpression of the Ephrin B2.Western blots probed with an antibody specific for human Ephrin B2.Protein was isolated from cell lysates of Ephrin B2 overexpressed hMSCs, dsREd transduced control hMSCs and untransduced hMSCs. The blots were then reprobed to detect the loading control (GAPDH).B) Quantification of band intensity normalised to GAPDH

5.3.5 Ephrin B2 overexpression significantly enhanced ALP activity and calcium production by hMSCs

5.3.5.1 Calcium quantification

Ephrin-B2 -hMSCs, dsRED hMSCs, and UT-hMSCs were cultured in osteogenic media for a period of 2 weeks. Ephrin-B2 overexpressing hMSCs displayed increased calcium deposition compared to dsRED and untransduced controls. The level of calcium deposition was assessed using the Stanbio calcium assay kit (Figure 5.3.6).

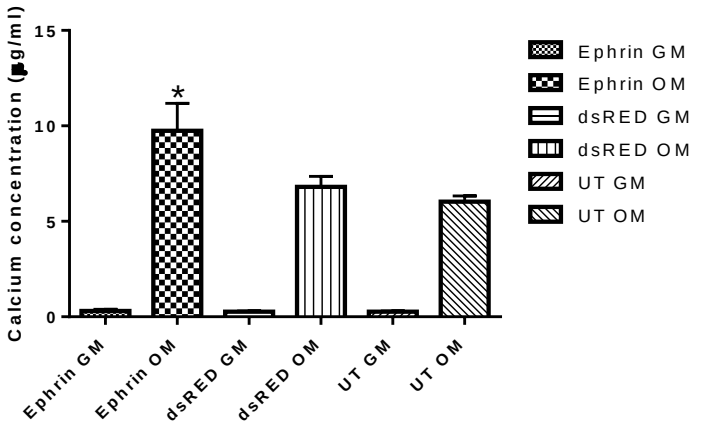

Figure 5.3.6: Calcium quantification at 14 days post osteogenic induction. A significant increase in calcium production was observed in EphrinB2 overexpressing hMSCs compared to dsRED controls. Data represents mean ± SD for 3 hMSC donors per condition, one-way ANOVA and Tukey post hoc analysis, ($^{*}p<0.05$).

5.3.5.2 ALP activity

Production of ALP as an early marker for osteogenesis was investigated by quantifying cell lysates using a colorimetric assay as described. There was a significant increase in alkaline phosphatase ($p<0.001$) in ephrinB2 overexpressed hMSC lysates compared to dsRED and untransduced hMSC lysates (Figure 5.3.7).

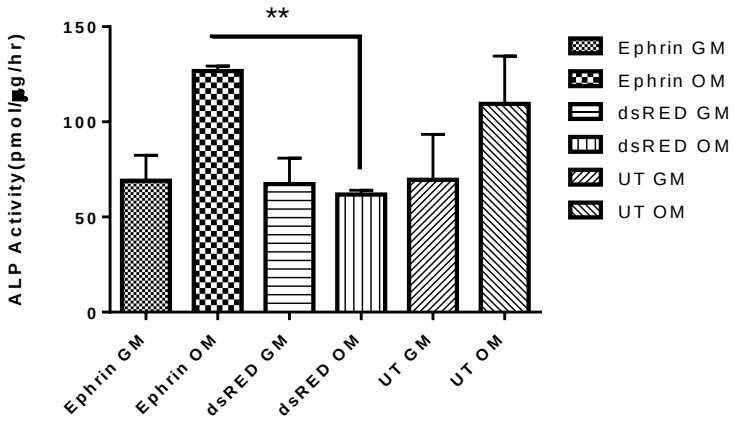

Figure 5.3.7: ALP quantification at 7 days post osteogenic induction. A significant increase in ALP activity was observed in EphrinB2 overexpressing hMSCs compared to dsRED controls. Data represents mean ± SD for 3 hMSC donors per condition, one-way ANOVA and Tukey post hoc analysis, ($^{**}p<0.01$).

5.3.6 Gene expression

The effect of Ephrin B2 overexpression was assessed by testing a range of osteoblastic gene expression markers as well as VEGF. Although ALP is a generic gene occurring in a wide variety of cell types, various studies have observed its upregulation as an early marker of bone formation. ALP gene expression was detected only in the untransduced population at day 7. No expression of the ALP gene was detected in the transduced hMSC populations. ALP gene expression was undetected at day 14 in all groups.

COL1A1 is another marker for the early bone formation and a critical component of the bone extracellular matrix[216]. COL1A1 was significantly increased in osteogenically differentiated Ephrin B2 overexpressing hMSCs at day 7 in comparison to osteogenically differentiated dsRED and untransduced populations. The gene was downregulated in all groups except the osteogenically differentiated untransduced group which showed a slight increase in COL1a1 gene expression. Bone sialoprotein, another gene specific to the bone extracellular matrix[216] was unregulated in all osteogenically differentiated groups at day 14, with no significant differences between differentiated Ephrin B2 overexpressing hMSCs and the dsRED and untransduced controls. Osteocalcin, a late marker of bone formation was increased only in the differentiated untransduced population at day 14. Interestingly, significant gene expression of the VEGF gene was observed in Ephrin B2 overexpressed undifferentiated hMSCs compared to dsRED and UT controls at day 14.Of note, the VEGF gene was not detected in any of the differentiated populations (Figure 5.3.8).

ALP DAY 7

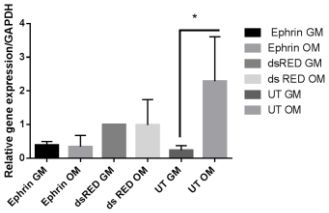

COL1A1 DAY 7

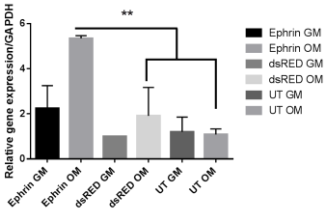

COL1A1 DAY 14

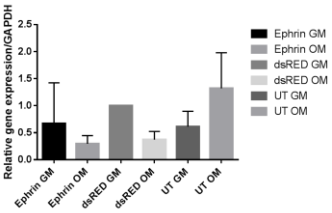

IBSP DAY 7

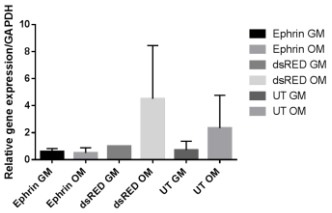

IBSP DAY 14

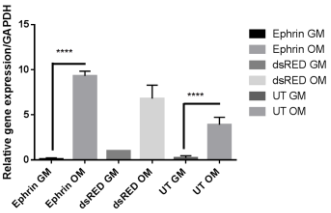

OCN DAY 7

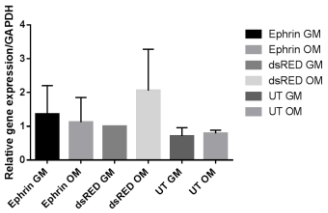

OCN DAY 14

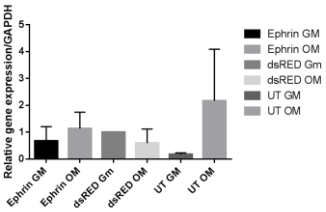

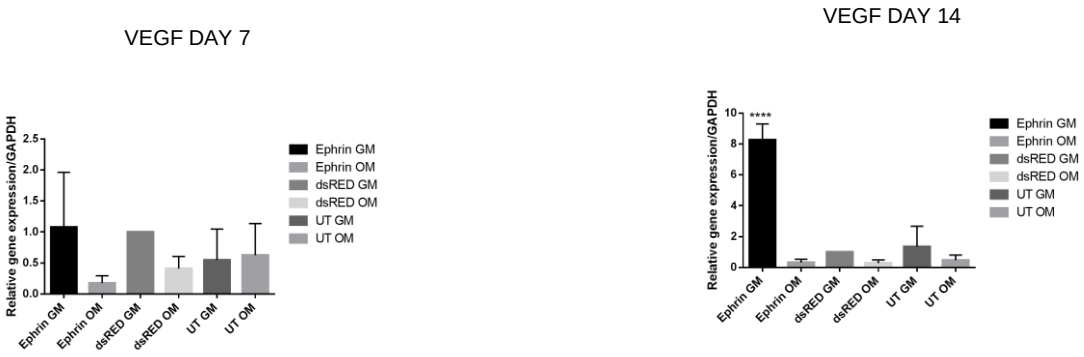

Figure 5.3.8 :Effect of Ephrin B2 gene overexpression on the expression of osteogenic and angiogenic gene expression at day 7 and day 14: Ephrin B2 overexpressing hMSC, dsRED hMSC, and untransduced hMSCs were differentiated along the osteogenic lineage. The cells were harvested at day 7 and day 14 post differentiated along with their respective untransduced controls, RNA was isolated and gene expression of ALP,COL1A1 ,IBSP ,OCN(Osteocalcin) and VEGF was assessed by real -time PCR. Expression levels were normalised to the corresponding GAPDH transcript levels and then normalised to dsRED hMSCs in GM. Data represents mean ± SD for 3 hMSC donors per condition , one-way ANOVA and Tukey post hoc analysis,(*p<0.05),(**p<0.05),(****p<0.0001).

5.3.7 VEGF Protein secretion

VEGF protein secretion in cell culture supernatant (collected at day 7 post osteogenic induction), as a measure of angiogenesis, was evaluated using the Quantikine ELISA kit as described previously. In all groups, increased VEGF protein secretion was observed in hMSCs cultured in Growth media compared to osteogenic media, with the highest protein secretion observed in hMSCs overexpressing Ephrin B2, although these differences were not statistically significant (Figure 5.3.9).

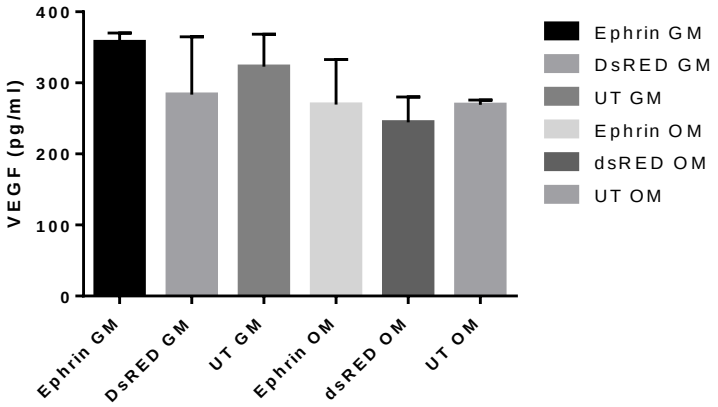

Figure 5.3.9: VEGF secretion quantified from media collected at day 7 post osteogenic induction. Data represents mean ± SD for 3 hMSC donors per condition, one-way ANOVA and Tukey post hoc analysis, p≥0.05.

5.3.8 Ephrin B2 overexpression significantly enhanced tubule formation by HUVECs

As a functional measure of angiogenesis, the ability of Ephrin B2 overexpressing hMSCs to form tubules was assayed using conditioned medium at day 14 from all three groups cultured with both growth media and osteogenic medium. Interestingly, no tubule formation was observed with osteogenic media from across all three groups (Figure 5.3.11). Remarkably, there was a significant increase in tubular formation (by counting the average number of branch points from 4 fields of view) (Figure 5.3.10) in conditioned media (GM) obtained from hMSCs overexpressing Ephrin B2 compared to dsRED and untransduced controls ($p<0.0001$) (Figure 5.3.12).

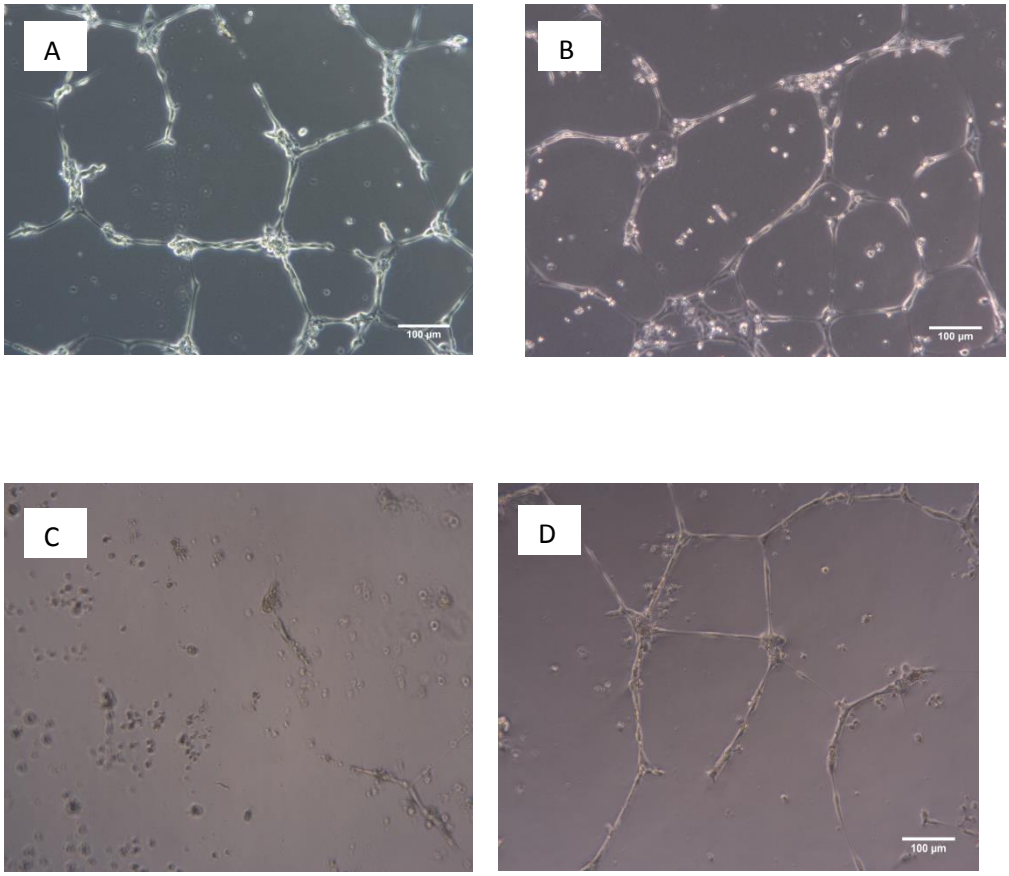

Figure 5.3.10: (Clockwise from left): A) HUVEC cultured with Endothelial growth medium (Positive control); B) HUVEC cultured with conditioned hMSC medium from Ephrin overexpressed hMSCs , C) HUVEC cultured with conditioned medium from untransduced hMSCs, D) HUVEC cultured with conditioned medium from dsRED transduced hMSCs (All are representative images).(N=3) Scale bars, 100µm.

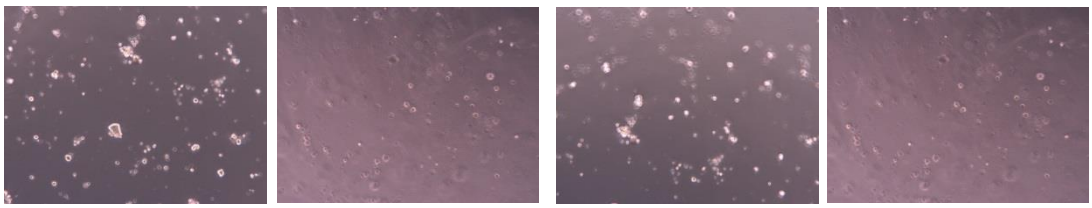

Figure 5.3.11: (from left to right): Osteogenically conditioned medium from Ephrin B2 overexpressed hMSCs, dsREd hMSCs, and untransduced hMSCs. No tubules were formed in any of the osteogenic conditions. Additionally, no tubules were formed in unconditioned hMSC or osteogenic medium (Negative control; Representative image with hMSC growth medium)

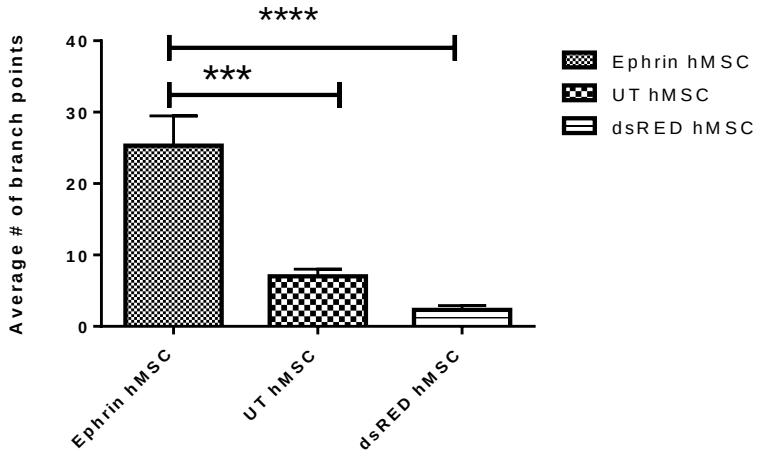

Figure 5.3.12: Quantification of the average number of tubules per well (four fields of view). A significant number of branch points was observed in the Ephrin B2 overexpressing population (in GM) compared to dsRED and UT controls in GM. Data represents mean ± SD for 3 hMSC donors per condition , one-way ANOVA and Tukey post hoc analysis,(***p<0.001),(****p<0.0001).

5.4 DISCUSSION

The aim of this chapter was to lentivirally overexpress Ephrin B2, a molecule shown to be involved in Osteogenesis and Angiogenesis. Previous studies by Duffy *et al*., has shown enhanced osteogenic and angiogenic potential in separate studies[319,320].

The success of the LR Clonase reaction was validated by a restriction digest (**Figure 5.3.1**). Overexpression was confirmed by western blotting (Figure 5.3.5) and gene expression data (Figure 4.3.4). An MOI=5 was used to transduce hMSCs using protamine sulphate at a concentration of 100µg/ml as indicated by Lin *et al*.[317]

They suggest using protamine sulphate at a concentration of 100µg/ml as an alternative to polybrene (Polybrene significantly suppresses proliferation in hMSCs). The study observed consistent expression of the transgene *in vitro* and *in vivo* over a period of 6 weeks at an MOI=5 using 100µg/ml protamine sulphate. Additionally the study also observed the use of FGF-2 to enhance transduction efficiency[318]. FGF-2 was used in our study as well. The cells

were viable throughout the study period. Additionally, efficient transduction was achieved as observed by red fluorescence in dsRED control transduced hMSCs. Also, Ephrin B2 was significantly overexpressed at the gene and protein level one week after puromycin selection as observed by qPCR and Western Blot results. There was a significant increase in the levels of Ephrin B2 expression in the overexpressing population compared to the dsRED and UT controls, establishing the functionality of the plasmid. The advantage of viral gene delivery is it that it offsets the limitations of protein therapy such as short half-life, diffusion and cost limitations.

Studies by Tierney *et al*[320] made use of a transiet non-viral vector approach for overexpressing Ephrin B2, employing Polyethylene amine (PEI) for gene transfer. However, non-viral methods only exhibit transient gene expression which could "go off" before we can observe desirable outcomes *in vivo*. Further, our understanding of cellular mechanisms involved is limited. Lentiviral gene delivery methods allow stable and long term gene expression and transduce both diving and non-dividing cells. The vector's genome integrates into the genome of the host cell. However, it is important to ensure an optimum MOI value, because high MOI values lead to mass cell death. We used a previously optimised MOI for transducing hMSCs as mentioned earlier. Additionally, the integrative nature of these viruses carries the possible risk of insertional mutagenesis. Non-viral methods, on the other hand, avoid undesirable side effects such as ectopic bone formation and safety concerns associated with lentiviral methods[321].The next objective was to evaluate the *in vitro* osteogenic and angiogenic capabilities of Ephrin B2 overexpressed hMSCs and compare outcomes with dsRED and Untransduced controls. The pro-osteogenic potential of Ephrin-B2 has been investigated in a number of studies.

Ephrin B2 overexpressed hMSCs cultured in osteogenic media exhibited significant alkaline phosphatase activity (Figure 5.3.7) and mineralisation (Figure 5.3.6) compared to dsRED-hMSCs and UT-hMSCs cultured in osteogenic media. However Tierney *et al*.,[320] show comparable mineralisation with a lower plating density of Ephrin B2 hMSCs (when cultured in osteogenic

media). We observed increased osteogenesis only in osteogenic media in our study as well, implying that Ephrin B2 requires the presence of osteogenic factors for differentiation.

With regard to the RT-PCR results, gene expression profiles at day 7 and day 14 did not show appreciable increase in osteogenic gene expression with Ephrin-B2 overexpressed hMSCs, in fact, a reduction in gene expression was observed with some osteogenic genes compared to dsRED and UT controls (Figure 5.3.8). Studies by Tierney *et al*.,[322] only showed increased gene expression in only Osterix at day 7 and day 14 and Dlx5 at day 7 in Ephrin B2 overexpressing hMSCs. Moreover, a study by Lee *et al*.,[174] observed that DLX5 is involved in the control of Osterix which could explain the results by Tierney et *al.*

It is important to know the genes involved in Ephrin B2 related osteogenesis. Tonna *et al*. have shown a role of Ephrin B2 in endochondral ossification – therefore assessing endochondral gene expression can be performed[314,323] Gerber *et al*. (1999)[324] showed that expression of VEGF in hypertrophic chondrocytes is critical to the endochondral bone formation as it stimulates resorption of cartilage and vascular invasion. Interestingly, in this study, we observed a significant increase in VEGF gene expression in hMSCs cultured in growth media (Figure 5.3.8). Tonna *et al*.[323] investigated the role of Ephrin B2 in endochondral ossification by use of neonatal osx1 Cre.Efn b2 $^{\Delta/\Delta}$ gene deletion mouse model. These mice exhibited transient osteopetrosis and osteoclasts at the growth plate displayed abnormal morphology and poor attachment. Additionally, cultured chondrocytes from these mice displayed compromised osteoclastogenesis as well as significant reduction in levels of Adamts 4. These data indicate the role of Ephrin B2 in regulating osteoclast resorption during endochondral ossification.

The next major goal of this study was to study the effects of Ephrin B2 in angiogenesis. The highest secretion of the potent angiogenic protein was found in Ephrin B2 overexpressed hMSCs. Of note, it was observed that in all groups; VEGF secretion was higher in hMSCs cultured in GM vis – a-vis

osteogenic media, although these differences were insignificant (Figure 5.3.9).

Our data is in agreement with studies by Hoch *et al*.[325] and Mayer *et al*.,[151] who observed a differentiation-dependent secretion of VEGF wherein VEGF secretion decreased in the presence of osteogenic media. While VEGF secretion was not significantly increased, we observed significantly increased VEGF gene expression in GM compared to OM (Figure 5.3.8). Additionally, Mayer *et al*. suggested VEGF-A plays an autocrine role in osteoblast differentiation as they observed that a high expression of VEGF-A increased mineralisation whereas an antagonist to VEFF-A; sFLT-1 decreased mineralisation. They also suggest a paracrine role of VEGF-A in stimulating sprouting angiogenesis, which is in agreement with this study.

Helmrich *et al*., (2013) modified hMSCs to express rat VEGF. Following eight weeks of implantation, constructs seeded with rat VEGF-expressing hMSCs showed significant vascularisation in comparison to controls. Interestingly, they also found a reduction in bone quantity and observed an active recruitment of osteoclasts[326]. Further, Hoch *et al*., (2012)[325] and Bara *et al*., (2013)[327] observed increased VEGF expression in GM and decreased expression in OM, in agreement with our study.

We observed sprouting angiogenesis was very significant in conditioned media from ephrin-B2 overexpressed hMSCs and it was comparable to endothelial growth medium (EGM) positive control. Studies have shown that blocking VEGF in BMSC conditioned media did not interfere with its potential to drive endothelial tubule migration and formation. This could be due to insufficient quantities of VEGF required to evaluate its effects[328]. Further, VEGF probably collaborates with other secreted pro-angiogenic molecules to drive Ephrin B2 mediated endothelial cell sprouting. Additional experiments to evaluate these possible factors need to be carried out in order to enhance our understanding. In their first study, Duffy *et al*.,[329] reported that transfected cells adapted an early endothelial morphology post osteogenic differentiation. Also, they observed that Ephrin B2 overexpressing hMSCs had reduced cell number and calcium deposition at day 15 post osteogenic induction in

comparison to controls. Furthermore;, they show enhanced tubular formation by Ephrin B2 overexpressing hMSCs cultured on matrigel with endothelial growth medium (for 24 hours) compared to controls. In our experimental setup, HUVECs were cultured in conditioned medium from Ephrin B2 overexpressing hMSCs and showed sprouting comparable to endothelial conditions. Our data more conclusively prove the angiogenic capabilities of Ephrin B2 because our experimental set up did not make use of endothelial growth medium, proving that Ephrin B2 overexpressing hMSCs alone promote significant angiogenic activity in comparison to controls.

Blocking Ephrin B2/Eph B4 signalling decreases expression of sclerostin, a powerful osteoblastogenesis inhibitor.[148,330] Ephrin B2 in osteoblasts, in a contact dependent manner with Eph B4 on osteoblasts, enables osteoblast differentiation and bone formation and via reverse signalling, Eph B4 in osteoblasts acts upon osteoclastic Ephrin B2 and suppresses formation of osteoclasts. BSP is a bone resorption marker and PCR data indicate increase expression of this marker in Ephrin B2 overexpressing hMSCs. Ephrin B2 has a known role in bone remodelling. Further, Riminucci *et al*., show that intracellular expression of BSP in osteoblasts is synchronized with their expression in early hypertrophic chondrocytes before extracellular BSP expression and mineralisation[331].

5.5 Chapter summary:

The lentiviral transduction of hMSCs at an MOI=5 effectively overexpress Ephrin B2 at the protein and transcript levels. Ephrin B2 overexpressing hMSCs displayed significant ALP activity and calcium deposition compared to dsRED controls (when cultured in osteogenic medium).

Ephrin B2 overexpressing hMSCs displayed a significantly increased VEGF gene expression in GM, although these changes were not significant at the protein level. Interestingly, Ephrin B2 overexpressing hMSCs significantly increased endothelial tubule formation (compared to the Endothelial growth

media positive control).Further studies would entail looking into an array of pro-angiogenic factors in Ephrin B2 conditioned medium.

Additionally, evaluating for endochondral genes may be considered, given that we noticed a significant increase in genes associated with hypertrophic chondrocytes (BSP and VEGF).

CHAPTER 6: CONCLUSIONS & FUTURE DIRECTIONS

6.1 CONCLUSIONS

Bone possesses an inherent capacity to regenerate during the development of the skeleton, remodeling as well as in response to injury. In fracture healing, the entire process of fetal skeletal osteogenesis (including intramembranous and endochondral ossification) is repeated without the formation of a scar tissue. However, in certain cases, this normal tissue healing is compromised (for example, tibial fractures) resulting in non-union or delayed union. Additionally there are cases where the amount of bone required for healing exceeds its normal healing capacity. Avascular necrosis, osteoporosis and skeletal reconstruction of long bones are examples of some conditions requiring a large amount of bone.

Current medical treatments for severe bone injuries are challenging and may yield poor results. Autografts have long been the “gold standard” for healing bone defects; however, there are limited sites where bone may be harvested without loss of function. Autografts-harvested from the iliac crest of the hip-are associated with a 10% complication rate as well as infection, fracture, pain, paraesthesia, nerve injury and donor-site morbidity Allografts -derived from cadavers/donors- are another commonly used bone graft material. Nevertheless, disease transmission and immunologic rejection are serious concerns with the use of unprocessed allografts, and processed allografts, like demineralized bone matrix, lack bone growth inducing factors that are essential for efficacy. Xenografts-or bone grafts obtained from different species-are also a poor option due to the threat of disease transmission and immunological rejection.

Use of metals such as iron, cobalt, and titanium may provide internal fixation but fatigue, corrosion, tissue infection, and poor implant-tissue interface create many problems for patients. Moreover metals typically possess mechanical properties considerably greater than that of natural bone, thereby absorbing much of the mechanical stimuli required for proper regrowth of bone. This stress-shielding effect causes bone resorption around the implant and may require whole- implant removal in the long run[7].

The emerging field of tissue engineering promises therapies for improved healing of damaged tissue devoid of the limitations and drawbacks of current treatments. The goal of tissue engineering is to restore structure and function to a defect by exploiting the body's natural healing response with the aid of one or more of three elements: cells, signaling molecules, and scaffolds. Thus, a bone defect will possibly be replaced by natural bone tissue with the complete union and full restoration of function without using a permanent implant.

6.1.1 Properties to be considered while designing HA/TCP scaffolds for Bone Tissue Engineering applications

An ideal bone substitute scaffold having optimal mechanical properties, cytocompatibility with an ability to form mineralised tissue still remains to be identified[332]. In terms of osteoinductive properties, there exist considerable differences between calcium phosphate based ceramics owing to differences in their physical and chemical properties like surface chemistry or surface roughness, for example, which influences osteoblastic differentiation.

Despite the proven osteoblastic capacities of a range of calcium phosphate based materials, further investigations need to be done in developing materials with intrinsic osteoinductivity. Systematically evaluating the contribution of individual physical and chemical properties in aiding osteogenic differentiation in a range of bone tissue engineering scaffolds needs to be undertaken. Additionally, assessment of osteogenic differentiation on materials in the absence of osteogenic media would more stringently evaluate the impact of material properties. Bypassing the differentiation step using the inherent osteoinductive material capacities would save significant time, cost, and proves safer for translational studies. Further studies could also look into definite signaling pathways that are activated, providing important insights into material induced osteogenesis.

While brittleness is a major shortcoming of certain calcium phosphate ceramics, the problem is further compounded in scaffolds with high porosity and large pore size. Therefore, a challenging requirement is to fabricate a scaffold with a balance of properties. Further research could involve studying signaling pathways at the cellular level by studying interactions between cells/biomaterial/host and by probably looking at receptor binding of Ca^{2+} and PO_4^{3-} ions released from the material as well as activation of specific osteogenesis pathways[333].

Notwithstanding the many advantages of using ceramics for bone repair, a significant disadvantage is their low degradability. HA is hardly degradable while the degradability of TCP is faster. BCP ceramics tend to remain for several months in the body while only a few weeks are required for the bone to repair. Ideally, a BCP scaffold needs to be fabricated so that it degrades at a rate proportional to bone formation; or capable of undergoing remodeling by osteoclasts.

a. Role of porosity

Larger pores favor direct osteogenesis, because they allow for higher oxygenation and vascularisation. Nonetheless, smaller pores lead to osteochondral ossification, although this type of bone ingrowth is influenced by the type of biomaterial and pore geometry. However, there is an upper limit in porosity and pore size due to constraints associated with mechanical properties. An increase in the void volume leads to a reduction in mechanical strength of the scaffold, which can be critical for regeneration of load-bearing bones. In our study we found that the Biosel was more stable in culture compared to a highly porous material like the $MBCP^+$.The extent to which pore size can be increased while maintaining mechanical requirements depends on many parameters including the nature of the biomaterial and its processing conditions. An upper limit is also set based on the dimensions of the pores of the specific bone-tissue to be repaired[334].

A scaffold with porous interconnected structure is advantageous because it allows enhanced nutrient and waste exchange, enhanced migration and

thereby enables the formation of bone and vascular structures. Our confocal images showed poor penetration in the interior of the Biosel scaffold whereas the MBCP$^+$, showed uniform cell distribution. Chang *et al.,* (2016) compared titanium scaffolds of varying pore sizes and report that larger pore sizes enable better water penetration as a consequence of high wettability; enable superior penetration of cells and body fluids leading to the enhanced bone formation. The group found that although *in vitro* expression of bone markers were increased with scaffolds of lower pore size, this did not correlate to the *in vivo* situation wherein scaffolds with higher pore sizes showed more bone growth compared to scaffolds of smaller pore sizes[335].

b. *Role of scaffold architecture: Solid scaffold (Biosel) versus Particulate scaffolds (MBCP$^+$)*

Although studies have employed both block based and particulate scaffolds, particulate scaffolds offer the advantage of greater cell-cell contact that would favour osteogenesis. Indeed, our confocal images showed greater clustering of cells on the MBCP$^+$ in comparision to the Biosel. Fedorovich *et al*.,(2011)[336] observed that compared to MSCs loaded on solid scaffolds, cells in porous constructs exhibited enhanced expression of ALP, collagen type I and osteocalcin.Further, Krebsbach *et al*[337] observed sparse bone formation in the periphery and interior in solid scaffold, whereas particulate scaffolds exhibited abundant bone formation throughout. We found expression of osteogenic markers in the MBCP$^+$ constructs even in the absence of osteoinducive medium- a true mark of an osteoinductive material, which could probably be due to improved cell-cell contact.

c. *Role of HA/TCP ratio*

According to our study, the Biosel consisting of a higher HA component did not significantly enhance expression of osteogenic markers. However, the MBCP$^+$, consisting of a higher TCP component exhibited expression of osteogenic markers even in the absence of osteogenic medium. This could be

due to higher degradability and release of calcium in the milieu which could have contributed to osteogenesis.

Table 6.1 shows a comparision of scaffold properties between the Biosel and MBCP$^+$

Table 6.6.1.1: Comparision of outcomes between the Biosel and MBCP$^+$ scaffolds

Scaffold property	Biosel(DePuy Synthes)	MBCP$^+$ (Biomatlante)
Osteoconductive?	✓	✓
Osteoinductive?	x	✓
Biodegradable?	Degrades slowly	Degrades quickly
Cell distribution	Poor cell distribution in the scaffold interior	Homogenous cell distribution
Ease of handling	Easy to handle	Difficult to handle as the material degrades quickly

6.1.2 Effect of culture conditions: Static versus dynamic cell culture systems

Improved methods for *in vitro* hMSC culture, harvesting, and subsequent implant need investigation. However *in vitro* expansion of MSCs is time-consuming and could add to the overall costs and risks. Research into alternative sources of bone marrow-derived MSCs, for example; MSCs derived from adipose tissue, Wharton's jelly and dental pulp can be investigated for their bone regeneration potential. Additionally, seeding of freshly isolated cells into scaffolds, avoiding the two-dimension culture step can be conducted. Papadimitropoulos *et al*.[239] demonstrated that seeding of freshly isolated hMSCs not only eliminated laborious two-dimensional culture but was more representative of the *in vivo* environment by supporting hematopoietic lineage cell maintenance. Further, they applied this system for expansion of hMSC.

Modulation of fluid-flow-induced mechanical stimuli by increasing fluid shear stress could lead to enhanced mineralisation of scaffolds[250]. Further research could also assess any osteogenic growth factor production occurring as a result of fluid shear stress to further understand the mechanism of mechanically induced osteogenesis. It would be interesting to test different

time frames of *in vitro* osteogenic differentiation before implant to check for the best *in vivo* outcomes in subcutaneous models. An investigation by Tasso *et al*., demonstrated that implanted MSCs on ceramic recruited circulating osteoprogenitors of host origin and that these host cells appeared to play the major role overall in bone tissue formation[338]. Possibly subcutaneous implant of Biosel could be performed in an animal model to check for bone formation and then stain to detect cells of human origin. The outcomes can be compared to MBCP^{+} scaffolds cultured under dynamic conditions.

6.1.3 Enhancing the angiogenic potential of hMSCs by overexpressing Ephrin B2.

Angiogenic therapy has been proposed in fracture management strategies[282]. Angiogenic growth factor therapy, enhanced HIF signaling, use of endothelial cells, preventing angiogenic inhibitors are all options for therapeutic angiogenesis. Growth factors BMP-2 and BMP-7 have been granted approval by the United States Food and Drug Administration (US-FDA) for the management of fracture and non-unions. A number of studies have focussed on VEGF[152,339-341], FGF[342-349], and PDGF[350,351] in animal models of bone repair. Another molecule of interest, Thrombin-peptide 508 (TP-508), is known to play a role in angiogenesis, cell chemotaxis and proliferation. This molecule stimulates thrombin healing response devoid of the associated clotting. Its effect on fracture healing has been explored in a number of studies[352-355]. Erythropoietin (EPO) - a cytokine that is similar to VEGF in homology and hypoxia stimulation to VEGF[356]- is studied as a therapeutic target[357-359]. Further, increasing HIF-1α production by inhibiting proyly hydroxylase is evaluated as a potential therapy to promote fracture healing[360]. Blocking of angiogenesis inhibitors such as thrombospndin-2 (TSP-2) is an additional approach to treating fractures[361,362] Cell-based therapies for angiogenic based bone repair have mostly considered mesenchymal progenitor cells[363,364].

Previous studies using hMSCs seeded on ceramic scaffolds have only focussed on evaluating the osteogenic capabilities of MSCs on the scaffold. Bone tissue contains a multitude of cell types, including osteogenic and

endothelial cells. Additionally, it has been well established that angiogenesis is necessary for in vivo osteogenesis. Furthermore, inadequate vascularisation of tissue engineered constructs has been shown in studies to be a cause of hypoxia and cell necrosis. Therefore, vascularisation of the scaffold is critical for the success of bone tissue engineering strategies. Consequently, it is justifiable to enhance the inherent angiogenic capacity of hMSCs by overexpressing ephrin B2 as this is of high clinical relevance.

A probable shortcoming of the Ephrin B2 study is the inherent risks involved with genetic modification during translation to clinical use. The biological effects of gene overexpression cannot be anticipated *in vivo*. Use of "switchable" promoters that react to external stimuli could be used to modulate gene overexpression. Another factor that needs to be addressed while using genetically modified cells is the possibility of their turning malignant once transplanted. Also, the obvious risk of using viral vectors is a concern. Further research needs to evaluate safety issues related to their use in animal models[365].

Finally, it must be stated that the current study lacks an in vivo proof of concept experimentation. Although alternatives to animal experimentation such as engineered organs and in vitro disease models are being researched, pre-clinical testing remains the gold standard for bone regeneration therapies. Animal models possess the capacity to mimic human physiological features as well as bone mechanics: an advantage that is absent in non animal models. These features become more critical when testing new medicinal products and for preclinical stages of drug development. Current biomedical research is concentrating on applying the concepts of "3Rs" for human experimentation in animals with a focus on the principles of Replacement, Reduction and Refinement[366].

6.2 Future directions

Core decompression, a procedure described by Ficat and Arlet[367] is the current gold standard treatment for osteonecrosis. As stated previously, this procedure aims to reduce intraosseous pressure and stimulates

vascularisation at the site of osteonecrosis by providing channels for blood flow.

Mesenchymal stem cells are promising candidates to treat necrotic bone[368]. Mesenchymal stem cells are capable of homing to these sites of injury when delivered intravenously and help regeneration of bone tissue at the site of injury either by plasticity or paracrine mechanisms[369]. Although Core decompression is the standard technique for treating osteonecrosis its efficiency is limited only to the early stages of the diseases. Combining MSC therapy with core decompression is a promising therapy for treating AVN because it provides an additional material to enable bone formation.

6.2.1 Potential of the Biosel and MBCP^{+} scaffolds in the clinic

The Biosel has been used previously in a clinical as well as pre-clinical study.Nich *et al*., (2006) [370]used Biosel in granular form to treat 20 patients (Age range:30-79,Avg age: 65.7) with grade II or grade III femoral peri-prosthetic bone defect revision cases. Treatment groups consisted of Biosel granules (14 patients), Biosel granules and cancellous grafts (5 patients) and Biosel granules + autograft (2 patients). At an average follow-up of 36 months, (time period: 14-76 months) Merle d'aubigne score indicated 90% of the cases as good or very good. A couple of diaphyseal femoral fractures ensued; however, they were subsequently reunited. Aseptic loosening and septic occurrence necessitated re-revision in 2 hips. Radiology indicated no osteolysis in 17 cases and implies that the implanted Biosel granules bonded with bone. Therefore, it was suggested that ceramic Biosel granules were as promising as the gold standard bone grafts in femoral bone repair strategies.

Further Bodde *et al.,* (2006) [371]used cell-free Biosel (3mm cubes) and compared it to Conduit TCP granules, and tested their effects on sheep trabecular bone defects. As expected, the conduit TCP showed more degradability compared to the Biosel, which did not degrade. Both materials were conducive to *in vivo* osteogenesis with conduit TCP implants showing higher bone formation. These differences however were not significant. Homogenous bone formation was observed in the Conduit TCP, while the

Biosel showed higher bone formation in its outer surface as compared to its center. However it must be noted that the above studies used the Biosel only in granular form and not solid form as used in this study.

The Reborne project (http://biomatlante.com/) has demonstrated the effective use of the $MBCP^{+}$ and culture expanded hMSCs as bone tissue engineered constructsin bone regeneration from a regulatory, scientific as well as a clinical standpoint. The project has demonstrated the fruitful of hMSCs and $MBCP^{+}$ being osteogenic, osteoinductive with high clinical success especially in the treatment of long bone non-unions. Combining the MBCP+ construct with Ephrin B2 modified hMSCs has the potential for enhanced outcomes, combining the osteogenicity of the MBCP+ with the angiogenicity of the Ephrin B2 hMSCs.

There are currently over 30 biphasic calcium phosphate tissue replacement products available commercially, with respect to orthopaedic and maxillofacial applications[372]. Additionally, studies have employed BCP as a carrier or delivery system for therapeutic drugs, antibiotics, hormones and growth factors to enhance performance of tissue engineered bone therapies.

A material TCH, (Kasios, France) that is similar in composition to the Biosel (75% HA and 25% TCP) has been successfully used in the following conditions (Ref: http://www.kasios.com/doc-pdf/TCH-90-fren.pdf):

> for both epiphyseal and diaphyseal

> simple and complex fractures

> filling after removal of osteosynthesis

> materials and after benign synovioma curettage

> non-union or pseudarthrosis, arthrod-esis and osteotomies

> prosthesis revision surgery

> spinal fusion

The material is available as porous granules, blocks, cylinders and wedges.

However, there are more products available that are similar in composition to the MBCP$^+$ (20% HA, 80% TCP) for various orthopaedic, dental and spinal applications:

BoneCeramic (Straumann, Switzerland)

BoneSave (Stryker Orthopaedics, NJ)

Kainos (Signus, Germany)

MBCP+ (Biomatlante SA, France)

OsSatura BCP (Integra Orthobiologics, CA)

Osteosynt (Einco, Brazil)

ReproBone (Ceramisys, UK)

Tribone 80 (Stryker, Europe)

6.2.2 Potential of Ephrin B2 in the clinic:

A study by Kwan Tat *et al*.[373] showed that Eph B4 receptor activation that was catalysed by Ephrin B2 in OA subchondral bone osteoblasts downregulates a variety of bone remodeling factors. Additionally, factors that caused increased activity of Ephrin B2 / Eph B4 inhibited bone resorption. Therefore, it was suggested that Ephrin B2 can be a therapeutic drug target to stop abnormal metabolism in OA tissue. Additionally, the authors suggest that Ephrin B2 as a therapeutic target could be extended to other diseases characterised by bone remodelling: post-menopausal osteoporosis, Rheumatoid Arthritis (RA), multiple myeloma and breast cancer. Further in a separate study, the group showed that treating OA chondrocytes incubated with human recombinant Ephrin B2 attenuates abnormal metabolism in these cells by suppressing catabolic activity and promoting anabolic activity[323,374].

It would be interesting to evaluate conditioned media from Ephrin B2 overexpressing hMSCs and look for specific growth factors released to get more insight into ephrin-B2 catalysed angiogenesis. Future studies entail

looking into factors that regulate Ephrin B2 and Eph B4 regulation. Additionally,; their relationship to known genes and pathways involved in osteoclast and osteoblast differentiation can be investigated[147].

It would be interesting to co-culture HUVEC's with Ephrin B2 modified hMSCs as HUVEC/non modified MSC co-culture has been shown to increase ALP activity in the absence of osteoinductive factors. Conversely, Meury *et al*., [375] observed inhibition of Osterix expression when HUVEC's were co-cultured with dexamethasone. Therefore, it has been proposed that endothelial cells play a role in MSC differentiation rate by recruiting osteoprogenitor cells at bone remodeling sites and preserve them at a pre-osteoblastic state so as to prevent their mineralisation within the vessel. Once the osteoprogenitors home to the sites of bone remodeling, they would functionally differentiate into mature osteoblasts that would lay down new osteoid tissue[376].

Recognizing the paracrine activity between osteoblast and endothelial cells would enhance our understanding of the critical processes involved in bone remodeling and would help develop new therapies for engineering vascularised bone constructs.

A study by Kusumbe *et al*., [377] improved our understanding of the bone vasculature. Imaging of the vasculature revealed the presence of structurally distinct capillary subsets, distinguishable by immunostaining for CD31 and endomucin. Strong CD31 and endomucin staining was seen in a subtype termed Type H, while weak staining was seen in another subtype, termed Type L. Osterix, collagenase type 1α and Runx 2 positive cells were detected in the vicinity of Type H cells but absent near the Type L domain. The significant decline of osteoprogenitors seen in bone from aged mice was associated with a simultaneous decrease in Type H blood vessels with advancing age. Further, Xie *et al*., [378] showed that platelet-derived growth factor-BB (PDGF-BB) secreted by preosteoclasts induces formation of Type H vessels during bone formation and remodeling.

As stated previously, a series of healing events occur following fracture. Growth factors and cytokines in the fracture environment recruit cells and

promote their differentiation, ultimately leading to new bone formation. This normal fracture healing is impaired in a condition like avascular necrosis wherein blood supply is compromised. Autologous bone grafting has the best clinical outcome in such situations, but comes with many limitations as stated previously.

An endochondral route would also be a promising strategy for bone repair because it mimics the *in vivo* bone development process. As stated previously Ephrin B2 has a known role in endochondral ossification. It has been suggested that the cartilage could possibly be responsible for recruitment and formation of bone marrow and associated vasculature in the newly developed bone[379]. The invading vasculature plays a key role in converting cartilage to bone. Additionally, transdifferentiation of cartilage to bone has been observed in a number of studies- suggesting the presence of additional cell types contributing to endochondral ossification[380-385]. Further, use of cartilage grafts over direct osteogenesis is a significant advantage because it exploits the inherent ability of cartilage to adapt to avascular conditions. As chondrocytes undergo hypertrophy, a range of factors promoting new bone formation is secreted:

1. VEGF (to aid in vascular invasion)
2. MMP-13 (promotes matrix mineralisation)
3. BMPs (promote osteogenic differentiation) [324,380,386-388]

For bone substitutes to be successful, pro-osteogenic cells seeded on an osteoinductive osteoconductive scaffold, while avoiding donor site morbidity is required. Therefore, seeding of ephrin-B2 overexpressing hMSCs on the MBCP scaffold is proposed as an attractive option as it fulfills all requirements of an ideal substitute to treat an osteonecrotic condition.

BIBLIOGRAPHY

1. Bancroft, G. & Mikos, A. Bone Tissue Engineering by Cell Transplantation. in *Polymer Based Systems on Tissue Engineering, Replacement and Regeneration* 251-263 (Springer, 2002).
2. Yaszemski, M.J., Payne, R.G., Hayes, W.C., Langer, R. & Mikos, A.G. Evolution of bone transplantation: molecular, cellular and tissue strategies to engineer human bone. *Biomaterials* **17**, 175-185 (1996).
3. Bruder, S.P. & Caplan, A.I. Bone regeneration through cellular engineering. *Principles of tissue engineering* **2**, 683-696 (2000).
4. Athanasiou, K.A., Zhu, C.-F., Lanctot, D., Agrawal, C. & Wang, X. Fundamentals of biomechanics in tissue engineering of bone. *Tissue engineering* **6**, 361-381 (2000).
5. Clarke, B. Normal bone anatomy and physiology. *Clinical journal of the American Society of Nephrology* **3**, S131-S139 (2008).
6. Sikavitsas, V.I., Temenoff, J.S. & Mikos, A.G. Biomaterials and bone mechanotransduction. *Biomaterials* **22**, 2581-2593 (2001).
7. Mistry, A.S. & Mikos, A.G. Tissue engineering strategies for bone regeneration. *Advances in biochemical engineering/biotechnology* **94**, 1-22 (2005).
8. Jilka, R.L. Biology of the basic multicellular unit and the pathophysiology of osteoporosis. *Medical and pediatric oncology* **41**, 182-185 (2003).
9. Clarke, B. Normal bone anatomy and physiology. *Clinical journal of the American Society of Nephrology : CJASN* **3 Suppl 3**, S131-139 (2008).
10. Jordan, C.T. & Lemischka, I.R. Clonal and systemic analysis of long-term hematopoiesis in the mouse. *Genes & development* **4**, 220-232 (1990).
11. Osawa, M., Hanada, K.-i., Hamada, H. & Nakauchi, H. Long-term lymphohematopoietic reconstitution by a single CD34-low/negative hematopoietic stem cell. *Science* **273**, 242 (1996).
12. Matsuzaki, Y., Kinjo, K., Mulligan, R.C. & Okano, H. Unexpectedly efficient homing capacity of purified murine hematopoietic stem cells. *Immunity* **20**, 87-93 (2004).
13. Wilson, A. & Trumpp, A. Bone-marrow haematopoietic-stem-cell niches. *Nature reviews. Immunology* **6**, 93 (2006).

14. Deguchi, K.*, et al.* Excessive extramedullary hematopoiesis in Cbfa1-deficient mice with a congenital lack of bone marrow. *Biochemical and biophysical research communications* **255**, 352-359 (1999).
15. Sasaki, K.*, et al.* Absence of fetal liver hematopoiesis in mice deficient in transcriptional coactivator core binding factor beta. *Proceedings of the National Academy of Sciences* **93**, 12359-12363 (1996).
16. Wang, Q.*, et al.* Disruption of the Cbfa2 gene causes necrosis and hemorrhaging in the central nervous system and blocks definitive hematopoiesis. *Proceedings of the National Academy of Sciences* **93**, 3444-3449 (1996).
17. Taichman, R.S. & Emerson, S.G. The role of osteoblasts in the hematopoietic microenvironment. *Stem cells* **16**, 7-15 (1998).
18. Greenfield, E.M., Horowitz, M.C. & Lavish, S.A. Stimulation by parathyroid hormone of interleukin-6 and leukemia inhibitory factor expression in osteoblasts is an immediate-early gene response induced by cAMP signal transduction. *Journal of Biological Chemistry* **271**, 10984-10989 (1996).
19. Ponomaryov, T.*, et al.* Increased production of SDF-1 following treatment with DNA damaging agents: relevance for human stem cell homing and repopulation of NOD/SCID mice. *J Clin Invest* **106**, 1331-1339 (2000).
20. Hofbauer, L.C.*, et al.* The roles of osteoprotegerin and osteoprotegerin ligand in the paracrine regulation of bone resorption. *Journal of Bone and Mineral Research* **15**, 2-12 (2000).
21. Taichman, R.S. Blood and bone: two tissues whose fates are intertwined to create the hematopoietic stem-cell niche. *Blood* **105**, 2631-2639 (2005).
22. Scadden, D.T. Blood and Bone. *The New England journal of medicine* **374**, 1891-1893 (2016).
23. Morrison, S.J. & Scadden, D.T. The bone marrow niche for haematopoietic stem cells. *Nature* **505**, 327-334 (2014).
24. Bianco, P. Bone and the hematopoietic niche: a tale of two stem cells. *Blood* **117**, 5281-5288 (2011).

25. Charles, J.F. & Aliprantis, A.O. Osteoclasts: more than 'bone eaters'. *Trends in molecular medicine* **20**, 449-459 (2014).
26. Sims, N.A. & Martin, T.J. Coupling the activities of bone formation and resorption: a multitude of signals within the basic multicellular unit. *BoneKEy reports* **3**, 481 (2014).
27. Bonewald, L.F. The amazing osteocyte. *Journal of bone and mineral research : the official journal of the American Society for Bone and Mineral Research* **26**, 229-238 (2011).
28. Porter, J.R., Ruckh, T.T. & Popat, K.C. Bone tissue engineering: a review in bone biomimetics and drug delivery strategies. *Biotechnology progress* **25**, 1539-1560 (2009).
29. Einhorn, T.A. & Gerstenfeld, L.C. Fracture healing: mechanisms and interventions. *Nature reviews. Rheumatology* **11**, 45-54 (2015).
30. Kalfas, I.H. Principles of bone healing. *Neurosurgical focus* **10**, E1 (2001).
31. Dimitriou, R., Jones, E., McGonagle, D. & Giannoudis, P.V. Bone regeneration: current concepts and future directions. *BMC medicine* **9**, 66 (2011).
32. Tien, W.C.*, et al.* A population-based study of prevalence and hospital charges in total hip and knee replacement. *International orthopaedics* **33**, 949-954 (2009).
33. Pavelka, K. Osteonecrosis. *Bailliere's best practice & research. Clinical rheumatology* **14**, 399-414 (2000).
34. Rackwitz, L.*, et al.* Stem cell- and growth factor-based regenerative therapies for avascular necrosis of the femoral head. *Stem cell research & therapy* **3**, 7 (2012).
35. Petrigliano, F.A. & Lieberman, J.R. Osteonecrosis of the hip: novel approaches to evaluation and treatment. *Clinical orthopaedics and related research* **465**, 53-62 (2007).
36. Bohr, H. & Larsen, E.H. On Necrosis of the Femoral Head after Fracture of the Neck of the Femur. *The Journal of bone and joint surgery. British volume* **47**, 330-338 (1965).
37. Giannoudis, P.V., Einhorn, T.A. & Marsh, D. Fracture healing: The diamond concept. *Injury* **38**, S3-S6 (2007).

38. Phemister, D.B. The classic: repair of bone in the presence of aseptic necrosis resulting from fractures, transplantations, and vascular obstruction. *Clinical orthopaedics and related research* **466**, 1021-1033 (2008).
39. Fondi, C. & Franchi, A. Definition of bone necrosis by the pathologist. *Clinical cases in mineral and bone metabolism : the official journal of the Italian Society of Osteoporosis, Mineral Metabolism, and Skeletal Diseases* **4**, 21-26 (2007).
40. Hungerford, D.S. & Jones, L.C. Asymptomatic osteonecrosis: should it be treated? *Clinical orthopaedics and related research*, 124-130 (2004).
41. Fukushima, W.*, et al.* Nationwide epidemiologic survey of idiopathic osteonecrosis of the femoral head. *Clinical orthopaedics and related research* **468**, 2715-2724 (2010).
42. Kang, J.S.*, et al.* Prevalence of osteonecrosis of the femoral head: a nationwide epidemiologic analysis in Korea. *The Journal of arthroplasty* **24**, 1178-1183 (2009).
43. Lai, Y.S., Wei, H.W. & Cheng, C.K. Incidence of hip replacement among national health insurance enrollees in Taiwan. *Journal of orthopaedic surgery and research* **3**, 42 (2008).
44. Lai, K.A.*, et al.* The use of alendronate to prevent early collapse of the femoral head in patients with nontraumatic osteonecrosis. A randomized clinical study. *The Journal of bone and joint surgery. American volume* **87**, 2155-2159 (2005).
45. Chen, W.M.*, et al.* Autosomal dominant avascular necrosis of femoral head in two Taiwanese pedigrees and linkage to chromosome 12q13. *American journal of human genetics* **75**, 310-317 (2004).
46. Liu, Y.F.*, et al.* Type II collagen gene variants and inherited osteonecrosis of the femoral head. *The New England journal of medicine* **352**, 2294-2301 (2005).
47. Miyamoto, Y.*, et al.* A recurrent mutation in type II collagen gene causes Legg-Calve-Perthes disease in a Japanese family. *Human genetics* **121**, 625-629 (2007).

48. Wang, L., Pan, H. & Zhu, Z.A. A genetic pedigree analysis to identify gene mutations involved in femoral head necrosis. *Molecular medicine reports* **10**, 1835-1838 (2014).
49. Pouya, F. & Kerachian, M.A. Avascular Necrosis of the Femoral Head: Are Any Genes Involved? *The archives of bone and joint surgery* **3**, 149-155 (2015).
50. Liu, Y., Zhang, Z., Liu, S., Su, X. & Zhou, S. Association between VEGF -634G/C polymorphism and osteonecrosis of the femoral head susceptibility: a meta analysis. *International journal of clinical and experimental medicine* **8**, 10979-10985 (2015).
51. Filvaroff, E.H. VEGF and bone. *Journal of musculoskeletal & neuronal interactions* **3**, 304-307; discussion 320-301 (2003).
52. Hunter, J. A treatise on the blood, inflammation, and gun-shot wounds. 1794. *Clinical orthopaedics and related research* **458**, 27-34 (2007).
53. Trueta, J. & Buhr, A.J. The Vascular Contribution to Osteogenesis. V. The Vasculature Supplying the Epiphysial Cartilage in Rachitic Rats. *The Journal of bone and joint surgery. British volume* **45**, 572-581 (1963).
54. Hausman, M.R., Schaffler, M.B. & Majeska, R.J. Prevention of fracture healing in rats by an inhibitor of angiogenesis. *Bone* **29**, 560-564 (2001).
55. Fang, T.D.*, et al.* Angiogenesis is required for successful bone induction during distraction osteogenesis. *Journal of bone and mineral research : the official journal of the American Society for Bone and Mineral Research* **20**, 1114-1124 (2005).
56. Gerstenfeld, L.C., Cullinane, D.M., Barnes, G.L., Graves, D.T. & Einhorn, T.A. Fracture healing as a post-natal developmental process: molecular, spatial, and temporal aspects of its regulation. *Journal of cellular biochemistry* **88**, 873-884 (2003).
57. Carano, R.A. & Filvaroff, E.H. Angiogenesis and bone repair. *Drug discovery today* **8**, 980-989 (2003).
58. Cenni, E., Perut, F. & Baldini, N. In vitro models for the evaluation of angiogenic potential in bone engineering. *Acta pharmacologica Sinica* **32**, 21-30 (2011).

59. Lu, C., Marcucio, R. & Miclau, T. Assessing angiogenesis during fracture healing. *The Iowa orthopaedic journal* **26**, 17-26 (2006).
60. Lavernia, C.J., Sierra, R.J. & Grieco, F.R. Osteonecrosis of the femoral head. *The Journal of the American Academy of Orthopaedic Surgeons* **7**, 250-261 (1999).
61. Cheng, E.Y., Thongtrangan, I., Laorr, A. & Saleh, K.J. Spontaneous resolution of osteonecrosis of the femoral head. *The Journal of bone and joint surgery. American volume* **86-A**, 2594-2599 (2004).
62. Hernigou, P. & Beaujean, F. Treatment of osteonecrosis with autologous bone marrow grafting. *Clinical orthopaedics and related research*, 14-23 (2002).
63. Hernigou, P., Poignard, A., Nogier, A. & Manicom, O. Fate of very small asymptomatic stage-I osteonecrotic lesions of the hip. *The Journal of bone and joint surgery. American volume* **86**, 2589-2593 (2004).
64. Seamon, J., Keller, T., Saleh, J. & Cui, Q. The pathogenesis of nontraumatic osteonecrosis. *Arthritis* **2012**(2012).
65. Mont, M.A., Carbone, J.J. & Fairbank, A.C. Core decompression versus nonoperative management for osteonecrosis of the hip. *Clinical orthopaedics and related research*, 169-178 (1996).
66. Rajagopal, M., Balch Samora, J. & Ellis, T.J. Efficacy of core decompression as treatment for osteonecrosis of the hip: a systematic review. *Hip international : the journal of clinical and experimental research on hip pathology and therapy* **22**, 489-493 (2012).
67. Ficat, R.P. Idiopathic bone necrosis of the femoral head. Early diagnosis and treatment. *The Journal of bone and joint surgery. British volume* **67**, 3-9 (1985).
68. Chan, T.W., Dalinka, M.K., Steinberg, M.E. & Kressel, H.Y. MRI appearance of femoral head osteonecrosis following core decompression and bone grafting. *Skeletal radiology* **20**, 103-107 (1991).
69. Smith, S.W., Fehring, T.K., Griffin, W.L. & Beaver, W.B. Core decompression of the osteonecrotic femoral head. *The Journal of bone and joint surgery. American volume* **77**, 674-680 (1995).

70. Koo, K.H.*, et al.* Preventing collapse in early osteonecrosis of the femoral head. A randomised clinical trial of core decompression. *The Journal of bone and joint surgery. British volume* **77**, 870-874 (1995).
71. Mont, M.A., Einhorn, T.A., Sponseller, P.D. & Hungerford, D.S. The trapdoor procedure using autogenous cortical and cancellous bone grafts for osteonecrosis of the femoral head. *Bone & Joint Journal* **80**, 56-62 (1998).
72. Phemister, D.B. Treatment of the necrotic head of the femur in adults. *The Journal of bone and joint surgery. American volume* **31**, 55-66 (1949).
73. Sen, R.K. Management of avascular necrosis of femoral head at pre-collapse stage. *Indian journal of orthopaedics* **43**, 6 (2009).
74. Lieberman, J.R.*, et al.* Osteonecrosis of the hip: management in the 21st century. *Instructional course lectures* **52**, 337-355 (2003).
75. Garino, J.P. & Steinberg, M.E. Total hip arthroplasty in patients with avascular necrosis of the femoral head: a 2- to 10-year follow-up. *Clinical orthopaedics and related research*, 108-115 (1997).
76. Mistry, A.S. & Mikos, A.G. Tissue engineering strategies for bone regeneration. in *Regenerative medicine II* 1-22 (Springer, 2005).
77. Urist, M.R. Bone: formation by autoinduction. *Science* **150**, 893-899 (1965).
78. Hench, L.L. & Polak, J.M. Third-generation biomedical materials. *Science* **295**, 1014-1017 (2002).
79. Zijderveld, S.A., Zerbo, I.R., van den Bergh, J., Schulten, E. & Bruggenkate, C.M.t. Maxillary Sinus Floor Augmentation Using a β3-Tricalcium Phosphate (Cerasorb) Alone Compared to Autogenous Bone Grafts. *International Journal of Oral & Maxillofacial Implants* **20**(2005).
80. Jell, G. & Stevens, M.M. Gene activation by bioactive glasses. *Journal of Materials Science: Materials in Medicine* **17**, 997-1002 (2006).
81. Tsigkou, O., Hench, L., Boccaccini, A., Polak, J. & Stevens, M. Enhanced differentiation and mineralization of human fetal osteoblasts on PDLLA containing Bioglass® composite films in the absence of

osteogenic supplements. *Journal of Biomedical Materials Research Part A* **80**, 837-851 (2007).

82. Ma, P.X. & Choi, J.-W. Biodegradable polymer scaffolds with well-defined interconnected spherical pore network. *Tissue engineering* **7**, 23-33 (2001).
83. Zhao, F.*, et al.* Preparation and histological evaluation of biomimetic three-dimensional hydroxyapatite/chitosan-gelatin network composite scaffolds. *Biomaterials* **23**, 3227-3234 (2002).
84. Liu, X. & Ma, P.X. Polymeric scaffolds for bone tissue engineering. *Annals of biomedical engineering* **32**, 477-486 (2004).
85. Vacanti, J.P. & Langer, R.S. Preparation of three-dimensional fibrous scaffold for attaching cells to produce vascularized tissue in vivo. (Google Patents, 1998).
86. Ginty, P.J.*, et al.* Mammalian cell survival and processing in supercritical CO2. *Proceedings of the National Academy of Sciences* **103**, 7426-7431 (2006).
87. Sherwood, J.K.*, et al.* A three-dimensional osteochondral composite scaffold for articular cartilage repair. *Biomaterials* **23**, 4739-4751 (2002).
88. Cushing, M.C. & Anseth, K.S. Hydrogel cell cultures. *Science* **316**, 1133-1134 (2007).
89. Lutolf, M.*, et al.* Synthetic matrix metalloproteinase-sensitive hydrogels for the conduction of tissue regeneration: engineering cell-invasion characteristics. *Proceedings of the National Academy of Sciences* **100**, 5413-5418 (2003).
90. Lutolf, M.P.*, et al.* Repair of bone defects using synthetic mimetics of collagenous extracellular matrices. *Nature biotechnology* **21**, 513-518 (2003).
91. Koh, W.-G., Revzin, A. & Pishko, M.V. Poly (ethylene glycol) hydrogel microstructures encapsulating living cells. *Langmuir : the ACS journal of surfaces and colloids* **18**, 2459-2462 (2002).
92. Tsang, V.L. & Bhatia, S.N. Three-dimensional tissue fabrication. *Advanced drug delivery reviews* **56**, 1635-1647 (2004).

93. Linhart, W.*, et al.* Biologically and chemically optimized composites of carbonated apatite and polyglycolide as bone substitution materials. *Journal of biomedical materials research* **54**, 162-171 (2001).
94. Hu, Y., Zhang, C., Zhang, S., Xiong, Z. & Xu, J. Development of a porous poly (L-lactic acid)/hydroxyapatite/collagen scaffold as a BMP delivery system and its use in healing canine segmental bone defect. *Journal of Biomedical Materials Research Part A* **67**, 591-598 (2003).
95. Place, E.S., Evans, N.D. & Stevens, M.M. Complexity in biomaterials for tissue engineering. *Nature materials* **8**, 457-470 (2009).
96. Stevens, M.M. Biomaterials for bone tissue engineering. *Materials Today* **5**, 18-25 (2008).
97. Liao, S., Cui, F. & Zhu, Y. Osteoblasts adherence and migration through three-dimensional porous mineralized collagen based composite: nHAC/PLA. *Journal of Bioactive and Compatible polymers* **19**, 117-130 (2004).
98. Smith, B.D. & Grande, D.A. The current state of scaffolds for musculoskeletal regenerative applications. *Nature Reviews Rheumatology* **11**, 213-222 (2015).
99. Bose, S., Roy, M. & Bandyopadhyay, A. Recent advances in bone tissue engineering scaffolds. *Trends in biotechnology* **30**, 546-554 (2012).
100. Hutmacher, D.W. & Sittinger, M. Periosteal cells in bone tissue engineering. *Tissue engineering* **9 Suppl 1**, S45-64 (2003).
101. Nakahara, H.*, et al.* In vitro differentiation of bone and hypertrophic cartilage from periosteal-derived cells. *Experimental cell research* **195**, 492-503 (1991).
102. Mateizel, I.*, et al.* Efficient differentiation of human embryonic stem cells into a homogeneous population of osteoprogenitor-like cells. *Reproductive biomedicine online* **16**, 741-753 (2008).
103. Tian, X.F.*, et al.* Comparison of osteogenesis of human embryonic stem cells within 2D and 3D culture systems. *Scandinavian journal of clinical and laboratory investigation* **68**, 58-67 (2008).
104. Bielby, R.C., Boccaccini, A.R., Polak, J.M. & Buttery, L.D. In vitro differentiation and in vivo mineralization of osteogenic cells derived

from human embryonic stem cells. *Tissue engineering* **10**, 1518-1525 (2004).

105. Ahn, S.E.*, et al.* Primary bone-derived cells induce osteogenic differentiation without exogenous factors in human embryonic stem cells. *Biochemical and biophysical research communications* **340**, 403-408 (2006).
106. Inanc, B., Elcin, A.E. & Elcin, Y.M. Effect of osteogenic induction on the in vitro differentiation of human embryonic stem cells cocultured with periodontal ligament fibroblasts. *Artificial organs* **31**, 792-800 (2007).
107. Olivier, E.N., Rybicki, A.C. & Bouhassira, E.E. Differentiation of human embryonic stem cells into bipotent mesenchymal stem cells. *Stem cells* **24**, 1914-1922 (2006).
108. Barberi, T., Willis, L.M., Socci, N.D. & Studer, L. Derivation of multipotent mesenchymal precursors from human embryonic stem cells. *PLoS medicine* **2**, e161 (2005).
109. Boyd, N.L., Robbins, K.R., Dhara, S.K., West, F.D. & Stice, S.L. Human embryonic stem cell-derived mesoderm-like epithelium transitions to mesenchymal progenitor cells. *Tissue engineering. Part A* **15**, 1897-1907 (2009).
110. Kim, S.*, et al.* In vivo bone formation from human embryonic stem cell-derived osteogenic cells in poly(d,l-lactic-co-glycolic acid)/hydroxyapatite composite scaffolds. *Biomaterials* **29**, 1043-1053 (2008).
111. Takahashi, K. & Yamanaka, S. Induction of pluripotent stem cells from mouse embryonic and adult fibroblast cultures by defined factors. *Cell* **126**, 663-676 (2006).
112. Feng, B., Ng, J.-H., Heng, J.-C.D. & Ng, H.-H. Molecules that promote or enhance reprogramming of somatic cells to induced pluripotent stem cells. *Cell stem cell* **4**, 301-312 (2009).
113. Friedenstein, A.J., Piatetzky, S., II & Petrakova, K.V. Osteogenesis in transplants of bone marrow cells. *Journal of embryology and experimental morphology* **16**, 381-390 (1966).

114. Castro-Malaspina, H., *et al.* Characterization of human bone marrow fibroblast colony-forming cells (CFU-F) and their progeny. *Blood* **56**, 289-301 (1980).
115. Prockop, D.J. Marrow stromal cells as stem cells for nonhematopoietic tissues. *Science* **276**, 71-74 (1997).
116. Caplan, A.I. & Bruder, S.P. Mesenchymal stem cells: building blocks for molecular medicine in the 21st century. *Trends in molecular medicine* **7**, 259-264 (2001).
117. Pittenger, M.F., *et al.* Multilineage potential of adult human mesenchymal stem cells. *Science* **284**, 143-147 (1999).
118. da Silva Meirelles, L., Chagastelles, P.C. & Nardi, N.B. Mesenchymal stem cells reside in virtually all post-natal organs and tissues. *Journal of cell science* **119**, 2204-2213 (2006).
119. Zuk, P.A., *et al.* Human adipose tissue is a source of multipotent stem cells. *Molecular biology of the cell* **13**, 4279-4295 (2002).
120. De Bari, C., Dell'Accio, F., Tylzanowski, P. & Luyten, F.P. Multipotent mesenchymal stem cells from adult human synovial membrane. *Arthritis and rheumatism* **44**, 1928-1942 (2001).
121. De Bari, C., *et al.* Mesenchymal multipotency of adult human periosteal cells demonstrated by single-cell lineage analysis. *Arthritis and rheumatism* **54**, 1209-1221 (2006).
122. De Bari, C., *et al.* Skeletal muscle repair by adult human mesenchymal stem cells from synovial membrane. *The Journal of cell biology* **160**, 909-918 (2003).
123. Caplan, A.I. All MSCs are pericytes? *Cell stem cell* **3**, 229-230 (2008).
124. Dominici, M., *et al.* Minimal criteria for defining multipotent mesenchymal stromal cells. The International Society for Cellular Therapy position statement. *Cytotherapy* **8**, 315-317 (2006).
125. Augello, A. & De Bari, C. The regulation of differentiation in mesenchymal stem cells. *Human gene therapy* **21**, 1226-1238 (2010).
126. Haynesworth, S.E., Goshima, J., Goldberg, V.M. & Caplan, A.I. Characterization of cells with osteogenic potential from human marrow. *Bone* **13**, 81-88 (1992).

127. Noth, U., Rackwitz, L., Steinert, A.F. & Tuan, R.S. Cell delivery therapeutics for musculoskeletal regeneration. *Advanced drug delivery reviews* **62**, 765-783 (2010).
128. Barry, F. & Murphy, M. Mesenchymal stem cells in joint disease and repair. *Nature reviews. Rheumatology* **9**, 584-594 (2013).
129. Meirelles Lda, S., Fontes, A.M., Covas, D.T. & Caplan, A.I. Mechanisms involved in the therapeutic properties of mesenchymal stem cells. *Cytokine & growth factor reviews* **20**, 419-427 (2009).
130. Huang, Y.X., Ren, J., Chen, C., Ren, T.B. & Zhou, X.Y. Preparation and properties of poly(lactide-co-glycolide) (PLGA)/ nano-hydroxyapatite (NHA) scaffolds by thermally induced phase separation and rabbit MSCs culture on scaffolds. *Journal of biomaterials applications* **22**, 409-432 (2008).
131. Sorrell, J.M., Baber, M.A. & Caplan, A.I. Influence of adult mesenchymal stem cells on in vitro vascular formation. *Tissue engineering. Part A* **15**, 1751-1761 (2009).
132. Tombran-Tink, J. & Barnstable, C.J. Osteoblasts and osteoclasts express PEDF, VEGF-A isoforms, and VEGF receptors: possible mediators of angiogenesis and matrix remodeling in the bone. *Biochemical and biophysical research communications* **316**, 573-579 (2004).
133. Barry, F.P. & Murphy, J.M. Mesenchymal stem cells: clinical applications and biological characterization. *The international journal of biochemistry & cell biology* **36**, 568-584 (2004).
134. Ryan, J.M., Barry, F.P., Murphy, J.M. & Mahon, B.P. Mesenchymal stem cells avoid allogeneic rejection. *Journal of inflammation* **2**, 8 (2005).
135. Bhattacharya, V.*, et al.* Enhanced endothelialization and microvessel formation in polyester grafts seeded with CD34+ bone marrow cells. *Blood* **95**, 581-585 (2000).
136. Kocher, A.*, et al.* Neovascularization of ischemic myocardium by human bone-marrow–derived angioblasts prevents cardiomyocyte apoptosis, reduces remodeling and improves cardiac function. *Nature medicine* **7**, 430-436 (2001).

137. Murohara, T.*, et al.* Transplanted cord blood–derived endothelial precursor cells augment postnatal neovascularization. *The Journal of clinical investigation* **105**, 1527-1536 (2000).
138. Szmitko, P.E.*, et al.* Endothelial progenitor cells new hope for a broken heart. *Circulation* **107**, 3093-3100 (2003).
139. Urbich, C. & Dimmeler, S. Endothelial progenitor cells characterization and role in vascular biology. *Circulation research* **95**, 343-353 (2004).
140. Evans, C.H. Gene delivery to bone. *Advanced drug delivery reviews* **64**, 1331-1340 (2012).
141. Kofron, M.D. & Laurencin, C.T. Bone tissue engineering by gene delivery. *Advanced drug delivery reviews* **58**, 555-576 (2006).
142. Szmitko, P.E.*, et al.* Endothelial progenitor cells: new hope for a broken heart. *Circulation* **107**, 3093-3100 (2003).
143. Urbich, C. & Dimmeler, S. Endothelial progenitor cells: characterization and role in vascular biology. *Circulation research* **95**, 343-353 (2004).
144. Saik, J.E., McHale, M.K. & West, J.L. Biofunctional materials for directing vascular development. *Current vascular pharmacology* **10**, 331-341 (2012).
145. Zhao, C.*, et al.* Bidirectional ephrinB2-EphB4 signaling controls bone homeostasis. *Cell metabolism* **4**, 111-121 (2006).
146. Mundy, G.R. & Elefteriou, F. Boning up on ephrin signaling. *Cell* **126**, 441-443 (2006).
147. Sims, N.A. EPHs and ephrins: Many pathways to regulate osteoblasts and osteoclasts. *IBMS BoneKEy* **7**, 304-313 (2010).
148. Matsuo, K. & Otaki, N. Bone cell interactions through Eph/ephrin: bone modeling, remodeling and associated diseases. *Cell adhesion & migration* **6**, 148-156 (2012).
149. Sawamiphak, S.*, et al.* Ephrin-B2 regulates VEGFR2 function in developmental and tumour angiogenesis. *Nature* **465**, 487-491 (2010).
150. Wang, Y.*, et al.* Ephrin-B2 controls VEGF-induced angiogenesis and lymphangiogenesis. *Nature* **465**, 483-486 (2010).
151. Mayer, H.*, et al.* Vascular endothelial growth factor (VEGF-A) expression in human mesenchymal stem cells: autocrine and paracrine

role on osteoblastic and endothelial differentiation. *Journal of cellular biochemistry* **95**, 827-839 (2005).

152. Street, J.*, et al.* Vascular endothelial growth factor stimulates bone repair by promoting angiogenesis and bone turnover. *Proceedings of the National Academy of Sciences of the United States of America* **99**, 9656-9661 (2002).
153. Engsig, M.T.*, et al.* Matrix metalloproteinase 9 and vascular endothelial growth factor are essential for osteoclast recruitment into developing long bones. *The Journal of cell biology* **151**, 879-889 (2000).
154. Aldridge, S.E., Lennard, T.W., Williams, J.R. & Birch, M.A. Vascular endothelial growth factor receptors in osteoclast differentiation and function. *Biochemical and biophysical research communications* **335**, 793-798 (2005).
155. Cuneyt Tas, A., Korkusuz, F., Timucin, M. & Akkas, N. An investigation of the chemical synthesis and high-temperature sintering behaviour of calcium hydroxyapatite (HA) and tricalcium phosphate (TCP) bioceramics. *Journal of materials science. Materials in medicine* **8**, 91-96 (1997).
156. Dressmann, H. Ueber knochenplombierung bei hohlenformigen defekten des knochens. *Beitr Klin Chir* **9**, 804-810 (1892).
157. Albee, F.H. Studies in Bone Growth: Triple Calcium Phosphate as a Stimulus to Osteogenesis. *Annals of surgery* **71**, 32-39 (1920).
158. McGee, T.D. & Wood, J.L. Calcium-phosphate magnesium-aluminate osteoceramics. *Journal of biomedical materials research* **8**, 137-144 (1974).
159. Samavedi, S., Whittington, A.R. & Goldstein, A.S. Calcium phosphate ceramics in bone tissue engineering: a review of properties and their influence on cell behavior. *Acta biomaterialia* **9**, 8037-8045 (2013).
160. Kawasaki, T. Hydroxyapatite as a liquid chromatographic packing. *Journal of Chromatography A* **544**, 147-184 (1991).
161. Wakae, H.*, et al.* Preparation of carbonate apatite foam by hydrothermal treatment of a-TCP foam in carbonate salt solutions. *Arch Bioceram Res* **6**, 103-105 (2006).

162. LeGeros, R., Lin, S., Rohanizadeh, R., Mijares, D. & LeGeros, J. Biphasic calcium phosphate bioceramics: preparation, properties and applications. *Journal of materials science: Materials in Medicine* **14**, 201-209 (2003).
163. Koerten, H. & Van der Meulen, J. Degradation of calcium phosphate ceramics. *Journal of biomedical materials research* **44**, 78-86 (1999).
164. Legeros, R.Z. Biodegradation and bioresorption of calcium phosphate ceramics. *Clinical materials* **14**, 65-88 (1993).
165. LeGeros, R.*, et al.* Comparative properties of bioactive bone graft materials. *Bioceramics* **8**, 81-87 (1995).
166. Hench, L.L., Splinter, R.J., Allen, W. & Greenlee, T. Bonding mechanisms at the interface of ceramic prosthetic materials. *Journal of biomedical materials research* **5**, 117-141 (1971).
167. LeGeros, R., Orly, I., Gregoire, M. & Daculsi, G. Substrate surface dissolution and interfacial biological mineralization. *The bone-biomaterial interface*, 76-88 (1991).
168. LeGeros, R.Z. Calcium phosphate-based osteoinductive materials. *Chemical reviews* **108**, 4742-4753 (2008).
169. Samavedi, S., Whittington, A.R. & Goldstein, A.S. Calcium phosphate ceramics in bone tissue engineering: a review of properties and their influence on cell behavior. *Acta biomaterialia* **9**, 8037-8045 (2013).
170. Fujii, E.*, et al.* Selective protein adsorption property and characterization of nano-crystalline zinc-containing hydroxyapatite. *Acta biomaterialia* **2**, 69-74 (2006).
171. Tsapikouni, T.S., Allen, S. & Missirlis, Y.F. Measurement of interaction forces between fibrinogen coated probes and mica surface with the atomic force microscope: The pH and ionic strength effect. *Biointerphases* **3**, 1-8 (2008).
172. Zhu, X.D., Zhang, H.J., Fan, H.S., Li, W. & Zhang, X.D. Effect of phase composition and microstructure of calcium phosphate ceramic particles on protein adsorption. *Acta biomaterialia* **6**, 1536-1541 (2010).
173. Zhu, X.D.*, et al.* Effect of surface structure on protein adsorption to biphasic calcium-phosphate ceramics in vitro and in vivo. *Acta biomaterialia* **5**, 1311-1318 (2009).

174. Lee, J.H., Rim, N.G., Jung, H.S. & Shin, H. Control of osteogenic differentiation and mineralization of human mesenchymal stem cells on composite nanofibers containing poly[lactic-co-(glycolic acid)] and hydroxyapatite. *Macromolecular bioscience* **10**, 173-182 (2010).
175. Lee, K.W., Wang, S., Yaszemski, M.J. & Lu, L. Physical properties and cellular responses to crosslinkable poly(propylene fumarate)/hydroxyapatite nanocomposites. *Biomaterials* **29**, 2839-2848 (2008).
176. Keselowsky, B.G., Collard, D.M. & Garcia, A.J. Surface chemistry modulates fibronectin conformation and directs integrin binding and specificity to control cell adhesion. *Journal of biomedical materials research. Part A* **66**, 247-259 (2003).
177. Kandori, K., Miyagawa, K. & Ishikawa, T. Adsorption of immunogamma globulin onto various synthetic calcium hydroxyapatite particles. *Journal of colloid and interface science* **273**, 406-413 (2004).
178. Kandori, K., Murata, K. & Ishikawa, T. Microcalorimetric study of protein adsorption onto calcium hydroxyapatites. *Langmuir : the ACS journal of surfaces and colloids* **23**, 2064-2070 (2007).
179. Barradas, A.M.*, et al.* A calcium-induced signaling cascade leading to osteogenic differentiation of human bone marrow-derived mesenchymal stromal cells. *Biomaterials* **33**, 3205-3215 (2012).
180. Barradas, A.M.*, et al.* Molecular mechanisms of biomaterial-driven osteogenic differentiation in human mesenchymal stromal cells. *Integrative biology : quantitative biosciences from nano to macro* **5**, 920-931 (2013).
181. Khoshniat, S.*, et al.* Phosphate-dependent stimulation of MGP and OPN expression in osteoblasts via the ERK1/2 pathway is modulated by calcium. *Bone* **48**, 894-902 (2011).
182. LeGeros, R.Z. Calcium phosphate-based osteoinductive materials. *Chemical reviews* **108**, 4742-4753 (2008).
183. Dang, P.N.*, et al.* Controlled dual growth factor delivery from microparticles incorporated within human bone marrow-derived mesenchymal stem cell aggregates for enhanced bone tissue

engineering via endochondral ossification. *Stem cells translational medicine* **5**, 206-217 (2016).

184. Berzina-Cimdina, L. & Borodajenko, N. Research of calcium phosphates using Fourier transform infrared spectroscopy. in *Infrared Spectroscopy-Materials Science, Engineering and Technology* (InTech, 2012).
185. Pattanayak, D.K.*, et al.* Synthesis and evaluation of hydroxyapatite ceramics. *Trends Biomater Artif Organs* **18**, 87-92 (2005).
186. Bouler, J.M.*, et al.* Macroporous biphasic calcium phosphate ceramics: influence of five synthesis parameters on compressive strength. *Journal of biomedical materials research* **32**, 603-609 (1996).
187. Houmard, M., Fu, Q., Genet, M., Saiz, E. & Tomsia, A.P. On the structural, mechanical, and biodegradation properties of HA/β-TCP robocast scaffolds. *Journal of Biomedical Materials Research Part B: Applied Biomaterials* **101**, 1233-1242 (2013).
188. Mygind, T.*, et al.* Mesenchymal stem cell ingrowth and differentiation on coralline hydroxyapatite scaffolds. *Biomaterials* **28**, 1036-1047 (2007).
189. Itoh, M.*, et al.* Characterization of CO 3 Ap-collagen sponges using X-ray high-resolution microtomography. *Biomaterials* **25**, 2577-2583 (2004).
190. Takahashi, Y. & Tabata, Y. Effect of the fiber diameter and porosity of non-woven PET fabrics on the osteogenic differentiation of mesenchymal stem cells. *Journal of Biomaterials Science, Polymer Edition* **15**, 41-57 (2004).
191. García, A.J., Ducheyne, P. & Boettiger, D. Quantification of cell adhesion using a spinning disc device and application to surface-reactive materials. *Biomaterials* **18**, 1091-1098 (1997).
192. Zeng, H., Chittur, K.K. & Lacefield, W.R. Analysis of bovine serum albumin adsorption on calcium phosphate and titanium surfaces. *Biomaterials* **20**, 377-384 (1999).
193. Wang, K., Zhou, C., Hong, Y. & Zhang, X. A review of protein adsorption on bioceramics. *Interface focus* **2**, 259-277 (2012).

194. Malmsten, M. Formation of Adsorbed Protein Layers. *Journal of colloid and interface science* **207**, 186-199 (1998).
195. Lopes, M.A., Monteiro, F.J., Santos, J.D., Serro, A.P. & Saramago, B. Hydrophobicity, surface tension, and zeta potential measurements of glass-reinforced hydroxyapatite composites. *Journal of biomedical materials research* **45**, 370-375 (1999).
196. Osborn, J.F. & Newesely, H. The material science of calcium phosphate ceramics. *Biomaterials* **1**, 108-111 (1980).
197. Webster, T.J., Ergun, C., Doremus, R.H., Siegel, R.W. & Bizios, R. Specific proteins mediate enhanced osteoblast adhesion on nanophase ceramics. *Journal of biomedical materials research* **51**, 475-483 (2000).
198. Webster, T.J., Siegel, R.W. & Bizios, R. Osteoblast adhesion on nanophase ceramics. *Biomaterials* **20**, 1221-1227 (1999).
199. Woo, K., Zhang, R., Deng, H. & Ma, P. Protein-mediated osteoblast survival and migration on biodegradable polymer/hydroxyapatite composite scaffolds. in *Transaction of the 28th Annual Meeting of the Society for Biomaterial*, Vol. 605 (2002).
200. Woo, K., Wei, G. & Ma, P. Enhancement of fibronectin-and vitronectin-adsorption to polymer/hydroxyapatite scaffolds suppresses the apoptosis of osteoblasts. in *JOURNAL OF BONE AND MINERAL RESEARCH*, Vol. 17 S407-S407 (AMER SOC BONE & MINERAL RES 2025 M ST, NW, STE 800, WASHINGTON, DC 20036-3309 USA, 2002).
201. Wei, G. & Ma, P.X. Structure and properties of nano-hydroxyapatite/polymer composite scaffolds for bone tissue engineering. *Biomaterials* **25**, 4749-4757 (2004).
202. Cancedda, R., Giannoni, P. & Mastrogiacomo, M. A tissue engineering approach to bone repair in large animal models and in clinical practice. *Biomaterials* **28**, 4240-4250 (2007).
203. Daculsi, G., LeGeros, R.Z., Nery, E., Lynch, K. & Kerebel, B. Transformation of biphasic calcium phosphate ceramics in vivo: ultrastructural and physicochemical characterization. *Journal of biomedical materials research* **23**, 883-894 (1989).

204. Goshima, J., Goldberg, V.M. & Caplan, A.I. The osteogenic potential of culture-expanded rat marrow mesenchymal cells assayed in vivo in calcium phosphate ceramic blocks. *Clinical orthopaedics and related research*, 298-311 (1991).
205. Goshima, J., Goldberg, V.M. & Caplan, A.I. The origin of bone formed in composite grafts of porous calcium phosphate ceramic loaded with marrow cells. *Clinical orthopaedics and related research*, 274-283 (1991).
206. Martin, I., Muraglia, A., Campanile, G., Cancedda, R. & Quarto, R. Fibroblast growth factor-2 supports ex vivo expansion and maintenance of osteogenic precursors from human bone marrow. *Endocrinology* **138**, 4456-4462 (1997).
207. Kadiyala, S., Young, R.G., Thiede, M.A. & Bruder, S.P. Culture expanded canine mesenchymal stem cells possess osteochondrogenic potential in vivo and in vitro. *Cell transplantation* **6**, 125-134 (1997).
208. Krebsbach, P.H.*, et al.* Bone formation in vivo: comparison of osteogenesis by transplanted mouse and human marrow stromal fibroblasts. *Transplantation* **63**, 1059-1069 (1997).
209. Mastrogiacomo, M.*, et al.* Synchrotron radiation microtomography of bone engineered from bone marrow stromal cells. *Tissue engineering* **10**, 1767-1774 (2004).
210. Komlev, V.S.*, et al.* Kinetics of in vivo bone deposition by bone marrow stromal cells into porous calcium phosphate scaffolds: an X-ray computed microtomography study. *Tissue engineering* **12**, 3449-3458 (2006).
211. Casabona, F.*, et al.* Prefabricated engineered bone flaps: an experimental model of tissue reconstruction in plastic surgery. *Plastic and reconstructive surgery* **101**, 577-581 (1998).
212. Mankani, M.H.*, et al.* Pedicled bone flap formation using transplanted bone marrow stromal cells. *Archives of surgery* **136**, 263-270 (2001).
213. Dahl, M., Jorgensen, N.R., Horberg, M. & Pinholt, E.M. Carriers in mesenchymal stem cell osteoblast mineralization--state-of-the-art. *Journal of cranio-maxillo-facial surgery : official publication of the*

European Association for Cranio-Maxillo-Facial Surgery **42**, 41-47 (2014).

214. Wang, M. Developing bioactive composite materials for tissue replacement. *Biomaterials* **24**, 2133-2151 (2003).
215. Shin, H., Zygourakis, K., Farach-Carson, M.C., Yaszemski, M.J. & Mikos, A.G. Modulation of differentiation and mineralization of marrow stromal cells cultured on biomimetic hydrogels modified with Arg-Gly-Asp containing peptides. *Journal of biomedical materials research. Part A* **69**, 535-543 (2004).
216. Kirkham, G. & Cartmell, S. Genes and proteins involved in the regulation of osteogenesis. *Ashammakhi N, Reis R, Chiellini E, editores. Topics in Tissue Engineering* **3**(2007).
217. Nguyen, L.H.*, et al.* Vascularized bone tissue engineering: approaches for potential improvement. *Tissue engineering. Part B, Reviews* **18**, 363-382 (2012).
218. Mercado-Pagan, A.E., Stahl, A.M., Shanjani, Y. & Yang, Y. Vascularization in bone tissue engineering constructs. *Annals of biomedical engineering* **43**, 718-729 (2015).
219. Costa, P.F.*, et al.* Biofabrication of customized bone grafts by combination of additive manufacturing and bioreactor knowhow. *Biofabrication* **6**, 035006 (2014).
220. Tang, D.*, et al.* Biofabrication of bone tissue: approaches, challenges and translation for bone regeneration. *Biomaterials* **83**, 363-382 (2016).
221. Tandon, N., Marolt, D., Cimetta, E. & Vunjak-Novakovic, G. Bioreactor engineering of stem cell environments. *Biotechnology advances* **31**, 1020-1031 (2013).
222. Ingber, D.E.*, et al.* Cellular tensegrity: exploring how mechanical changes in the cytoskeleton regulate cell growth, migration, and tissue pattern during morphogenesis. *International review of cytology* **150**, 173-224 (1994).
223. Mauney, J.R.*, et al.* Mechanical stimulation promotes osteogenic differentiation of human bone marrow stromal cells on 3-D partially demineralized bone scaffolds in vitro. *Calcified tissue international* **74**, 458-468 (2004).

224. Rubin, C.T.*, et al.* Adipogenesis is inhibited by brief, daily exposure to high-frequency, extremely low-magnitude mechanical signals. *Proceedings of the National Academy of Sciences of the United States of America* **104**, 17879-17884 (2007).
225. Schumacher, M., Uhl, F., Detsch, R., Deisinger, U. & Ziegler, G. Static and dynamic cultivation of bone marrow stromal cells on biphasic calcium phosphate scaffolds derived from an indirect rapid prototyping technique. *Journal of materials science. Materials in medicine* **21**, 3039-3048 (2010).
226. Yu, X., Botchwey, E.A., Levine, E.M., Pollack, S.R. & Laurencin, C.T. Bioreactor-based bone tissue engineering: the influence of dynamic flow on osteoblast phenotypic expression and matrix mineralization. *Proceedings of the National Academy of Sciences of the United States of America* **101**, 11203-11208 (2004).
227. Bjerre, L., Bunger, C.E., Kassem, M. & Mygind, T. Flow perfusion culture of human mesenchymal stem cells on silicate-substituted tricalcium phosphate scaffolds. *Biomaterials* **29**, 2616-2627 (2008).
228. Xie, Y.*, et al.* Three-dimensional flow perfusion culture system for stem cell proliferation inside the critical-size beta-tricalcium phosphate scaffold. *Tissue engineering* **12**, 3535-3543 (2006).
229. Braccini, A.*, et al.* Three-dimensional perfusion culture of human bone marrow cells and generation of osteoinductive grafts. *Stem cells* **23**, 1066-1072 (2005).
230. Scherberich, A., Galli, R., Jaquiery, C., Farhadi, J. & Martin, I. Three-Dimensional Perfusion Culture of Human Adipose Tissue-Derived Endothelial and Osteoblastic Progenitors Generates Osteogenic Constructs with Intrinsic Vascularization Capacity. *Stem cells* **25**, 1823-1829 (2007).
231. Güven, S.*, et al.* Engineering of large osteogenic grafts with rapid engraftment capacity using mesenchymal and endothelial progenitors from human adipose tissue. *Biomaterials* **32**, 5801-5809 (2011).

232. Wendt, D., Stroebel, S., Jakob, M., John, G. & Martin, I. Uniform tissues engineered by seeding and culturing cells in 3D scaffolds under perfusion at defined oxygen tensions. *Biorheology* **43**, 481-488 (2006).
233. Santoro, R.*, et al.* Bioreactor based engineering of large-scale human cartilage grafts for joint resurfacing. *Biomaterials* **31**, 8946-8952 (2010).
234. Di Maggio, N.*, et al.* Toward modeling the bone marrow niche using scaffold-based 3D culture systems. *Biomaterials* **32**, 321-329 (2011).
235. Papadimitropoulos, A.*, et al.* A 3D in vitro bone organ model using human progenitor cells. *European cells & materials* **21**, 445-458 (2011).
236. Sadr, N.*, et al.* Enhancing the biological performance of synthetic polymeric materials by decoration with engineered, decellularized extracellular matrix. *Biomaterials* **33**, 5085-5093 (2012).
237. Scherberich, A., Galli, R., Jaquiery, C., Farhadi, J. & Martin, I. Three-dimensional perfusion culture of human adipose tissue-derived endothelial and osteoblastic progenitors generates osteogenic constructs with intrinsic vascularization capacity. *Stem cells* **25**, 1823-1829 (2007).
238. Papadimitropoulos, A.*, et al.* A 3D in vitro bone organ model using human progenitor cells. *European cells & materials* **21**, 445-458; discussion 458 (2011).
239. Papadimitropoulos, A.*, et al.* Expansion of human mesenchymal stromal cells from fresh bone marrow in a 3D scaffold-based system under direct perfusion. *PloS one* **9**, e102359 (2014).
240. Vahabi, S.*, et al.* A comparison between the efficacy of Bio-Oss, hydroxyapatite tricalcium phosphate and combination of mesenchymal stem cells in inducing bone regeneration. *Chang Gung medical journal* **35**, 28-37 (2011).
241. Livak, K.J. & Schmittgen, T.D. Analysis of relative gene expression data using real-time quantitative PCR and the 2− ΔΔCT method. *methods* **25**, 402-408 (2001).
242. Pfaffl, M.W. A new mathematical model for relative quantification in real-time RT–PCR. *Nucleic acids research* **29**, e45-e45 (2001).

243. Piccinini, E., Sadr, N. & Martin, I. Ceramic materials lead to underestimated DNA quantifications: a method for reliable measurements. *European cells & materials* **20**, 38-44 (2010).
244. Nich, C. & Sedel, L. Bone substitution in revision hip replacement. *International orthopaedics* **30**, 525-531 (2006).
245. Bodde, E.W., Wolke, J.G., Kowalski, R.S. & Jansen, J.A. Bone regeneration of porous β-tricalcium phosphate (Conduit™ TCP) and of biphasic calcium phosphate ceramic (Biosel®) in trabecular defects in sheep. *Journal of Biomedical Materials Research Part A* **82**, 711-722 (2007).
246. Orimo, H. The mechanism of mineralization and the role of alkaline phosphatase in health and disease. *Journal of Nippon Medical School = Nippon Ika Daigaku zasshi* **77**, 4-12 (2010).
247. Ogata, K.*, et al.* Comparison of osteoblast responses to hydroxyapatite and hydroxyapatite/soluble calcium phosphate composites. *Journal of biomedical materials research. Part A* **72**, 127-135 (2005).
248. Yang, W.*, et al.* Performance of different three-dimensional scaffolds for in vivo endochondral bone generation. *European cells & materials* **27**, 350-364 (2014).
249. Holtorf, H.L., Sheffield, T.L., Ambrose, C.G., Jansen, J.A. & Mikos, A.G. Flow perfusion culture of marrow stromal cells seeded on porous biphasic calcium phosphate ceramics. *Annals of biomedical engineering* **33**, 1238-1248 (2005).
250. Bancroft, G.N.*, et al.* Fluid flow increases mineralized matrix deposition in 3D perfusion culture of marrow stromal osteoblasts in a dose-dependent manner. *Proceedings of the National Academy of Sciences of the United States of America* **99**, 12600-12605 (2002).
251. Amarilio, R.*, et al.* HIF1alpha regulation of Sox9 is necessary to maintain differentiation of hypoxic prechondrogenic cells during early skeletogenesis. *Development* **134**, 3917-3928 (2007).
252. Le Guehennec, L., Layrolle, P. & Daculsi, G. A review of bioceramics and fibrin sealant. *European cells & materials* **8**, 1-10; discussion 10-11 (2004).

253. Koolwijk, P.*, et al.* Cooperative effect of TNFalpha, bFGF, and VEGF on the formation of tubular structures of human microvascular endothelial cells in a fibrin matrix. Role of urokinase activity. *The Journal of cell biology* **132**, 1177-1188 (1996).
254. Takei, A., Tashiro, Y., Nakashima, Y. & Sueishi, K. Effects of fibrin on the angiogenesis in vitro of bovine endothelial cells in collagen gel. *In vitro cellular & developmental biology. Animal* **31**, 467-472 (1995).
255. Nakamura, K., Koshino, T. & Saito, T. Osteogenic response of the rabbit femur to a hydroxyapatite thermal decomposition product-fibrin glue mixture. *Biomaterials* **19**, 1901-1907 (1998).
256. Bluteau, G.*, et al.* The modulation of gene expression in osteoblasts by thrombin coated on biphasic calcium phosphate ceramic. *Biomaterials* **27**, 2934-2943 (2006).
257. Arinzeh, T.L., Tran, T., McAlary, J. & Daculsi, G. A comparative study of biphasic calcium phosphate ceramics for human mesenchymal stem-cell-induced bone formation. *Biomaterials* **26**, 3631-3638 (2005).
258. Muller, P.*, et al.* Calcium phosphate surfaces promote osteogenic differentiation of mesenchymal stem cells. *Journal of cellular and molecular medicine* **12**, 281-291 (2008).
259. Polini, A., Pisignano, D., Parodi, M., Quarto, R. & Scaglione, S. Osteoinduction of human mesenchymal stem cells by bioactive composite scaffolds without supplemental osteogenic growth factors. *PloS one* **6**, e26211 (2011).
260. Guha, A.K., Singh, S., Kumaresan, R., Nayar, S. & Sinha, A. Mesenchymal cell response to nanosized biphasic calcium phosphate composites. *Colloids and surfaces. B, Biointerfaces* **73**, 146-151 (2009).
261. Kasten, P.*, et al.* Porosity and pore size of beta-tricalcium phosphate scaffold can influence protein production and osteogenic differentiation of human mesenchymal stem cells: an in vitro and in vivo study. *Acta biomaterialia* **4**, 1904-1915 (2008).
262. Kurashina, K., Kurita, H., Wu, Q., Ohtsuka, A. & Kobayashi, H. Ectopic osteogenesis with biphasic ceramics of hydroxyapatite and tricalcium phosphate in rabbits. *Biomaterials* **23**, 407-412 (2002).

263. Yuan, H.*, et al.* Bone morphogenetic protein and ceramic-induced osteogenesis. *Journal of materials science. Materials in medicine* **9**, 717-721 (1998).
264. Frayssinet, P., Trouillet, J.L., Rouquet, N., Azimus, E. & Autefage, A. Osseointegration of macroporous calcium phosphate ceramics having a different chemical composition. *Biomaterials* **14**, 423-429 (1993).
265. Alam, I., Asahina, I., Ohmamiuda, K. & Enomoto, S. Comparative study of biphasic calcium phosphate ceramics impregnated with rhBMP-2 as bone substitutes. *Journal of biomedical materials research* **54**, 129-138 (2001).
266. Giachelli, C.M.*, et al.* Vascular calcification and inorganic phosphate. *American journal of kidney diseases : the official journal of the National Kidney Foundation* **38**, S34-37 (2001).
267. Nielsen, L.B., Pedersen, F.S. & Pedersen, L. Expression of type III sodium-dependent phosphate transporters/retroviral receptors mRNAs during osteoblast differentiation. *Bone* **28**, 160-166 (2001).
268. Li, Z., Zhou, Z., Yellowley, C.E. & Donahue, H.J. Inhibiting gap junctional intercellular communication alters expression of differentiation markers in osteoblastic cells. *Bone* **25**, 661-666 (1999).
269. Schiller, P.C., D'Ippolito, G., Balkan, W., Roos, B.A. & Howard, G.A. Gap-junctional communication is required for the maturation process of osteoblastic cells in culture. *Bone* **28**, 362-369 (2001).
270. Liu, G.*, et al.* Effect of type I collagen on the adhesion, proliferation, and osteoblastic gene expression of bone marrow-derived mesenchymal stem cells. *Chinese journal of traumatology = Zhonghua chuang shang za zhi / Chinese Medical Association* **7**, 358-362 (2004).
271. Liu, Y., Hunziker, E.B., Layrolle, P., De Bruijn, J.D. & De Groot, K. Bone morphogenetic protein 2 incorporated into biomimetic coatings retains its biological activity. *Tissue engineering* **10**, 101-108 (2004).
272. Cool, S.M. & Nurcombe, V. Substrate induction of osteogenesis from marrow-derived mesenchymal precursors. *Stem cells and development* **14**, 632-642 (2005).
273. Valarmathi, M.T., Yost, M.J., Goodwin, R.L. & Potts, J.D. A three-dimensional tubular scaffold that modulates the osteogenic and

vasculogenic differentiation of rat bone marrow stromal cells. *Tissue engineering. Part A* **14**, 491-504 (2008).

274. Cordonnier, T.*, et al.* 3D environment on human mesenchymal stem cells differentiation for bone tissue engineering. *Journal of materials science. Materials in medicine* **21**, 981-987 (2010).
275. Cordonnier, T., Sohier, J., Rosset, P. & Layrolle, P. Biomimetic Materials for Bone Tissue Engineering - State of the Art and Future Trends. *Advanced Engineering Materials* **13**, B135-B150 (2011).
276. Cordonnier, T.*, et al.* Osteoblastic differentiation and potent osteogenicity of three-dimensional hBMSC-BCP particle constructs. *Journal of tissue engineering and regenerative medicine* **8**, 364-376 (2014).
277. Heughebaert, M., LeGeros, R., Gineste, M., Guilhem, A. & Bonel, G. Physicochemical characterization of deposits associated with HA ceramics implanted in nonosseous sites. *Journal of Biomedical Materials Research Part A* **22**, 257-268 (1988).
278. Daculsi, G., LeGeros, R., Heughebaert, M. & Barbieux, I. Formation of carbonate-apatite crystals after implantation of calcium phosphate ceramics. *Calcified tissue international* **46**, 20-27 (1990).
279. Daculsi, G., LeGeros, R., Nery, E., Lynch, K. & Kerebel, B. Transformation of biphasic calcium phosphate ceramics in vivo: ultrastructural and physicochemical characterization. *Journal of Biomedical Materials Research Part A* **23**, 883-894 (1989).
280. Jung, G.-Y., Park, Y.-J. & Han, J.-S. Effects of HA released calcium ion on osteoblast differentiation. *Journal of Materials Science: Materials in Medicine* **21**, 1649-1654 (2010).
281. Portal-Nunez, S., Lozano, D. & Esbrit, P. Role of angiogenesis on bone formation. *Histology and histopathology* **27**, 559-566 (2012).
282. Hankenson, K.D., Dishowitz, M., Gray, C. & Schenker, M. Angiogenesis in bone regeneration. *Injury* **42**, 556-561 (2011).
283. Patel, Z.S.*, et al.* Dual delivery of an angiogenic and an osteogenic growth factor for bone regeneration in a critical size defect model. *Bone* **43**, 931-940 (2008).

284. Shah, N.J., *et al.* Tunable dual growth factor delivery from polyelectrolyte multilayer films. *Biomaterials* **32**, 6183-6193 (2011).
285. Young, S., *et al.* Dose effect of dual delivery of vascular endothelial growth factor and bone morphogenetic protein-2 on bone regeneration in a rat critical-size defect model. *Tissue Engineering Part A* **15**, 2347-2362 (2009).
286. Yu, H., *et al.* Promotion of osteogenesis in tissue-engineered bone by pre-seeding endothelial progenitor cells-derived endothelial cells. *Journal of orthopaedic research* **26**, 1147-1152 (2008).
287. Zhou, J., *et al.* The repair of large segmental bone defects in the rabbit with vascularized tissue engineered bone. *Biomaterials* **31**, 1171-1179 (2010).
288. Villars, F., Bordenave, L., Bareille, R. & Amedee, J. Effect of human endothelial cells on human bone marrow stromal cell phenotype: role of VEGF? *Journal of cellular biochemistry* **79**, 672-685 (2000).
289. Sweeney, N.V.O., *et al.* Cyclic strain-mediated regulation of vascular endothelial cell migration and tube formation. *Biochemical and biophysical research communications* **329**, 573-582 (2005).
290. Iba, T. & Sumpio, B.E. Morphological response of human endothelial cells subjected to cyclic strain in vitro. *Microvascular research* **42**, 245-254 (1991).
291. Azuma, N., *et al.* Endothelial cell response to different mechanical forces. *Journal of vascular surgery* **32**, 789-794 (2000).
292. Cheung, W.Y., Liu, C., Tonelli-Zasarsky, R.M., Simmons, C.A. & You, L. Osteocyte apoptosis is mechanically regulated and induces angiogenesis in vitro. *Journal of Orthopaedic Research* **29**, 523-530 (2011).
293. Liu, C., *et al.* Influence of perfusion and compression on the proliferation and differentiation of bone mesenchymal stromal cells seeded on polyurethane scaffolds. *Biomaterials* **33**, 1052-1064 (2012).
294. Yu, H., *et al.* Promotion of osteogenesis in tissue-engineered bone by pre-seeding endothelial progenitor cells-derived endothelial cells.

Journal of orthopaedic research : official publication of the Orthopaedic Research Society **26**, 1147-1152 (2008).

295. Kuboki, Y., Jin, Q. & Takita, H. Geometry of carriers controlling phenotypic expression in BMP-induced osteogenesis and chondrogenesis. *The Journal of bone and joint surgery. American volume* **83**, S105-S115 (2001).
296. Gomes, M.E., Sikavitsas, V.I., Behravesh, E., Reis, R.L. & Mikos, A.G. Effect of flow perfusion on the osteogenic differentiation of bone marrow stromal cells cultured on starch-based three-dimensional scaffolds. *Journal of Biomedical Materials Research Part A* **67**, 87-95 (2003).
297. Muller, I.*, et al.* Secretion of angiogenic proteins by human multipotent mesenchymal stromal cells and their clinical potential in the treatment of avascular osteonecrosis. *Leukemia* **22**, 2054-2061 (2008).
298. Zhang, Z.Y.*, et al.* A biaxial rotating bioreactor for the culture of fetal mesenchymal stem cells for bone tissue engineering. *Biomaterials* **30**, 2694-2704 (2009).
299. Davy, A. & Soriano, P. Ephrin signaling in vivo: look both ways. *Developmental dynamics* **232**, 1-10 (2005).
300. Santiago, A. & Erickson, C.A. Ephrin-B ligands play a dual role in the control of neural crest cell migration. *Development* **129**, 3621-3632 (2002).
301. Hruska, M. & Dalva, M.B. Ephrin regulation of synapse formation, function and plasticity. *Molecular and Cellular Neuroscience* **50**, 35-44 (2012).
302. Wang, Y.*, et al.* Ephrin B2/EphB4 mediates the actions of IGF-I signaling in regulating endochondral bone formation. *Journal of bone and mineral research : the official journal of the American Society for Bone and Mineral Research* **29**, 1900-1913 (2014).
303. Wang, Y.*, et al.* Ephrin-B2 controls VEGF-induced angiogenesis and lymphangiogenesis. *Nature* **465**, 483-486 (2010).
304. Gerety, S.S., Wang, H.U., Chen, Z.-F. & Anderson, D.J. Symmetrical mutant phenotypes of the receptor EphB4 and its specific

transmembrane ligand ephrin-B2 in cardiovascular development. *Molecular cell* **4**, 403-414 (1999).

305. Foo, S.S.*, et al.* Ephrin-B2 controls cell motility and adhesion during blood-vessel-wall assembly. *Cell* **124**, 161-173 (2006).
306. Abengozar, M.A.*, et al.* Blocking ephrinB2 with highly specific antibodies inhibits angiogenesis, lymphangiogenesis, and tumor growth. *Blood* **119**, 4565-4576 (2012).
307. Takyar, F.M.*, et al.* EphrinB2/EphB4 inhibition in the osteoblast lineage modifies the anabolic response to parathyroid hormone. *Journal of bone and mineral research : the official journal of the American Society for Bone and Mineral Research* **28**, 912-925 (2013).
308. Xing, W.*, et al.* Global gene expression analysis in the bones reveals involvement of several novel genes and pathways in mediating an anabolic response of mechanical loading in mice. *Journal of cellular biochemistry* **96**, 1049-1060 (2005).
309. Broqueres-You, D.*, et al.* Ephrin-B2-activated peripheral blood mononuclear cells from diabetic patients restore diabetes-induced impairment of postischemic neovascularization. *Diabetes* **61**, 2621-2632 (2012).
310. Katsu, M.*, et al.* Ex vivo gene delivery of ephrin-B2 induces development of functional collateral vessels in a rabbit model of hind limb ischemia. *Journal of vascular surgery* **49**, 192-198 (2009).
311. Salvucci, O.*, et al.* EphrinB reverse signaling contributes to endothelial and mural cell assembly into vascular structures. *Blood* **114**, 1707-1716 (2009).
312. Bochenek, M.L., Dickinson, S., Astin, J.W., Adams, R.H. & Nobes, C.D. Ephrin-B2 regulates endothelial cell morphology and motility independently of Eph-receptor binding. *Journal of cell science* **123**, 1235-1246 (2010).
313. Arthur, A.*, et al.* EphB/ephrin-B interactions mediate human MSC attachment, migration and osteochondral differentiation. *Bone* **48**, 533-542 (2011).
314. Tonna, S.*, et al.* EphrinB2 signaling in osteoblasts promotes bone mineralization by preventing apoptosis. *FASEB journal : official*

publication of the Federation of American Societies for Experimental Biology **28**, 4482-4496 (2014).

315. Kutner, R.H., Zhang, X.-Y. & Reiser, J. Production, concentration and titration of pseudotyped HIV-1-based lentiviral vectors. *Nature protocols* **4**, 495-505 (2009).
316. Sastry, L., Johnson, T., Hobson, M., Smucker, B. & Cornetta, K. Titering lentiviral vectors: comparison of DNA, RNA and marker expression methods. *Gene therapy* **9**(2002).
317. Lin, P.*, et al.* Efficient Lentiviral Transduction of Human Mesenchymal Stem Cells That Preserves Proliferation and Differentiation Capabilities. *Stem Cells Translational Medicine* **1**, 886 (2012).
318. Lin, P.*, et al.* Efficient lentiviral transduction of human mesenchymal stem cells that preserves proliferation and differentiation capabilities. *Stem cells translational medicine* **1**, 886-897 (2012).
319. Duffy, G.P.*, et al.* Mesenchymal stem cells overexpressing ephrin-b2 rapidly adopt an early endothelial phenotype with simultaneous reduction of osteogenic potential. *Tissue Engineering Part A* **16**, 2755-2768 (2010).
320. Tierney, E.G.*, et al.* High levels of ephrinB2 over-expression increases the osteogenic differentiation of human mesenchymal stem cells and promotes enhanced cell mediated mineralisation in a polyethyleneimine-ephrinB2 gene-activated matrix. *Journal of controlled release* **165**, 173-182 (2013).
321. Grinev, V., Seviaryn, I., Posrednik, D., Kosmacheva, S. & Potapnev, M. Highly efficient transfer and stable expression of two genes upon lentivirus transduction of mesenchymal stem cells from human bone marrow. *Russian journal of genetics* **48**, 336-346 (2012).
322. Tierney, E.G.*, et al.* High levels of ephrinB2 over-expression increases the osteogenic differentiation of human mesenchymal stem cells and promotes enhanced cell mediated mineralisation in a polyethyleneimine-ephrinB2 gene-activated matrix. *Journal of controlled release : official journal of the Controlled Release Society* **165**, 173-182 (2013).

323. Tonna, S.*, et al.* Chondrocytic ephrin B2 promotes cartilage destruction by osteoclasts in endochondral ossification. *Development* **143**, 648-657 (2016).
324. Gerber, H.P.*, et al.* VEGF couples hypertrophic cartilage remodeling, ossification and angiogenesis during endochondral bone formation. *Nature medicine* **5**, 623-628 (1999).
325. Hoch, A.I., Binder, B.Y., Genetos, D.C. & Leach, J.K. Differentiation-dependent secretion of proangiogenic factors by mesenchymal stem cells. *PloS one* **7**, e35579 (2012).
326. Helmrich, U.*, et al.* Osteogenic graft vascularization and bone resorption by VEGF-expressing human mesenchymal progenitors. *Biomaterials* **34**, 5025-5035 (2013).
327. Bara, J.J., McCarthy, H.E., Humphrey, E., Johnson, W.E. & Roberts, S. Bone marrow-derived mesenchymal stem cells become antiangiogenic when chondrogenically or osteogenically differentiated: implications for bone and cartilage tissue engineering. *Tissue engineering. Part A* **20**, 147-159 (2014).
328. Gruber, R.*, et al.* Bone marrow stromal cells can provide a local environment that favors migration and formation of tubular structures of endothelial cells. *Tissue engineering* **11**, 896-903 (2005).
329. Duffy, G.P.*, et al.* Mesenchymal stem cells overexpressing ephrin-b2 rapidly adopt an early endothelial phenotype with simultaneous reduction of osteogenic potential. *Tissue engineering. Part A* **16**, 2755-2768 (2010).
330. Martin, T.J.*, et al.* Communication between ephrinB2 and EphB4 within the osteoblast lineage. *Advances in experimental medicine and biology* **658**, 51-60 (2010).
331. Riminucci, M.*, et al.* Vis-a-vis cells and the priming of bone formation. *Journal of Bone and Mineral Research* **13**, 1852-1861 (1998).
332. Frohbergh, M.E.*, et al.* Electrospun hydroxyapatite-containing chitosan nanofibers crosslinked with genipin for bone tissue engineering. *Biomaterials* **33**, 9167-9178 (2012).

333. Chai, Y.C., *et al.* Current views on calcium phosphate osteogenicity and the translation into effective bone regeneration strategies. *Acta biomaterialia* **8**, 3876-3887 (2012).
334. Karageorgiou, V. & Kaplan, D. Porosity of 3D biomaterial scaffolds and osteogenesis. *Biomaterials* **26**, 5474-5491 (2005).
335. Chang, B., *et al.* Influence of pore size of porous titanium fabricated by vacuum diffusion bonding of titanium meshes on cell penetration and bone ingrowth. *Acta biomaterialia* **33**, 311-321 (2016).
336. Fedorovich, N.E., Kuipers, E., Gawlitta, D., Dhert, W.J. & Alblas, J. Scaffold porosity and oxygenation of printed hydrogel constructs affect functionality of embedded osteogenic progenitors. *Tissue engineering. Part A* **17**, 2473-2486 (2011).
337. Krebsbach, P.H., *et al.* Bone formation in vivo: comparison of osteogenesis by transplanted mouse and human marrow stromal fibroblasts. *Transplantation* **63**, 1059-1069 (1997).
338. Tasso, R., *et al.* Recruitment of a host's osteoprogenitor cells using exogenous mesenchymal stem cells seeded on porous ceramic. *Tissue engineering. Part A* **15**, 2203-2212 (2009).
339. Eckardt, H., *et al.* Effects of locally applied vascular endothelial growth factor (VEGF) and VEGF-inhibitor to the rabbit tibia during distraction osteogenesis. *Journal of orthopaedic research : official publication of the Orthopaedic Research Society* **21**, 335-340 (2003).
340. Li, R., Stewart, D.J., von Schroeder, H.P., Mackinnon, E.S. & Schemitsch, E.H. Effect of cell-based VEGF gene therapy on healing of a segmental bone defect. *Journal of orthopaedic research : official publication of the Orthopaedic Research Society* **27**, 8-14 (2009).
341. Tarkka, T., *et al.* Adenoviral VEGF-A gene transfer induces angiogenesis and promotes bone formation in healing osseous tissues. *The journal of gene medicine* **5**, 560-566 (2003).
342. Andreshak, J.L., Rabin, S.I., Patwardhan, A.G. & Wezeman, F.H. Tibial segmental defect repair: chondrogenesis and biomechanical strength modulated by basic fibroblast growth factor. *The Anatomical record* **248**, 198-204 (1997).

343. Bland, Y.S., Critchlow, M.A. & Ashhurst, D.E. Exogenous fibroblast growth factors-1 and -2 do not accelerate fracture healing in the rabbit. *Acta orthopaedica Scandinavica* **66**, 543-548 (1995).
344. Chen, W.J.*, et al.* Effects of FGF-2 on metaphyseal fracture repair in rabbit tibiae. *Journal of bone and mineral metabolism* **22**, 303-309 (2004).
345. Kawaguchi, H.*, et al.* Stimulation of fracture repair by recombinant human basic fibroblast growth factor in normal and streptozotocin-diabetic rats. *Endocrinology* **135**, 774-781 (1994).
346. Kawaguchi, H.*, et al.* Acceleration of fracture healing in nonhuman primates by fibroblast growth factor-2. *The Journal of clinical endocrinology and metabolism* **86**, 875-880 (2001).
347. Nakajima, F.*, et al.* Spatial and temporal gene expression in chondrogenesis during fracture healing and the effects of basic fibroblast growth factor. *Journal of orthopaedic research : official publication of the Orthopaedic Research Society* **19**, 935-944 (2001).
348. Nakamura, T.*, et al.* Recombinant human basic fibroblast growth factor accelerates fracture healing by enhancing callus remodeling in experimental dog tibial fracture. *Journal of bone and mineral research : the official journal of the American Society for Bone and Mineral Research* **13**, 942-949 (1998).
349. Radomsky, M.L.*, et al.* Novel formulation of fibroblast growth factor-2 in a hyaluronan gel accelerates fracture healing in nonhuman primates. *Journal of orthopaedic research : official publication of the Orthopaedic Research Society* **17**, 607-614 (1999).
350. Hollinger, J.O.*, et al.* Accelerated fracture healing in the geriatric, osteoporotic rat with recombinant human platelet-derived growth factor-BB and an injectable beta-tricalcium phosphate/collagen matrix. *Journal of orthopaedic research : official publication of the Orthopaedic Research Society* **26**, 83-90 (2008).
351. Nash, T.J.*, et al.* Effect of platelet-derived growth factor on tibial osteotomies in rabbits. *Bone* **15**, 203-208 (1994).
352. Li, G., Ryaby, J.T., Carney, D.H. & Wang, H. Bone formation is enhanced by thrombin-related peptide TP508 during distraction

osteogenesis. *Journal of orthopaedic research : official publication of the Orthopaedic Research Society* **23**, 196-202 (2005).

353. Ryaby, J.T.*, et al.* Thrombin peptide TP508 stimulates cellular events leading to angiogenesis, revascularization, and repair of dermal and musculoskeletal tissues. *The Journal of bone and joint surgery. American volume* **88 Suppl 3**, 132-139 (2006).
354. Sheller, M.R.*, et al.* Repair of rabbit segmental defects with the thrombin peptide, TP508. *Journal of orthopaedic research : official publication of the Orthopaedic Research Society* **22**, 1094-1099 (2004).
355. Wang, H.*, et al.* Thrombin peptide (TP508) promotes fracture repair by up-regulating inflammatory mediators, early growth factors, and increasing angiogenesis. *Journal of orthopaedic research : official publication of the Orthopaedic Research Society* **23**, 671-679 (2005).
356. Steinbrech, D.S.*, et al.* VEGF expression in an osteoblast-like cell line is regulated by a hypoxia response mechanism. *American journal of physiology. Cell physiology* **278**, C853-860 (2000).
357. Anagnostou, A., Lee, E.S., Kessimian, N., Levinson, R. & Steiner, M. Erythropoietin has a mitogenic and positive chemotactic effect on endothelial cells. *Proceedings of the National Academy of Sciences of the United States of America* **87**, 5978-5982 (1990).
358. Goldberg, M.A., Dunning, S.P. & Bunn, H.F. Regulation of the erythropoietin gene: evidence that the oxygen sensor is a heme protein. *Science* **242**, 1412-1415 (1988).
359. Holstein, J.H.*, et al.* Erythropoietin (EPO): EPO-receptor signaling improves early endochondral ossification and mechanical strength in fracture healing. *Life sciences* **80**, 893-900 (2007).
360. Shen, X.*, et al.* Prolyl hydroxylase inhibitors increase neoangiogenesis and callus formation following femur fracture in mice. *Journal of orthopaedic research : official publication of the Orthopaedic Research Society* **27**, 1298-1305 (2009).
361. Isenberg, J.S.*, et al.* CD47 is necessary for inhibition of nitric oxide-stimulated vascular cell responses by thrombospondin-1. *The Journal of biological chemistry* **281**, 26069-26080 (2006).

362. Taylor, D.K., *et al.* Thrombospondin-2 influences the proportion of cartilage and bone during fracture healing. *Journal of bone and mineral research : the official journal of the American Society for Bone and Mineral Research* **24**, 1043-1054 (2009).
363. Caplan, A.I. & Dennis, J.E. Mesenchymal stem cells as trophic mediators. *Journal of cellular biochemistry* **98**, 1076-1084 (2006).
364. Tang, Y.L., *et al.* Paracrine action enhances the effects of autologous mesenchymal stem cell transplantation on vascular regeneration in rat model of myocardial infarction. *The Annals of thoracic surgery* **80**, 229-236; discussion 236-227 (2005).
365. Heng, B.C., Haider, H., Sim, E.K., Cao, T. & Ng, S.C. Strategies for directing the differentiation of stem cells into the cardiomyogenic lineage in vitro. *Cardiovascular research* **62**, 34-42 (2004).
366. Peric, M., *et al.* The rational use of animal models in the evaluation of novel bone regenerative therapies. *Bone* **70**, 73-86 (2015).
367. Ficat, R. & Arlet, J. Functional investigation of bone under normal conditions in ischemia and necrosis of bone. *Ischemia and necrosis of bone. Baltimore: Williams and Wilkins*, 29 (1980).
368. Tzaribachev, N., *et al.* Mesenchymal stromal cells: a novel treatment option for steroid-induced avascular osteonecrosis. *The Israel Medical Association journal : IMAJ* **10**, 232-234 (2008).
369. Yan, Z., Hang, D., Guo, C. & Chen, Z. Fate of mesenchymal stem cells transplanted to osteonecrosis of femoral head. *Journal of orthopaedic research : official publication of the Orthopaedic Research Society* **27**, 442-446 (2009).
370. Nich, C. & Sedel, L. Bone substitution in revision hip replacement. *International orthopaedics* **30**, 525-531 (2006).
371. Bodde, E.W., Wolke, J.G., Kowalski, R.S. & Jansen, J.A. Bone regeneration of porous beta-tricalcium phosphate (Conduit TCP) and of biphasic calcium phosphate ceramic (Biosel) in trabecular defects in sheep. *Journal of biomedical materials research. Part A* **82**, 711-722 (2007).
372. Ebrahimi, M. & Botelho, M. Biphasic calcium phosphates (BCP) of hydroxyapatite (HA) and tricalcium phosphate (TCP) as bone

substitutes: Importance of physicochemical characterizations in biomaterials studies. *Data in brief* **10**, 93-97 (2017).

373. Kwan Tat, S.*, et al.* Treatment with ephrin B2 positively impacts the abnormal metabolism of human osteoarthritic chondrocytes. *Arthritis research & therapy* **11**, R119 (2009).
374. Kwan Tat, S.*, et al.* Activation of the receptor EphB4 by its specific ligand ephrin B2 in human osteoarthritic subchondral bone osteoblasts. *Arthritis and rheumatism* **58**, 3820-3830 (2008).
375. Meury, T., Verrier, S. & Alini, M. Human endothelial cells inhibit BMSC differentiation into mature osteoblasts in vitro by interfering with osterix expression. *Journal of cellular biochemistry* **98**, 992-1006 (2006).
376. Kanczler, J.M. & Oreffo, R.O. Osteogenesis and angiogenesis: the potential for engineering bone. *European cells & materials* **15**, 100-114 (2008).
377. Kusumbe, A.P., Ramasamy, S.K. & Adams, R.H. Coupling of angiogenesis and osteogenesis by a specific vessel subtype in bone. *Nature* **507**, 323-328 (2014).
378. Xie, H.*, et al.* PDGF-BB secreted by preosteoclasts induces angiogenesis during coupling with osteogenesis. *Nature medicine* **20**, 1270-1278 (2014).
379. Bahney, C.S., Hu, D.P., Miclau, T., 3rd & Marcucio, R.S. The multifaceted role of the vasculature in endochondral fracture repair. *Frontiers in endocrinology* **6**, 4 (2015).
380. Bahney, C.S.*, et al.* Stem cell-derived endochondral cartilage stimulates bone healing by tissue transformation. *Journal of bone and mineral research : the official journal of the American Society for Bone and Mineral Research* **29**, 1269-1282 (2014).
381. Yang, L., Tsang, K.Y., Tang, H.C., Chan, D. & Cheah, K.S. Hypertrophic chondrocytes can become osteoblasts and osteocytes in endochondral bone formation. *Proceedings of the National Academy of Sciences of the United States of America* **111**, 12097-12102 (2014).
382. Zhou, X.*, et al.* Chondrocytes transdifferentiate into osteoblasts in endochondral bone during development, postnatal growth and fracture healing in mice. *PLoS genetics* **10**, e1004820 (2014).

383. Scammell, B.E. & Roach, H.I. A new role for the chondrocyte in fracture repair: endochondral ossification includes direct bone formation by former chondrocytes. *Journal of bone and mineral research : the official journal of the American Society for Bone and Mineral Research* **11**, 737-745 (1996).
384. Yasui, N.*, et al.* Three modes of ossification during distraction osteogenesis in the rat. *The Journal of bone and joint surgery. British volume* **79**, 824-830 (1997).
385. Song, L. & Tuan, R.S. Transdifferentiation potential of human mesenchymal stem cells derived from bone marrow. *FASEB journal : official publication of the Federation of American Societies for Experimental Biology* **18**, 980-982 (2004).
386. Behonick, D.J.*, et al.* Role of matrix metalloproteinase 13 in both endochondral and intramembranous ossification during skeletal regeneration. *PloS one* **2**, e1150 (2007).
387. Yu, Y.Y.*, et al.* Immunolocalization of BMPs, BMP antagonists, receptors, and effectors during fracture repair. *Bone* **46**, 841-851 (2010).
388. Gerstenfeld, L.C.*, et al.* Chondrocytes provide morphogenic signals that selectively induce osteogenic differentiation of mesenchymal stem cells. *Journal of bone and mineral research : the official journal of the American Society for Bone and Mineral Research* **17**, 221-230 (2002).